Title
page

PEAK AND RESIDUAL STRENGTH ENVELOPES ESTABLISHED BY CONFINED SHEAR TEST METHOD

M. GYENGE

CANADIAN MINE TECHNOLOGY LABORATORY

MRL 88-35 (TR) MAY 1988

PEAK AND RESIDUAL STRENGTH ENVELOPES ESTABLISHED BY CONFINED SHEAR TEST METHOD

M. Gyenge*

ABSTRACT

This report provides a detailed account of the development and verification of a novel testing concept for establishing the frictional and strength properties of jointed rocks.

A set of four cylindrical specimens is easily prepared from readily available diamond cores. In the test apparatus, three equal normal forces are applied on the three outside specimens in a radial direction. The latter are in sliding contact with the central specimen along three equally-spaced generatrices. A concentric shear force is applied to the central core in an axial direction. The central core is free to move along the shear direction, but it is otherwise confined along the lines of contact, by the triangular application of normal forces.

The technique had been verified by successfully testing several rocks, including both ductile and brittle types. Strength and frictional properties were established for smooth joints, as well as, for joints with simulated asperities.

The results obtained by the completed tests revealed that this technique is superior to any of the previously-used shear testing methods. Due to the inherent advantages of the method, a large quantity of highly reliable joint-property data can be obtained from a single set of test specimens.

Based on the reliable, reproducible and consistent data thus obtained, it is seemingly possible to evolve a data analysis method to distinguish between the various components of the coefficient of friction, and relationships between them.

---

*Research Scientist, Canadian Mine Technology Laboratory, Canada Centre for Mineral and Energy Technology (CANMET), Energy, Mines and Resources Canada.

Analysed joint property data can be correlated with uniaxial and triaxial test data. Consequently, with this method of analysis all major strength and deformation properties can be linked.

The defined interrelationships between joint and rock substance strength properties were used to determine both the peak and the residual strength envelopes of jointed rock mass.

The test apparatus, due to its simplicity, is highly versatile. It can be used not only with a laboratory press, but also with a simple portable test frame operated by hydraulic hand pumps. Specimen preparation can be performed on site.

ENVELOPPES DE RESISTANCE MAXIMALE ET RESIDUELLE ETABLIES PAR LA METHODE D'ESSAI DE CISAILLEMENT CONFINE

M. Gyenge*

RESUME

Ce rapport décrit en détail comment a été élaboré et comment vérifier un nouveau principe d'essai pour établir les propriétés de frottement et de résistance des roches diaclasées.

Un jeu de quatre éprouvettes cylindriques est facile à préparer à partir de carottes de forage au diamant faciles à obtenir. Dans l'appareil d'essai, trois forces normales égales sont appliquées radialement sur les trois éprouvettes extérieures. Ces dernières sont en contact de glissement, le long de trois génératrices équidistantes, avec l'éprouvette centrale. Une force de cisaillement concentrique est appliquée axialement au noyau central. Ce dernier est libre de se déplacer le long de l'axe de cisaillement, mais il est autrement confiné le long des lignes de contact par l'application triangulaire des forces normales.

La technique a été vérifiée par des essais concluants sur plusieurs roches, tant ductiles que fragiles. Les propriétés de résistance et de frottement ont été établies pour des diaclases lisses ainsi que pour des diaclases avec aspérités simulées.

Les résultats des essais ont révélé que cette technique est supérieure à toutes les autres méthodes d'essai de cisaillement utilisées. A cause des avantages inhérents de la méthode, une grande quantité de données très fiables sur les propriétés des diaclases peuvent être obtenues d'un seul jeu d'éprouvettes.

D'après les données fiables, reproductibles et systématiques ainsi obtenues, il serait possible d'élaborer une méthode d'analyse des données pour distinguer les diverses composantes du coefficient de frottement, et les relations entre elles.

---

*Chercheur scientifique, Laboratoire canadien de technologie minière, Centre canadien de la technologie des minéraux et de l'énergie (CANMET), Energie, Mines et Ressources Canada.

Les données analysées sur les propriétés des diaclases peuvent être corrélées avec des données d'essais uniaxiaux et triaxiaux. Par conséquent, cette méthode d'analyse permet d'établir des relations entre toutes les grandes propriétés de résistance et de déformation.

Les relations définies entre les propriétés de résistance des diaclases et de la matière rocheuse ont servi à établir les enveloppes de résistance tant maximale que résiduelle de masses rocheuses diaclasées.

L'appareil d'essai, par sa simplicité, est très souple. Il peut être utilisé non seulement avec une presse de laboratoire, mais aussi avec un simple cadre d'essai portatif actionné par des pompes à main hydrauliques. Les éprouvettes peuvent être préparées sur place.

CONTENTS

CONTENTS (Cont'd)

TABLES

FIGURES

FIGURES (Cont'd)

FIGURES (Cont'd)

FIGURES (Cont'd)

FIGURES (Cont'd)

INTRODUCTION

An increasing amount of Canadian underground mining will, in the future, will take place under high stress, deep mining conditions. The increasingly sophisticated analysis, needed for good mine design, will require even more accurate constitutive equations to describe the strength and deformational properties of the rock mass. Consequently, new test methods and analytical procedures have to be developed to provide sufficiently accurate test data for this purpose.

The necessary development work is currently being handled within MRL's "Rock Properties and Support Systems" project. In the first phase of development, the post-failure strength properties tests were emphasized. The task of updating the test capabilities of CANMET's Canadian Mine Technology Laboratory (at MRL) was completed in two stages. First, the available 1.4 MN capacity universal press was modified and adapted for the requirements [1,2]. The present stage of updating activities involve the development of testing procedures for a recently purchased 4.5 MN capacity MTS 815 servo-hydraulic test system.

The second phase of the laboratory testing technology development is concerned with the strength properties of the joints. This report is an account of the development and verification of procedures involved in a novel test concept, which will be referred to as the "confined shear test method".

PREVIOUS TEST METHODS

The frictional and strength properties of joints are currently determined by either triaxial or direct shear test methods.

The triaxial method is used to establish the shear strength of a geological discontinuity in a cylindrical specimen under triaxial loading. This test provides data useful in determining the strength properties of the natural discontinuities, namely peak shear strengths at various lateral pressures, as well as the peak value of the coefficient of friction and apparent cohesion. The test is performed on a cylindrical rock specimen containing a single geological discontinuity with a certain degree of surface roughness and with an angle of orientation permitting sliding under the triaxial test conditions.

The limitation in the degree of surface roughness that can be tested represents one of the drawbacks of the method. The orientation requirement poses a further limitation on the use of the method, and presents problems in specimen preparation. A distinct advantage of the method is that triaxial test conditions are used. This permits the frictional and strength properties of the tested discontinuity to be obtained under confinement, i.e., under conditions which may simulate the actual field conditions around an underground opening.

The more popular of the two current methods in use is the direct shear test. The laboratory test is performed in a shear device consisting of a box made of two frames that hold the two halves of the specimen, separated by the plane of discontinuity. The test provides data useful in determining the strength properties of the natural discontinuities. The following relevant information is provided: (a) the shear strength on the plane at various normal pressures; (b) the geometrical component of the shear strength which results from the interlocking of surface irregularities; and (c) the frictional component of the shear strength due to sliding of the two surfaces. The test can be performed on a rock specimen of either irregular or cylindrical shape which contains the particular discontinuity of interest.

The shear device is provided with means for applying normal and shearing forces to the plane of discontinuity. The test method simulates the sliding condition of a surface block unconfined along its sides.

A specific type of direct shear test method is used to determine the residual shear strength and residual angle of friction of a rock substance. The test is usually performed on cylindrical specimens with a saw-cut plane of discontinuity. The test is used: (a) either to complement the triaxial shear tests which provide data relating only to the peak strength properties, or (b) to check the residual angle of friction of a natural discontinuity in the rock.

A field version of the direct shear method is used to measure the in situ peak and residual shear strengths as a function of the stress normal to the sheared plane. This test is usually employed in connection with foundation investigations of large structures, when the high cost of tests can be justified.

The field shear tests are carried out on intact blocks of the rock, which are isolated from the surrounding rock mass by excavation, or by drilling. The size of a block sample is governed by the capacities of the available loading systems. While a 0.1 m^2 area of tested discontinuity can be taken as a minimum, tests on a larger scale are expected to provide more representative results. A distinct disadvantage of field shear tests is the necessary costs involved in site preparation and the rather complex and large loading facilities required.

Regardless of the test method used, interpretation of the test results and their use for underground designs provide only uncertain answers. The uncertainties are inherent in the test method itself. The following problem areas are common to all of the specific tests mentioned above.

One of the interpreted laws of friction postulates, that in the case of dry surfaces the friction force is not dependent upon the total area of the surfaces in contact. Therefore, these methods should provide reliable data. However, problems arise at the stage of shear and normal stress calculations. The original contact area can, perhaps, be calculated or measured. However, once the normal and shear forces are applied, and once the normal and shear displacements have therefore occurred, the original contact area changes and is no longer known. Analysis, interpretation and use of the test results is, therefore, questionable.

Another interpreted law of friction states, that in the case of dry surfaces, the friction force is dependent upon the kinds of materials tested and upon the degree of roughness of the two surfaces in contact. However, to establish the strength and frictional properties along a plane of discontinuity, at least three, and preferably five, data pairs of the normal and shear stresses are required. Therefore, ideally an equivalent number of individual tests must be conducted at a range of normal loads, on specimens of identical material and of an equal degree of roughness along the two surfaces in contact. When dealing with geological materials, it is hard enough to meet the first requirement. The identical surface roughness of contact criterion probably never occurs. The test results obviously reflect the differences between the specimens, which in turn contributes to the uncertainty in the results achieved.

The third interpreted law of friction states, that the maximum friction force which can be developed is dependent upon the normal pressure between the two surfaces in contact, and is proportional to it.
One problem tied in with this law is the uncertainty with which the normal pressure and its distribution can be established. Because the contact area continually changes during the test, and since there is also a variation in the surface roughness along the contact area, the normal pressure cannot be calculated with any degree of certainty.

The second problem area is related to the magnitude of the normal stress which is usually applied when using these test methods. In order to run the tests on sliding surfaces that contain all of the representative features of the relevant discontinuity, the goal is to select its area as large as possible. Due to the constraints imposed by the capacities of the available loading devices, the tests are usually performed at rather low levels of normal stress. Consequently, the strength and frictional properties in case of higher normal stresses can only be estimated by the very uncertain means of extrapolation.

There are other shortcomings of these test methods as well. One such shortcoming, already touched upon, is related to the question of field-condition simulation. The failure mechanism due to the sliding of rock blocks, forming the periphery of an underground opening or the surface of an open pit, is adequately simulated by these methods. However, the movement of blocks within the rock mass is constrained. This condition is simulated only by the triaxial test method; this, however, has its own drawbacks, as discussed previously.

Moreover, specimen preparation for these tests is rather difficult, especially in the case of the in situ shear test. With the exception of the portable shearing device, the required special testing facilities are relatively complex.

Contact area related problems are eliminated by the test method suggested by Stimpson [3]. This simple test procedure measures the critical angle of sliding of cylindrical core surfaces in contact, by using three pieces of core and a tilt cable. The main problem with this method is that the frictional properties can only be established for a smooth surface and for a single normal load, namely, for the weight of the sliding core.

HIGHLIGHTS OF THE NEW TESTING METHOD

To reliably establish the frictional and strength properties of rock joints, a new testing technique had to be developed. It is based on a novel concept which is designed to eliminate the problems inherent in the use of the previous methods.

Following the conceptual and then the detailed designs, as well as in-house manufacturing and calibration, the test equipment and concept had been verified by means of test programs. Various rock types were tested and the frictional and strength properties established for smooth joints, as well as, for joints with simulated asperity. The tested rock materials included both ductile and brittle types. In addition, steel and teflon materials were also tested, in order to obtain comparative test data for ideal elastic and plastic materials. These data ideally suited for the development and verification of the analytical procedures.

The results of these test programs revealed that the method is superior to any previous shear testing technique. Due to the inherent advantages of the applied concept, a large quantity of highly-reliable data on joint properties can be obtained from a single set of test specimens.

Through the applied loading systems and instrumentation, it is possible to exercise full control over the normal stress acting along the joint represented by a single line of contact (i.e., the generatrix of the cylindrical test specimen). The test is conducted under confined conditions. The stress level acting on the specimen reaches, and even surpasses, the level required for underground mine design purposes.

Due to the obtained highly reliable, reproducible and consistent data, it is seemingly possible to determine and separate the various components of the coefficient of friction, and to establish the relationships between components and the involved stresses. Furthermore, it is seemingly also possible to define the relationship between the joint strength properties and the peak and residual strength properties of the rock substance. Consequently the testing technique, in combination with the analytical procedure, constitute a complete system which may be used for determination of design parameters of a jointed rock mass. In addition, due to its simplicity, the testing procedure can be used at the mine sites.

Because of the novelty of the concept involved in the testing, and especially because of the new approach to the relevant analysis, this report contains a plethora of details. This is done in order to assist the interested readers who may wish to study the details of the logic and reasoning involved in the analysis and interpretation. Furthermore, because of the additional information about the frictional behaviour of the rock obtained by this test method, it was difficult to identify the various components of the coefficient of friction by the usual terms in general use. Therefore, new terms were defined which are considered to be more descriptive for the observed mechanisms.

CONFINED SHEAR TEST METHOD

BASIC PRINCIPLE

The basic principle of the confined shear test technique is illustrated in Fig. 1. The specimen set comprises four cylindrical rock core specimens of same diameter. The three outside specimens are of equal length, while the centre core is longer.

Each of the outside cores is loaded by a normal force, P_n, of equal magnitude. The concentric shear force, S, is applied to the centre core.

The outside cores are all rigidly supported from both underneath and behind. Their movement in a vertical direction, i.e. in the direction of shearing, is constrained. However, their individual horizontal movement, i.e., their normal displacement, is unconstrained. The centre core, which moves freely in the vertical direction, is supported only by the shear and normal forces along the three vertical lines of contact with the outside cores.

In addition, the horizontal movement of the core set as a whole is unhindered. This provision of free movement is a further guarantee of the concentric application of the shear force. By virtue of the statically very stable triangular application of the normal forces, and the provision of free movements, a completely self-adjusting loading system is attained.

The diagram of forces is shown in Fig. 1(b). The centre core is confined laterally by the radially-applied normal forces, P_n. Axial displacement, i.e., shear displacement, of the centre core occurs when the applied shear force, S, is greater than the combined shear resistance along the three lines of contact with the outside cores. Equilibrium is reached when:

$$\frac{S}{3\mu} = P_n \qquad \text{Eq 1}$$

let

$$P_s = \frac{S}{3} \qquad \text{Eq 2}$$

therefore,

$$\frac{P_s}{\mu} = P_n \qquad \text{Eq 3}$$

and the coefficient of friction is:

$$\mu = \frac{P_s}{P_n} \qquad \text{Eq 4}$$

TEST APPARATUS

The test apparatus was developed and constructed in-house at the CMTL [4]. It is shown in Fig. 2 and 3.

The main component of the apparatus is its ring-frame. It contains three grooves, spaced at 120° along the inside diameter, to accommodate the vee blocks which are to seat the outside cores. At the groove locations, the ring-frame also contains through-holes equipped with hydraulic pistons. The ring-frame is carefully levelled by three levelling bolts, positioned at 120°.

The three through-holes, with the pistons inside them, are connected to the hydraulic power supply by a common line.

The ring-frame, is supported by three levelling bolts in an elevated and levelled position. The bolts rest on a polished steel plate. The vee blocks within the grooves are also resting on the polished steel plate. Underneath they are lubricated to facilitate normal displacement of the outside core. The vee blocks are L-shaped in their vertical cross-section, to allow for the support and vertical positioning of the outside cores.

Normal Force Application

The hydraulic pistons are activated by the pressurized hydraulic fluid in the common line. In the CMTL laboratory the line is pressurized from the confining pressure unit of the rock testing press. In field use, a hydraulic hand pump can be employed.

The activated pistons push the vee blocks, guided by the grooves, towards the centre of the assembly. The triangular loading arrangement and equal piston forces ensure that the three outside cores are loaded equally. Therefore, the applied normal forces along the contact lines (between the centre sliding core and the side cores) are also equal. Due to the applied lubrication, the radial movement of the vee blocks is virtually frictionless. Therefore the applied load is evenly distributed as a line load, along the entire length of the contact lines.

The evenly-distributed normal forces is directly proportional to the applied line pressure. The desired pressure was kept constant manually.

Measurement of Normal Displacement

The arrangement to measure normal displacement is shown in Fig. 3 and 4. A short pin is fastened to the top of each vee block. A very thin copper wire interlinks these pins. At one end the wire is fixed to one of these pins, while passing over the other two pins. The other end of the wire is fastened to the core of a LVDT. The LVDT is, in turn, securely clamped to the ring-frame.

The average normal displacement, be it dilation or contraction, can then be calculated for every test stage from the recorded movement of the LVDT core, by taking into consideration the geometry of the wire linkage.

The completed tests showed, however, that measurements obtained with this arrangement did not always provide an accurate reading of the normal displacement. The reason is quite clear. In order to ensure concentric shear force application, as mentioned before, the set of cores, as a whole, is allowed to move sideways. However, since the position of the LVDT is fixed (it being clamped to the ring-frame) any floating movement of the entire core set is added to the measured sum of the normal displacements occurring along the lines of contact.

If required, an accurate normal displacement measurement can be achieved by means of a simple modification. Small LVDT units can be placed within drill holes in the ring-frame, appropriately positioned at each groove, with the purpose of measuring the individual displacement of each vee block. These displacements would then be an accurate measure of the individual normal displacements that occur along the three lines of contact.

After analyzing the test results, the necessity for improved accuracy in normal displacement measurement became highly questionable. The magnitude of the normal displacement is not required for the analysis of strength and frictional properties. The existing system, as described, indicates whether the observed displacement is due to dilation or to contraction. This information is adequate to analyze the shear mechanism occurring during various phases of the test.

Shear Force Application

The test set-up in conjunction with the laboratory press, and with the portable field press is shown in Fig. 5 and 6, respectively. The axial load is supplied by the loading system of the rock testing press in the first instance. In the second case a hydraulic jack, activated by a hand pump, does so.

The shear force acting on the sliding centre core is measured and recorded by the strain-gauged ring load cell.

Measurement of Shear Displacement

The shear displacement is measured and recorded by a vertically-positioned LVDT. It is held in a vertical position by a horizontal arm which is connected to a cylindrical steel loading platen. This platen is located between the sliding centre core and the load cell.

The tip of the spring-loaded extension rod of LVDT core is rests on the ring-frame.

Data Recording

The outputs of the transducers (i.e., of the strain gauges of the load cell, of the LVDT for normal displacement and of the LVDT for shear displacement) are recorded by an XY_1Y_2 recorded on data sheets with convenient grids.

The shear force versus normal displacement relationship is recorded on XY_1 axes. Test data with respect to the shear force versus shear displacement are recorded on the XY_2 axes.

PREPARATION OF SPECIMEN SET

The test requires a set of four rock cores of same diameter. The test apparatus is designed for the preferred BX size cores (i.e., with a nominal diameter of 41.3 mm). However, specimen sets with a somewhat larger or smaller diameter are also acceptable.

Although the length of the core is not an essential dimension, the preferred length to diameter ratio for the outside cores is 2:1. The height of the sliding centre core is increased by the desired length of the shear displacement. Based on the results of the completed tests, the preferred shear displacement is in the order of 15 mm.

The parallel ends are cut perpendicular to the axis by a circular diamond saw. No special end preparation is necessary.

The core surface obtained by typical core-drilling procedures is acceptable for routine tests. However, the core surface is to be specially prepared if the test is aimed at simulated surface roughness investigation.

A smoother than core-drilled surface can be obtained, for example, by surface grinding in a machinist-lathe (Fig. 7). The simulated large asperities of sliding surfaces are prepared in the same way. The matching indents and protrusions of the simulated asperities are formed on the rotating cores by grinding wheels having the desired profile.

TEST PROCEDURES

One of the most important advantages of this test method is that each specimen set can be tested at several different levels of normal force. Each test, at the predetermined normal force level, is performed along a specific set of contact lines. The cores are rotated after each test. The predetermined test lines, together with the respective test number and core identification, are marked on the round labels attached to the top surface of the cores (Fig. 3 and 4).

The maximum number of tests that can be conducted on the same set of cores is governed by the diameter of the cores and by the extent of shear and crushing damage experienced along the lines of contact. The damage depends upon the normal force of the test run.

Experiments with BX size cores show that in the case of smooth core surfaces (core-drilled, ground, and lapped) up to nine tests can be performed on the same specimen set. The number of tests on cores with simulated large asperities must, however, be decreased to four, to avoid overlapping damage to the asperities.

There are two types of test procedures, namely: single-stage procedure and multi-stage procedure.

Single-Stage Procedure

The feature of the single-stage procedure is that along each set of contact lines only one shear test is performed. Various predetermined normal force is applied to each set of contact lines, which is kept constant for the test run.

Specimen sets with smooth surface finish can be tested either by single-stage or multi-stage procedure. However, to test specimen sets with simulated large asperities, the single-stage procedure must always be used.

The steps of the test procedure is explained by referring to Figure 8, which is the record of the shear test obtained for steel specimens with single large asperity, performed at P_n = 166.4 lbf (740 N) applied normal force. The steps of the test are as follows:

(a) Setting of contact lines - While the centre core rests on a spacer block and the outside cores are seated on the vee blocks, the cores are rotated until the respective markers with the number of the test run are matched up on all labels.

(b) Application of normal force - The hydraulic pistons are activated until the predetermined line pressure is reached. In this given case, this amounts to 2,000 psi (13.8 MPa) which results a normal force of 168.4 lbf (740 N) with the given piston area.

(c) Mounting of instruments - The LVDT transducers, as well as the strain-gauged ring load cell, are positioned and connected to the YX_1Y_2 recorder. The spacer block, supporting the centre core, is now removed.

(d) Setting of data recording procedures - The scales of the recording instrument are set, and the recording pens are moved and lowered into their recording positions. The cross-head of the press is lowered.

(e) Application of shear force - While the normal force is kept constant, the shear force is applied at a constant rate until the predetermined amount of shear displacement is reached. The latter is 0.45 in. (11.5 mm) in case of subject test run.

(f) Dismantling - First the shear force is released and the cross-head of the press raised. Then the transducers are dismantled next, the normal force is released, and finally the spacer block is placed underneath the centre core.

The shear force in Step (e) varies with the shear displacement. The relationship between the shear force, P_s, and shear displacement, δ_s, for that particular test condition is given by the XY_2 record of Figure 8.

Multi-Stage Procedure

The multi-stage procedure is used to test specimen sets with smooth surface finish, with the distinct advantage that an increased amount of test data can be obtained for each test run. The procedure is explained by referring to Figures 9 and 10.

The initial run of the multi-stage procedure follows Steps (a) to (f) of the single-stage procedure, that is, shear test is performed along the contact line for the entire shear test length. Figure 9 represents the test records of the initial run obtained for smooth steel specimens set tested at an applied normal force of P_n = 166.4 lbf (740 N). The total shear test length was 0.4 in. (10.2 mm).

The recorded relationship between the shear force, P_s and shear displacement, δ_s, is given by the XY_2 record in Figure 9(a). The relationship between the shear force and normal displacement, δ_n, is given by the XY_1 record in Figure 9(b).

To establish the strength and frictional properties of the joints the normal displacement is not a requirement. Figure 9(b), therefore, represents somewhat useful but unessential information. For example, Figure 9(b) indicates that along the contact lines contraction took place, due to the deformation of the minute asperities during the test.

In Figure 9(a) the shear force values are marked at two specific points of the recorded graph. These shear force values are: the peak value of P_{st} and shear force value for the first plateau on the graph P_y'. The significance of these values will be given during the course of data analysis.

Figure 10 represents the recorded results of the remaining steps, which involved a series of repeated shear tests along the contact lines already been tested by the initial run (Figure 9). Each repeated shear test is performed at various predetermined value of normal force. The continuation of the test steps of the multi-stage procedure is as follows:

(g) Re-application of the normal force - A repeat of Step (b);

in case of Figure 10, the re-applied normal force was 41.6 lbf (185 N).

(h) Re-mounting of all instruments - A repeat of Step (c).

(i) Re-setting of data recording procedures - A repeat of Step (d).

(j) Application of shear force - While the normal force is kept constant, a shear force is applied at a constant rate until the predetermined shear displacement, which, in the case of Figure 10, was 0.065 in, (1.7 mm), is reached.

(k) Increase of normal force - While the shear force is kept constant, the line pressure is swiftly increased to the next predetermined level, which in the case of Figure 10 produced the normal force of P_n = 83.2 lbf (370 N).

(l) Continuous application of shear force - While the normal force is kept constant at the new level, a shear force is continuously applied at a constant rate until an additional shear displacement of 0.065 in. (1.7 mm) is reached.

(m) Repeat Steps (k) and (l) for the additional predetermined normal force levels. In the case of Figure 10 these were:

P_n = 166.4 lbf (740 N)
P_n = 249.6 lbf (1110 N)
P_n = 332.8 lbf (1480 N)
P_n = 416.0 lbf (1850 N)

(n) Dismantling - A repeat of Step (f).

Figure 10(a) represents the relationship between the shear force, P_s, and shear displacement for the various levels of the multi-stage normal forces. The corresponding P_s, versus δ_n graph in Figure 10(b) indicates the increased amount of deformations of minute asperities along the contact line, as the normal force levels are increased.

In Figure 10(a) the average shear force value, for the multi-stage shear test at P_n = 166.4 lbf (740 N), is P_y'' = 32.9 lbf (146 N). The significance of this value will be explained during the course of data analysis.

TYPICAL TEST RESULTS

From the test results it can be concluded that the coefficient of friction is not a simple material property. It is composed of several components. The coefficient of friction between sliding surfaces is the results of the various combination of these components.

The relative contribution of the components depends on:

(a) the condition of the sliding interface, which is affected by the history of sliding;

(b) the topography of the irregularities of the sliding interface and the degree of their interlocking;

(c) the environment such as the prevailing stress level along the sliding interface and the confinement condition of the sliding solids;

(d) the strength and deformation properties of the sliding solids.

Due to the consistent and reliable data, obtained by the confined shear test method, it is possible to define the significant components of the coefficient of friction either through direct measurements or through logical deductions.

The test method and analytical procedures had been developed with the ultimate objective of providing sufficiently accurate data for use in underground rock mechanics investigations and in design and ground control calculations. Consequently, the test data were studied and analysed with the above practical use in mind. The refined theoretical analysis of the test data were not pursued this time.

To establish the components of the coefficient of friction and their combined effects under various conditions it is essential to remember to the mathematical meaning of it. That is, the coefficient of friction is nothing else but a dimensionless number, i.e. the ratio between the momentary shear and normal forces. Therefore, for any applied normal force kept constant during the test run, the variation in the coefficient of friction reflects the variation in the shear force value which is required to initiate or maintain shearing.

Three types of materials, with various sliding contacts, were tested, namely: steel, teflon and various rock materials.

Specimens of steel material were tested because of the essentially ideal elastic and elasto-plastic deformation properties of the steels. The teflon material was tested for two reasons. Firstly, to obtain frictional data on material with ideally plastic deformation properties. The second reason was to verify the testing technique for a material with extremely low value of coefficient of friction, which is occasionally even referred to as "frictionless" material. The main objective of the laboratory test program is, however, to establish the joint strength properties of the various rock types. So far, the following rock types were tested: diabase, limestone, sandstone, granite and INCO ore.

Typical test results obtained for steel, teflon and granite specimen sets with smooth sliding contacts are given in Figure 11. The recorded shear force versus shear displacement data shown, include both, the initial and the multi-stage test graphs.

Although the following brief comparative discussion are equally applicable to the data of multi-stage steps, only the graphs of the initial runs will be compared here. These presented data are comparable because: the specimen size was similar in all the cases, the smooth sliding contact prevailed for all materials, the same normal force magnitude of 83.2 lbf (370 N) was applied for each test. Consequently, the comparison needs to consider only one variable, which is the material properties. More specifically, because at the normal load level of 83.2 lbf (370 N) the minute asperities along the sliding contacts were only deformed during the tests, without crushing or other damage, the only variable in the comparison is the deformation property of the material. Any difference between the data presented in Figures 11(a), 11(b) and 11(c) is a reflection of the deformational respond of the material, as it is controlled by its deformation property.

In the case of steel the P_s versus δ_s graph, in Figure 11(a), shows an initial rise in shear force. This peak force is accompanied by a very small shear displacement. As the shear displacement increases the shear force decreases. The rate of decrease in shear force, from an initial higher rate, also decreases with increased displacement, with the tendency of reaching a plateau. After test the specimens showed only slight markings along the sliding contact. This indicates mainly elastic deformation of the minute asperities.

A somewhat similar picture is shown for the teflon material in

Figure 11(b). The shear force versus shear displacement graph has an initial peak again but at a lower value than for the steel. The change in the rate of the shear force decrease is much faster for the teflon. The local variation of shear force is much smaller than for the steel; it is practically negligible. It is so, despite the fact that by touching the specimens a similar surface roughness can be observed for both types of materials. Actually, the specimen of the two materials were prepared, by using the same cutting tool and procedures during the lathe turning. However, following the test the sliding contacts on the teflon specimens showed permanent, i.e. plastic deformation, of the minute asperities.

An entire different picture can be drawn for the deformational behaviour of the granite, based on the data presented in Figure 11(c). The most striking characteristic of the P_s versus δ_s graphs is the harmonic variation of the shear force. This is caused by the interacting thread-like asperities, produced by the lathe grinding specimen preparation. Note that the harmonic variation of shear force decreases in amplitude with increased displacement, but it remains the same in frequency. This means that in case of granite for the indicated values of normal forces the thread-like asperities survived the shearing. Only slight alteration occurred to them, as expressed by the decrease in amplitude. The magnitude of the shear force, consequently, the coefficient of friction for the granite is much higher than for the steel and especially for the teflon.

Another characteristical difference of the shear force graph for granite is that, unlike the steel and teflon graphs, it has no initial peak value. This difference is attributable to the different deformational behaviour of the granite.

Due to the elastic property of the teflon and especially of the steel, the interlocked minute asperities, prior to any shear displacement, can be deformed elastically. A shear displacement will be initiated when the yield load for the contact areas of the minute asperities is reached.

The granite is also considered as elastic material, although to a lesser degree than the steel. The elastic behaviour of rock substances is quite evident from other laboratory tests. However, the interlocked minute asperities do not behave elastically. The size of the minute asperities is in the order of rock particle size. The rock particles unable to sustain prolonged deformation caused by the concentrated stresses acting on the particle contacts. Instead, they break-off. Consequently, the initial peak shear force value cannot develop.

The typical test results obtained for steel and granite specimen sets with large single asperity sliding contacts are compared in Fig. 12, which was produced by superimposing the two test graphs. The dimensions of the simulated large single asperity and the directions of shearing are shown in Fig. 13. The recorded graph in Fig. 12 were obtained by the tests performed in the shear direction Case A.

The equivalent characteristical points of the two tests graphs are marked by the same numerals, circled by single and double circles for the steel and granite materials, respectively. The remarkable similarities of the two graphs is an affirmation of the testing technique. It marks the accuracy and reliability of the test data. The dissimilarities in the graphs indicate definable differences in the shearing meachanism and the associated deformation of the two materials. For example, in case of the elastic steel material the recorded graph section marked by point 4 suggests a continuous and steady deformation, while, for the brittle rock material, this graph section is obscured or even absent.

DATA ANALYSIS

CALCULATION OF STRESS ALONG CONTACT LINES

Following the contact line setting, the second step of the confined shear test is the application of the normal force P_n. The deformation and stress along the lines of contact, due to an applied normal force, can be calculated by using the solution given by Timoshenko and Goodier [5].

The general solution of pressure between two bodies in contact is being applied to the special case of contact between two cylinders with parallel axis. The surface of contact in this case is a narrow rectangle. The distribution of pressure, σ_n, along the width of the contact surface is represented by a semi-ellipse.

If b is half of the width of the contact surface, and P_n' is the load per unit length of the contact surface, from the semi-elliptic pressure distribution, one will obtain:

$$P_n' = 0.5 \pi b \sigma_n$$

from which

$$\sigma_n = \frac{2 P_n'}{\pi b} \qquad \text{Eq. 5}$$

The investigation of local deformation for the quantity of b gives the following expression:

$$b = \left[\frac{4 \; P_n' \; (k_1 + k_2) \; R_1 \; R_2}{R_1 + R_2} \right]^{1/2} \qquad \text{Eq. 6}$$

where, R_1 and R_2 are the radii of the cylinders, and k_1 and k_2 are constants defined by the following equations:

$$k_1 = \frac{1 - \nu_1^2}{\pi \; E_2}$$

$$\text{Eq. 7}$$

$$k_2 = \frac{1 - \nu_2^2}{\pi \; E_2}$$

where, ν_1 and ν_2 are the Poisson's ratios and E_1 and E_2 are the elastic modulii of the materials of the cylinders in contact.

Since both cylinders are of the same material and the two radii are equal, Eq 6 is greatly simplified. The value of the Poisson's ratio for the tested steel is $\nu = 0.269$, therefore

$$k_1 + k_2 = 2 \left[\frac{1 - 0.269^2}{\pi \; E} \right] = \frac{0.591}{E}$$

then,

$$b = \left[\frac{4 \; P_n' \; (0.591/E) \; R^2}{2R} \right]^{1/2}$$

or

$$b = 1.087 \left[\frac{P_n' \; R}{E} \right]^{1/2} \qquad \text{Eq. (6a)}$$

The stress along the contact line, due to the applied normal load, can then be calculated by Eq 5. This stress is an average value. At the tips of the minute asperities the stresses are much higher than the average. This is, however, not a concern of the analysis, which is aimed at a solution for practical use. Similarly, the actual deformation is much more complex than the average distribution given by Eq 6. Again, from a practical point of view, it does not matter. Whatever the actual stresses or the deformations of the minute asperities are, they define the initial condition of the particular shear test.

The change from this initial condition is entirely due to the shear force which is required to initiate and maintain shear displacement. The magnitude of the required shear force depends upon, beside the normal force, the type of tested material, the roughness of the sliding contact, the degree of engagement of the interlocking roughnesses, and the condition of the interlocking roughnesses. The change in the shear force is recorded by the shear force versus shear displacement graph of the shear test.

SHEAR MECHANISM ALONG SMOOTH CONTACT LINES

Steel Specimens

Figure 14(a) is a typical graph obtained by single-stage shear test procedure on steel specimens with smooth sliding contact. With respect to the test, represented by the graph, all the above mentioned variables are constant, except the condition of the interlocking roughnesses.

Shear displacement will take place only if the interlocked minute asperities were disengaged. This disengagement involves both asperity overriding and asperity deformation. The ruggedness of the graph in Figure 14(a) is the indication of asperity overriding. However, this overriding or dilation mechanism in case of smooth-walled steal specimens has only negligible, "background-noise" type, effect. The overall shape of the graph, which constitutes the essential test data, is unaffected by the ruggedness.

Therefore, the P_s versus δ_s graph in Figure 14(a) can be interpreted as minute asperity deformation versus δ_s graph, where the shear force value at a specific shear displacement distance is a measure of the extent of the minute asperity deformation which had been occured while that specific shear displacement took place. Those shear force values which are essential for the analysis, are labelled in Figure 14(a). Their definition are:

P_{st} = peak, or static shear force; the shear force which is required to initiate shear displacement; the shear force which is associated with the elastic deformation of the asperities.

P_s = slidings shear force; the shear force which is required to maintain shear displacement; the shear force which varies in value from P_{st} to P_u.

P_u = ultimate shear force; the shear force required to maintain continuous sliding in case of perfectly smooth sliding contacts; the shear force which is associated with the plastic deformation of the asperities.

P_y' = yielding shear force; the sliding shear force value at the first plateau of the graph; the shear force which is associated with the transition point between the elasto-plastic and the plastic deformation of the asperities.

P_d = deformation shear force; the shear force which is required to deform the asperities completely to result perfectly smooth sliding contacts; $P_d = P_{st} - P_u$.

P_{id} = initial deformation shear force; the shear force which is required to initiate plastic deformation of the asperities, therefore, to cause permanent deformation; $P_{id} = P_{st} - P_y'$.

P_{cd} = continuous deformation shear force; the shear force which is required in addition to the initial deformation shear force to deform the asperities completely to result perfectly smooth sliding contacts; $P_{cd} = P_d - P_{id}$ or $P_{id} = P_y' - P_u$.

Figure 14(a) can be compared with a complete stress-strain curve, such as shown in Figure 14(b), which can be obtained by stiff testing techniques. The rising leg of a typical complete stress-strain curve begins with a linear portion which ends at the proportional limit. The linear portion is followed by a slightly curved section, which ends at the elastic limit. Specimens stressed up to this limit, upon a load release, regain their original dimensions. The increased curvature beyond the elastic limit indicates permanent deformation. A release of load would result in an essentially linear stress-strain curve, parallel to the first section. The offset of this linear stress-strain curve is the permanent deformation.

The peak value is the upper yield stress. From this maximum value the stress decreases rapidly to a lower yield stress value, characterized by a small plateau in the post-failure section of the stress-strain curve. As the material continuously fails the stress-strain curve gradually decreases to the residual stress value which is defined by the second and larger plateau. When the load is released the stress diminishes as indicated by the linear end section of the stress-strain curve.

Admittedly, it is somewhat difficult to recognize in Figure 14(a) those data points which are comparable to the previously discussed characteristical points of a typical complete stress-strain curve. The main problem behind the interpretation difficulties is the scale of Figure 14(a).

This point is proven by Figure 15 where the results of two identical test runs performed along two sets of immediately adjacent contact lines, are shown. The shear displacement scale for the first test, Figure 15(a), was the same as for the test in Figure 14(a). The result for the rising leg is a straight shear force versus shear displacement graph, apparently without any shear displacement. However, when for the second test the shear displacement scale of the recorded graph was enlarged by five-fold, as shown in Figure 15(b), the shear displacement due to the elastic deformation of the interlocking asperities became evident. Beside the peak or static shear force, P_{st}, which is comparable to the upper yield stress, it is also possible now to identify the shear force values which are comparable to the proportional and the elastic limits.

Having this information, for the test data presented in Figure 14(a) an interpretation, analogous to the analysis of a complete stress-strain curve (Figure 14(b)), can be given. The initial conditions (interlocking between asperities, deformation and stress along contact lines) to the test data in Figure 14(a) were set by the applied normal force of P_n = 166.4 lbf (740 N). The initial conditions have effect on shear test results, consequently, they are interdependent.

The interlocked minute asperities, due to the shear force, will be elastically deformed. Passing the shear force magnitude equivalent to the proportional limit and then the elastic limit stress values of the interlocking minute asperities of the steel material, the shear force reaches a peak value of P_{st}. This static shear force is sufficiently high to deform and therefore disengage the interlocking minute asperities, or with other words to initiate shear displacement.

Following the peak, the shear force required to maintain shear displacement decreases drastically. Speaking in stress-strain terms, beyond the upper yield stress the failed minute asperities will continue to fail in the form of further deformation. The shear force decreases first steeply, and then more gradually. This is a reflection of the change in the deformation characteristics of the minute asperities with the progression of shear displacement.

Around the peak shear force the dominating deformation characteristic minute asperities of the steel is elastic. This is clearly demonstrated by the steep initial slopes of the descending graph. However, the deformation behaviour of the failing steel minute asperities becomes elasto-plastic which is indicated by a gradual decrease in the shear force.

With further displacement, the deformation of minute asperities increasingly continue. The deformation behaviour of the minute asperities ultimately changes to plastic. The transition from elasto-plastic to plastic behaviour is indicated by a plateau in the shear force versus shear displacement graph. The sliding shear force value at this plateau is yielding shear force P_y'. This corresponds to the lower yield stress of a complete stress-strain curve (Figure 14(b)).

Beyond the transition point a slowly progressing plastic deformation can be maintained by a correspondingly decreasing shear force. The ultimate shear force which is required to maintain continuous sliding, P_u, is the minimum shear force value of the shear force versus shear displacement graph (Figure 14(a)). The corresponding stress level is a complete stress-strain curve is the residual stress (Figure 14(b)).

Note that the deformation corresponds to the ultimate shear force P_u can be reached only at a considerably longer shear displacement path than the one used in the test case of Figure 14(a). As a matter of fact, the value of P_u given in Figure 14(a), had been obtained by the test series with large single asperity. The required long shear displacement path, for smooth sliding contacts, would have resulted an impractical specimen length.

After completion the shear test for a predetermined displacement length, as the shear load is slowly released, a straight descending line is obtained. Actually, in an enlarged shear displacement scale, it would show a deviation from the horizontal, similar to the rising leg of the graph in Figure 15(b), but in a negative sense. The descending leg in Figure 14(a) signifies the elastic relaxation of the deformed minute asperities.

Without providing sound analytical reasoning, the attention is drawn to the "textbook quality" stress-strain curve for steels, which can be obtained from the recorded shear force versus shear displacement graph, as shown in Figure 14(c). It represents the average values of Figure 14(a). Accordingly, the interlocked minute asperities, due to the applied normal force P_n and shear force P_{st}, are under such a state of stresses that the yield strength of the involved minute asperities is proportional to P_{id}. The remarkable analogy between the two graphs need only be noted, without further considerations in the analytical process.

In Figure 14(a) the shear force components were identified according to their relationship to the deformation of the minute asperities. The coefficient of friction is a dimensionless number. It expresses the ratio between the shear and normal forces. Therefore, the components of the coefficient of friction are being identified in the same way as the corresponding shear forces. The coefficient of friction components are to be referred as follows:

μ_{st} = static coefficient of friction; it prevails at the instant of shear displacement initiation.

μ_s = sliding coefficient of friction; it is related to the conditions of the continuously maintained shear displacement; its value falls between μ_{st} and μ_u.

μ_u = ultimate coefficient of friction; it corresponds to the continuously maintained shear displacement in case of perfectly smooth sliding contacts.

μ_y - yielding coefficient of friction; a specific value of the sliding coefficient of friction μ_s, related to the conditions required to change the deformation behaviour of the minute asperities from elasto-plastic to plastic.

μ_d = coefficient of friction of deformation; it is related to the total deformation of the minute asperities occurs between the initial state and the state of completely smooth sliding contacts; $\mu_d = \mu_{st} - \mu_u$.

μ_{id} = coefficient of friction of initial deformation; it is related to the elasto-plastic deformation stage of the minute asperities; $\mu_{id} = \mu_{st} - \mu_y$.

μ_{cd} - coefficient of friction of continuous deformation; it is related to the plastic deformation stage of the minute asperities; $\mu_{cd} = \mu_d - \mu_{id}$ or $\mu_{cd} = \mu_y - \mu_u$.

Typical test data records obtained by testing steel specimens with smooth sliding contacts are given in Figures 9 and 10. Figure 9 is the recorded data of the initial test run, performed at the normal load of 166.4 lbf (740 N). In the process of analysis two data points are used, namely the static shear force P_{st}, and the yielding shear force P_y'.

Figure 10 is the recorded data, for the same sliding contact, as obtained by the multi-stage procedure. The portions of the graph are identified by the normal forces at which they were obtained. For the immediate discussion the graph portion for the normal force of P_n = 166.4 lbf (740 N) will only be used. The average shear force of this portion is P_y", which is designated as the multi-stage yielding shear force.

The two graphs (Figures 9 and 10) which were obtained by two different testing modes, but along the same contact lines, are united in Figure 16, by repeated photocopy method. The study of the combined graph reveals several important information.

First of all, it shows the quality and reliability of the data which can be obtained by the testing technique. Although the graphs in Figure 16 are the results of two separate tests, they are actually the components of the same data set. This is convincingly expressed by the combined graph. The unifying elements of the two tests are: the applied normal force of P_n = 166.4 lbf (740 N) and the common sliding contact lines.

Due to the negligible magnitude of normal displacements of both tests, the two shear force versus normal displacement graphs in Figure 16(b) are completely and undistinguishably superimposed.

The most important information is given in Figure 16(a) by the practically identical values of yielding shear forces of P_y' and P_y". In order to properly emphasize the significance of this test result, the definition of these yielding shear forces, as well as, the modus operandi related to them, must be reiterated.

Yielding shear force P_y' is obtained by initial test run. It signifies the transition point between the elasto-plastic and the plastic deformation of the minute asperities along the tested sliding contact lines of the smooth walled steel specimens. The deformation of the minute asperities is caused by the prevailing stresses, which are due to the combined effect of P_n and P_s forces.

The applied normal force P_n is constant for the test run. However, the shear force P_s varies according to the requirement to initiate first, and then, to maintain the shear displacement. This requirement is controlled by the momentary deformation of the minute asperities. Therefore the change in shear force, required to maintain shear displacement, is related to the change in the deformation status of the asperities. Accordingly, the reason for the drop of shear force, vallue from P_{st} to P_y' is the initial deformation of the minute asperities. The final stage of minute asperity deformation of the initial test run, is a state of deformation which, at the applied normal force of P_n = 166.4 lbf (740 N), requires a shear force of P_s to maintain continuous shear displacement.

The multi-stage procedure is performed along the same sliding contacts, which had already been deformed by the initial test run. The value of P_s, which was required to maintain continuous shear displacement, can be regarded as a measure of the minute asperity deformation, for the maximum shear displacement of the initial test run conducted at an applied normal force of P_n = 166.4 lbf (740 N). Consequently, it is expected that the shear force value for the test stage of the multi-stage procedure performed at the applied normal force of P_n = 166.4 lbf (740 N), should be the same as P_s.

Indeed, as shown in Figure 16(a), the values for the shear forces of P_s and P_y'' are virtually identical. This evidence is the factual affirmation of one important result achieved by the testing technique, namely, that some of the components of the coefficient of friction are related to deformation.

As can be seen in Figure 16(a), the average values of P_y'' and P_s are, from practical point of view, equal, but the shape of the related graph sections are different. The graph section defined by P_s is flat, with small shear force variations. This relatively smooth graph section is the reflection of the continuous shear displacement along the contact lines with minute asperities had been deformed during the preceding shear displacement. The graph section defined by P_y'' displays a larger variation of shear forces. Although this shear displacement is a repeated one, it still can be regarded as an initial displacement, because it always follows the step of normal load application. The graph section of P_y'' shows a slight peak value. Like in the case of the initial test run, it corresponds to an initial deformation of the already deformed minute asperities, i.e. some reshaping of the deformed asperities takes place. However, in comparison with the peak value of P_{st} of the initial test run, this peak value can be ignored completely.

The shear force values obtained by multi-stage procedure, at various applied normal forces, are defined as:

> P_y'' = multi-stage yielding shear force; the average value of the shear forces which are required to initiate and then to maintain a repeated shear displacement for a predetermined length of δ_y.

With respect to the relationship between the asperity deformation and shear force, several important conclusions can be made by analyzing the shape of the test graphs. The peak value in shear force is caused by the interlocked undeformed minute asperities of the sliding contact lines. Due to the stresses, from the normal and shear forces, these interlocking asperities deform. Permanent deformation of the interlocking minute asperities is reached at a specific magnitude pair of P_n and P_y' forces and at a specific shear displacement value of δ'. Once this shear displacement had been reached, and consequently the yielding shear force is arrived at, the shear force required to initiate a repeated shear displacement is without peak value.

The initial deformation, associated with the peak value of shear force P_{st} is elastic. Consequently, peak shear force value can develop only for materials with truly elastic properties, such as steel. This fact had been convincingly proved by numerous tests involving various materials.

Although the yielding shear forces of P_y' and P_y'' are somewhat different, from practical point of view they are taken as same. One of the reasons for it, is the negligible difference in their values. For example, in the test case of Figure 19(a) the difference is $(33.7 - 32.9)/33.7 = 2.4\%$.

The second reason, of practical nature, is related to the testing procedure. Each initial test run provides one value of yielding shear force of P_y' which is applicable for the normal load of the test run. However, during the multi-stage phase of the test procedure a yielding shear force value of P_y'' is obtained for each normal load application. Consequently, the number of P_y'' values, that can be obtained, equals to the product of the number of the tested contact lines and the number of the normal load applications.

The third reason, which is practical again, is that the determination of the P_y'' shear force values is always easy. However, to determine the yielding shear force value of P_y', as it can be defined for the elastic materials, in the case of rock materials is not possible.

Rock Specimens

The rock material is generally regarded as elastic material, however, it behaves considerably different ways than a truly elastic material such as the steel. It does behave differently especially with respect to the deformation of the minute asperities.

The interlocking minute asperities of the steel material are capable to sustain the concentrated stresses up to the point of the yield strength. For steel, the deformation of the asperities is essentially elastic up to the yield strength, with only a small portion of permanent deformation. The peak shear force is interpreted as the expression of this mechanism of minute asperity deformation.

In case of rock material, the particles of the interlocking minute asperities are unable to sustain the deformation caused by the concentrated stresses. Instead, the particles break-off without an indication of elastic deformation and without showing any increase in shear force. Consequently, the recorded test graphs of rock materials are without peak shear force values, even for the initial test runs. There are some variations in the relative ruggedness or smoothness of the test graphs. Those variations are attributed to the specific characters of the sliding contact lines of the various rock types, represented by the tested specimens.

Granite

Typical recorded graphs, of the initial and multi-stage test runs performed on granite specimens with smooth sliding contact lines, are shown in Figure 17. The variation of shear forces follows a systematic pattern. It is due to the thread-like minute asperities of surface finish of the specimens produced by the lathe grinding operation used for reducing the 4.75 cm diameter of the core sticks to the specimen's diameter of 4.1 cm.

The systematic variations of shear forces are within the bands defined by their low and high values. As a general rule the width of the band increases with the increased normal forces. However, some test cases were exceptions from this general rule.

The yielding shear force values of P_y' and P_y'' are defined (Figure 17) as the mid-values of the bands. The difference between the two yielding shear force values is negligible, similarly to the steel. For example in the test case of Figure 17 the difference is $(15.2 - 14.8)/14.8 = 2.7\%$.

Sandstone

In contrast, the typical recorded graphs of Figure 18 obtained for the initial and multi-stage test runs on sandstone specimens, show essentially constant shear forces, with hardly any change in their values for the entire shear displacement length. The surface finish was obtained by diamond drill coring.

The fine and uniform sand grains along the sliding contact lines form the interlocking minute asperities. These sand grains can be sheared-off by a practically constant value of shear force. Some reduction in shear force can be seen for the initial test run, due to the wearing of sliding contact lines caused by the longer shear displacement.

Indiana Limestone

Typical recorded graphs obtained for Indiana limestone specimens with smooth sliding contact lines are shown in Figure 19. The surface finish of the specimens was obtained again by diamond drill coring. Although the smoothness along the sliding contact lines was similar to that of the sandstone specimens the graphs of the limestone are more rugged. It is caused probably by the variation in the size of grains along the sliding contact lines which require variable magnitude of force to shear-off. Heterogeneity in strength of various grain materials can also be a contributing factor.

Diabase

Typical test results for diabase specimens are presented in Figure 20. The specimens were cut from diamond drill core sticks, without further surface preparation.

The graphs obtained for the lower values of normal forces are smooth. The very uniform fine-grained particles of the diabase provides explanation for the small variation of shear forces, displayed by these graphs.

With the increasing normal forces the graphs become increasingly rougher. An extremely wide range of shear force variation is shown by the graph obtained for the multi-stage test step conducted at an applied normal force of 416.0 lbf (1850 N). The phenomenon of sudden reduction and regain of shear force is interpreted as "stick and slip" shear mechanism, which found to be characteristical to some rock types at normal stress levels in excess of 120 MPa.

INCO Ore

Figure 21 represents typical test results obtained for INCO ore material. The graphs are very similar to those of the diabase. Some differences can be noticed for the mid-range normal forces. These rougher graphs of the INCO ore are probably resulted by the material variation of the grains along the contact lines. The sudden wide-range changes of shear force at the 416.0 lbf normal force test stage is typical for this material.

SHEAR MECHANISM ALONG SLIDING CONTACTS WITH SIMULATED ASPERITY

Steel Specimens

The dimensions of the simulated single large asperity are shown in Figure 13(a). With respect to the shape of the interlocking asperity, two shear directions were tested. In Case A, the shear direction coincided with the longer and shallower slope. While in Case B, the direction of shear was reversed.

From the dimension of the asperity, shown in Figure 13(a), the slope angles were: $\alpha_A = 23.7°$ and $\alpha_B = 43.7°$.

Typical test data are presented in Figure 22. Figures 22(a) and 22(b) are the recorded graphs of the shear tests performed at an applied normal force of $P_n = 83.2$ lbf (370 N) in the shear direction of Case A and of Case B, respectively. In Figure 22(c) the two graphs are superimposed by repeated photocopy technique.

The comparison of the graphs given in Figure 22 reveals several similarities. The overall shape of the two graphs is similar. This is a strong affirmation of the testing principle and method.

Due to the different geometry of the simulated asperity with respect to the two shearing directions, there are however several differences in the two test graphs.

One obvious difference is the shear displacement of the total disengagement of the asperity, which is controlled by the vertical dimensions of the asperity, i.e., as shown in Figure 13(a), δ_A = 0.24 inch and δ_B = 0.11 inch.

Other equally obvious difference is the magnitude of shear forces. To initiate and then to maintain shear displacement, the required shear force in Case B is about double than that for Case A. One reason for it, is the slope angle of the shear, i.e., $\alpha_B = 43.7°$ versus $\alpha_A = 23.7°$. The other reason is the different deformation mechanism of the interlocking asperities in the two shear directions, involving both the deformation of the simulated large asperity and of the minute asperities along the lines of contacts.

The different mechanism is indicated by the markedly different rising legs of the two graphs. For Case B, it is almost linear with a slight deviation prior to the peak shear force value. It is a typical elastic load-deformation curve. This indicates that in Case B the initial phase of shearing mechanism is characterized by the elastic deformation of the large asperity. Because of the large asperity slope angle ($\alpha_B = 43.7°$), shear displacement along the sloping contact during the initial phase of shear force appliccation is restrained.

In contrast, the rising leg for Case A (Figure 22(a)) shows a deformation response which is resulted from the combination of the elastic deformation of the large asperity itself and of the minute asperities on the sloping surface of it. In the Case A, the asperity slope angle is low enough ($\alpha_A = 23.7°$) to allow some small shear displacement along the sloping surface during the initial phase of shear force application. Consequently, the associated deformations of the surface minute asperities and of the large asperity are superimposed. This combined mechanism of elastic deformations is quite obvious in Figure 22(c), where the magnitude of the shear displacements related to the rising legs can be easily compared.

The analysis of test results is based on the assumption that applied normal force and the shear force are uniformly distributed along the contact lines. Based on this assumption, it is possible to substitute the terms of normal and shear forces by the equivalent terms of normal and shear stresses.

This assumption, strictly speaking, can only be applied in the case of perfectly smooth contact lines. It must be recognized that at the contacts of the minute asperities, especially at their tips, high stress concentration occurs. Consequently, the actual stress levels associated with the deformation and yield of the minute asperities of the steel specimen are much higher than the stress levels of the analysis.

With respect to frictional properties investigations, however, the knowledge about the actual concentrated stress magnitude is not important. The coefficient of friction is a ratio between the shear and normal stresses. The result of the analysis, therefore, is the same, whether it is based on the calculated uniformly distributed or on the actual stresses between the interlocking asperities.

Furthermore, the practical application of the frictional properties in mine design always considers uniformly distributed stresses, i.e. ground stresses. Consequently, in analysing the test results, it is justifiable to use uniformly distributed stresses along the contact lines even in the case of large asperity. It must, however, clearly understand that the concentrated stress levels at the three tips of the asperity of the centre specimen, is much higher than the calculated uniformly distributed contact line stresses.

There are theoretical solutions to estimate the magnitude of the concentrated stresses between the interlocking asperities [6]. These calculations, however, failed to contribute to the results of the analyses.

For the test series with large asperity, the contacts between the three stationary outside specimen and the moving centre specimen are the three points of the protruding asperity profiled on the centre specimen. As the shear force is applied, these three points move upwards on the sloping faces of the indentated matching asperities, profiled on the outside specimens.

Specimens made out of materials with infinitely high elastic modulus and strength i.e. rigid body, would provide one extreme mode of disengagement of the interlocking asperity. The shear displacement of the total disengagement would be equal to the dimension of the asperity in the direction of shearing. At the same time, each outside specimen would move sideways, i.e. dilate, by a distance equal to the protruction of the asperity which in the case of the test series was 0.105 inch (Figure 13(a)).

The opposing extreme mode of disengagement would be provided by a specimen set with extremely low deformation and strength properties. The disengagement, in this case, would be characterized by a complete destruction of the protruding asperity at the contact points, either by deformation or by shearing. No dilation would occur.

The mode of disengagement of a real material is between these two extremes. The steel is an elastic material, up to the yield point. Beyond the yield point the behaviour of steel is elasto-plastic, which becomes more and more plastic under the continuous loading.

During the tests, dilations of the outside specimens had been observed. Based on previous test experience, however, the measurement of dilation had been omitted.

The three contact points of the protruding asperity are the subject of a very high degree of stress concentrations. The concentrated stresses, far beyond of yield stress, are causing in the asperity material simultaneous elastic and plastic deformations. For the instant of disengagement, the sum of these deformations in shear direction equals to a shear displacement value which is obtained by substracting the asperity dimension in shear direction from the shear displacement of total disengagement.

At the moment of test completion, when the stresses are released, the elastic portion of the deformation relaxes. Only the effects of the permanent plastic deformation on the asperity can be observed and measured on the specimen.

It had been observed that for the tests conducted at lower normal forces permanent plastic deformation generally occurred only on the protruding centre asperity. For the test at higher normal forces, however, permanent deformations can be observed on the indentated asperities of the outside specimens as well.

Further analytical details of the involved mechanisms are presented in Figure 23 for the Case B test run of Figure 22(b). Points of the recorded graph, with significant changes, were identified by numbers from 1 to 6. Each point is defined by its shear force and shear displacement coordinates, bearing the identification number of the point.

The relative positions of the matching asperity, for each point, are given in the scale of the recorded shear displacement. These drawings were prepared only to demonstrate the sliding on a sloping surface by assuming completely rigid asperity material, i.e. omitting the asperity deformations.

Point 1 represents the initial condition. The normal force of P_n = 83.2 lbf (370 N) is applied, causing the matching asperity elements to be pressed together. At the points of the asperity tip contacts with the sloping seat, concentration of stresses will take place.

As the shear force is applied, the magnitude of the concentrated stresses increases. Due to these stresses, the asperity tip contacts are elastically deformed, until the yield strength of the tip contact is reached. This condition is arrived at Point 2. The shear displacement value of δ_2 is the elastic deformation of the asperity tip contact. Actual shear displacement along the sloping seat does not occur at that stage.

Due to the yield of the over-stressed material of the contact tips a rearrangement of stresses takes place which is accompanied by some stress release. The stress release is elastic, therefore, the corresponding portion of graph is a mirror image of the immediate pre-yield portion. Point 3 represents this condition. The differential shear displacement of $\delta_3 - \delta_2$ represents a true displacement along the sloping seat.

The continuously maintained shear displacement causes the asperity tip contacts to slide along the contact lines on the sloping seats. While still further deformation of asperity tip contacts take place, the sliding mechanism now is mainly governed by the deformation of the minute asperities along the contact lines on the sloping seats. The relevant section of the graph is in close resemblance with the graph obtained for specimens with smooth sliding contact.

Point 4 identifies the plateau which corresponds to the yielding shear force of P_y' of the smooth sliding contact test series. The deformation behaviour of the minute asperities between Points 3 and 4 is elasto-plastic. Analogue with the smooth sliding contact, the plateau at Point 4 indicates the transition between elasto-plastic and plastic behaviour of the minute asperities.

Beyond the transition point, i.e. between Points 4 and 5 the deformation behaviour is plastic. At the beginning the rate of the deformation is low. However, as the sliding asperity tip contact approaches the edge of the sloping seat the concentration level of stresses within the seat edge material reaches the yield value. The result is an increased rate of shear force reduction, which is in turn, due to the latest recent deformations. This stage corresponds to Point 5.

The last stage of the test is represented by Point 6. It corresponds to the instant of the total disengagement. At this stage, the only contact between the stationary outside and the sliding centre specimens, are the perfectly smooth points of the asperity tips and the sloping seat edge, as they were deformed and polished while the shear displacement, under the prevailing yield stress level, was completed.

Point 6 identifies a limiting asperity deformation condition. It is produced by the limiting stress, i.e. yield stress. The contact area of sliding was at the minimum value, i.e. contact point, therefore, the shear force measurement was free from the influence of surface roughness. Furthermore, this surface roughness had been minimized by the shear deformation, i.e. perfectly smooth, polished contacts.

The sliding mechanisms and the variation of shear forces for the Case A test run, of Figure 22(a), follow the same general pattern. The analytical explanation and reasonings, made for Case B, are equally applicable.

The differences between the two cases were caused by the different angles of sloping seats. The slope angle value of Case B drops from $\alpha_B = 43.7°$ to $\alpha_A = 23.7°$. Because of this smaller sliding slope angle, the influence of the deformation of minute asperities, along the sliding contact lines on the sloping surfaces, was somewhat larger than in Case B.

From the superimposed graphs of Figure 22(c) it can be seen that the elastic shear displacement of the peak shear force in Case A is the sum of the elastic deformation of two elements. Caused by the shear force application, both the large asperity itself and the minute asperities on the sloping faces are simultaneously deformed. Having much smaller dimensions, the yield load of the interlocking minute asperities is reached first, which is given by the shear force value at the kink in the rising leg of the graph. The elastic deformation of the large asperity contact tip is continued then until the yield load of the contact tip itself is reached. The influence of minute asperities is merely an observation fact, without any effect on the analyses of test results.

Rock Specimens

Sliding contacts with simulated asperity were tested for three types of rock materials, namely: Indiana limestone, diabase and granite. Typical test results obtained for granite are shown in Figure 24.

For the purpose of comparison the recorded test graphs obtained in shear directions Case A and Case B are superimposed by using repeated photocopy technique. The superimposed graphs of Figure 24(a) were resulted by the single-stage procedure first test runs. The graphs in Figure 24(b) were obtained by the repeated test runs conducted along the same contact lines.

The remarkable similarities of the graphs, even for the repeated test runs, is an affirmation of the testing technique, with respect to the reliability and accuracy of the test data. The dissimilarities in the graphs indicate definable differences in the shearing mechanism and the associated deformation, as governed by the different dimensions of the asperity in the two shear directions.

In Figure 24(a) the characteristic points of the superimposed graphs are numbered. The equivalent poins of the two test graphs are marked by the same numerals. The numerals of the Case A and Case B graphs are circled by single and double circles, respectively.

The conclusions which were resulted by the detailed analyses of the test graphs for steel material, with slight modifications, are valid for the granite as well. The justification is given by the remarkable similarities, as shown for example in Figure 12, between the test graphs obtained under the same test circumstances for the steel and granite specimens. The modification in the interpretation of granite's test graph is required because of the different deformational characteristics of the two materials, as clearly expressed by the relevant test graphs.

As can be seen in Figure 24(a), the influence of the deformation mechanism of the interlocking asperities for the granite is similar to that of the steel. Due to the differences in the angles of the sloping contact surfaces and in the effects of the deformation of the large asperity and the minute asperities for Case A and Case B, the shear mechanism is, just like in the case of steel, somewhat different in the two shear directions.

The different mechanism is indicated again by the significantly different rising legs of the two graphs in Figure 24(a). For Case B it is practically linear up to the peak shear force value. The shear displacement at the peak shear force is equal again to the elastic deformation of the large asperity. The displacement at peak shear force in Case A is the sum of the elastic deformation of the large asperity itself and the shear displacement due to the crushing of the minute asperities along the sliding contact lines, which are at a slope angle of $\alpha_A = 26.6°$ (Figure 13(b)). The descending legs of the two graphs are very similar.

The detailed analysis of shear mechanism for the Case A test run is given in Figure 25. Occasional comparative remarks to steel test results are necessary because those are regarded as the reference data, due to the ideally elastic deformation properties of the steel.

At Point 1 the asperity is completely interlocked, under the applied normal force of P_n.

Caused by the shear force, applied to the centre sliding specimen, both the large asperity itself and the minute asperities on the sloping faces are simultaneously deformed. Because of their much smaller dimensions the yield load of the interlocking minute asperities is reached first, as indicated by the shear force value at the small kink in the rising leg of the graph.

The continued rise of the shear force cause further elastic deformation of the asperities until reaches a level equivalent to the shear strength of the interlocking minute asperities on the sloping contact faces. This force crushes the minute asperities, which is marked by the first small drop in shear force on the rising leg. The second smaller drop in shear force value marks further crushing of minute asperities. The peak shear force is reached at the value of P_2. The shear displacement value of δ_2 is the sum of the shear displacements related to the crushing of minute asperities and to the elastic deformation of the large asperity.

The breakdown of the large asperity starts at Point 2. The forces, concentrated at the asperity contacts, break the extreme tips. This results in an immediate elastic relaxation of the asperity, marked by the shear force value of P_3.

Due to the different deformational behaviours of the two materials, the test graphs of steel and granite becomes significantly different for those sections which is immediately beyond the point of elastic relaxation. In case of steel, as shown in Figures 8, 12, 22 and 23 the elastic relaxation phase is followed always by a phase of continuous and steady deformation, characterized by a plateau in the graphs with little variation of shear forces (Point 4 in Figure 23(a)). The deformation behaviour of minute asperities for the steel, between Points 3 and 4 is elasto-plastic. Point 4 represents the transition point between elasto-plastic and plastic behaviour of the minute asperities.

For the brittle rock material this graph section is obscured or even absent. As shown in Figure 25, the continuous shear displacement along the sloping contact faces is accompanied by further minute asperity crushings, marked by the ups-and-downs in shear force values, until Point 5 is reached. This point marks the shear force value at which the crushing of the asperity earnestly begins. The shear force P_5 is large enough to initiate the break of that volume of the asperity which is defined by the still existing contacts of the interlocking sections of the large asperity.

The continuous crushing of the asperity is characterized by an S shaped unloading curve, with the inflexion point at Point 5.5 and the lower end at Point 7.

The shear force of $P_{5.5}$ represents a mid shear strength value between the maximum value of P_5, associated with the initiation of break, and the minimum value of P_7.

The complete asperity disengagement occurs at Point 6. The shear force at this point drops to the value of P_6.

A comparison between the descending legs of the test graphs for steel and granite reveals the different shear mechanisms of asperity disengagement pertinent for the two materials. As shown in Figure 23 the descending leg of the test graph is a smooth S shaped line between Points 5 and 6. It reflects the elastic relaxation of the steel asperity with the tips which undergone plastic deformation by that stage. The descending leg for the granite, in Figure 25, exhibits the crushing process of the rock asperity tips. The descending leg has a similar S shape. However, due to the crushing process, it is jittery.

The asperity deformation and the asperity disengagement for the steel coincide at Point 6, which defines the ultimate shear force, P_u, associated with perfectly smooth sliding contacts produced by the plastic deformation of the asperity tips. As shown in Figure 25 the asperity crushing of granite material is completed at Point 7, which is the lower end point of the S shaped unloading curve. The corresponding shear force value at Point 6 is higher than the ultimate shear force value which is defined by the complete disengagement of asperity.

SHEAR PROPERTIES ALONG SMOOTH CONTACT LINES

Steel Specimens

The first test series along smooth contact lines of steel specimens was conducted at dry sliding condition, i.e. no lubricant was applied along the contacts. The test results are summarized in Tables 1 and 2.

In Table 1 the listed yielding shear forces, P_y'', were derived from the recorded graphs of the multi-stage tests by following the previously described conducts of data treatment.

The multi-stage procedure test resulted six shear force values for each applied normal force. The mean values and the standard deviation of yielding shear forces were calculated. Similar computations were performed for the values of yielding coefficient of friction, μ_y.

Table 2 summarizes the test results for the initial test runs, namely, the yielding shear forces and the peak or static shear force values, P_{st}. The calculated peak and yielding coefficient of friction values are also listed.

The values in the last line of Table 2 were established by the core sliding method [3]. The last two columns of Table 2 show the differences, expressed in percentages, between the values of P_y' and the mean values of P_y'' in Table 1, as well as, between the values of $\mu_y = P_y'/P_n$ and the mean values of $\mu_y = P_y''/P_n$. The percentages in Table 2 are similar to the percentage values of the standard deviations in Table 1. This similarity justifies the assumption that, from practical point of view, the yielding shear forces P_y' and P_y'' are interchangeable.

The peak shear forces, P_{st}, and the peak coefficient of frictions, μ_{st}, of Table 2 are ploted in Figures 26(a) and 26(b), respectively. To the shear force values plotted in Figure 26(a), a straight line can be drawn which starts at the origin. The slope of this straight line is the peak coefficient of friction $\mu_{st} = 0.415$. In Figure 26(b) it is represented by a straight line, parallel with the normal force axis, which is well fitted to the plotted μ_{st} values of Table 2.

Therefore, it can be stated that relationship between the applied normal forces and the static or peak shear forces, which are required to initiate shear displacement, is linear. The ratio between the forces, i.e. $\mu_{st} = P_{st}/P_n$ is constant. For the tested steel material the

Table 1 - Summarized test results for steel specimens with smooth sliding contact lines tested in dry condition by multi-stage procedure

P_n, lbf	TEST LINE	$P_y"$, lbf	μ_y, $P_y"/P_n$	P_n, lbf	TEST LINE	$P_y"$, lbf	μ_y, $P_y"/P_n$
41.6	1	6.8	0.163	249.6	1	50.7	0.203
	2	6.8	0.163		2	49.6	0.199
	3	7.8	0.188		3	48.1	0.193
	4	6.3	0.151		4	46.3	0.185
	5	7.0	0.168		5	49.6	0.199
	6	5.9	0.142		6	46.3	0.185
Mean Standard Deviation		6.7 1.2 (18%)	0.163 0.010 (6%)	Mean Standard Deviation		48.4 2.3 (5%)	0.194 0.006 (3%)
83.2	1	15.2	0.183	332.8	1	66.6	0.200
	2	15.2	0.183		2	66.6	0.200
	3	15.9	0.191		3	64.4	0.195
	4	14.1	0.169		4	61.8	0.186
	5	14.8	0.178		5	66.2	0.199
	6	14.1	0.169		6	62.5	0.188
Mean Standard Deviation		14.9 0.7 (5%)	0.179 0.005 (3%)	Mean Standard Deviation		64.7 1.4 (2%)	0.195 0.005 (3%)
166.4	1	32.9	0.198	416.0	1	81.4	0.196
	2	33.7	0.203		2	83.3	0.200
	3	32.9	0.198		3	80.7	0.194
	4	30.7	0.184		4	78.8	0.189
	5	32.9	0.198		5	82.5	0.198
	6	30.3	0.182		6	78.1	0.188
Mean Standard Deviation		32.2 1.4 (4%)	0.193 0.005 (3%)	Mean Standard Deviation		80.7 2.0 (2%)	0.194 0.006 (3%)

Table 2 - Summarized results of the initial test runs for steel specimens with smooth sliding contact lines tested in dry condition

P_n, lbf	P_{st}, lbf	μ_{st}, P_{st}/P_n	P_y', lbf	μ_y, P_y'/P_n	PERCENTAGE DIFFERENCES FROM THE MEAN VALUES OF MULTI-STAGE TEST	
					for P_y'	for μ_y
41.6	16.7	0.401	6.3	0.151	- 6	- 8
83.2	31.8	0.382	15.5	0.186	+ 4	+ 4
166.4	72.5	0.436	33.7	0.196	+ 4	+ 2
249.6	106.6	0.427	49.2	0.197	+ 2	+ 2
332.8	136.9	0.411	66.6	0.200	+ 3	+ 3
416.0	177.6	0.427	80.7	0.194	0	0
0.745	0.322	0.432	-----	-----	---	---

value of this constant coefficient of friction is 0.415. This value is, however, applicable only for the degree of roughness along the sliding contact lines which was represented by the tested specimens.

The mean values of yielding shear forces, P_y" in Table 1, are also plotted in Figure 26(a). The best fit for the normal force values above 150 lbf (667 N) is linear. Under this value, the relationship between the normal and shear force is slightly non-linear.

The non-linear relationship is more evident from the normal force versus yielding coefficient of friction plot in Figure 26(b). It can be seen that the yielding coefficient of friction, μ_y, for the normal force values of about 150 lbf (667 N) and above, is depicted by a straight line which is parallel with the normal force axis. However, for normal force values less than 150 lbf (667 N) the data points are on a curved line.

The extrapolated portion of the curve, which is indicated by broken line, intercepts the vertical axis at the value of ultimate coefficient of friction of $\mu_u = 0.130$. This numerical value had been confirmed independently by the simulated large asperity test series, which will be discussed elsewhere.

The percent values of standard deviations, listed in Table 1, are also shown in Figure 26(a) and 26(b). The highest percentage belongs to the lowest normal force. This indicates, that the scatter in the shear force data is largest for the low normal forces. The variation in shear force is due to the roughness along the contact lines. Since the deformation of the minute asperities decreases with decreasing normal force the data scattering expectantly increases with decreasing normal force.

The exceptionally low standard deviation percentage values, even including the higher values, is the manifestation of the highly reliable data set that can be obtained by the confined shear test method.

Figures 26(a) and 26(b) are the graphical presentation of results, based entirely on actually measured test data. Figures 26(c) and 26(d), in addition, also include the components of the coefficient of friction and the shear force, respectively. The deductive logics, which resulted the definition of these components, were already discussed extensively in connection with Figure 14.

The following discussion is to explain the steps of producing first Figure 26(c) and then Figure 26(d). The static coefficient of friction μ_{st} and the yielding coefficient of friction μ_y in

Figure 26(c) were replotted from Figure 26(b). Both of these coefficients were calculated from measured shear force data of P_{st} and P_y', respectively.

From Figure 14(a), $P_{st} = P_y + P_{id}$ or $P_{id} = P_{st} - P_y'$, therefore, $\mu_{id} = \mu_{st} - \mu_y$. The value of the coefficient of friction of initial deformation μ_{id} can be calculated for each applied normal force from the known values of μ_{st} and μ_y.

Furthermore, from Figure 14(a), $P_y' = P_{cd} + P_u$ or $P_{cd} = P_y' - P_u$, therefore, $\mu_{cd} = \mu_y - \mu_u$. Again, the values of coefficient of friction of continued deformation μ_{cd} are calculated from the known values of μ_y and μ_u.

In addition, from Figure 14(a), $P_{st} = P_u + P_d$ or $P_d = P_{st} - P_u$, therefore, $\mu_d = \mu_{st} - \mu_u$. Since both μ_{st} and μ_u are constant values, the coefficient of friction of deformation μ_d must also be constant, that is, represented in Figure 26(c) by a straight line parallel with the normal force axis.

All the coefficient of friction components and their variations with normal force are shown in Figure 26(c). The products of these coefficient of friction components and the normal forces are the relevant shear force components. Their variations with normal forces are shown in Figure 26(d).

The variation of P_{st}, P_d and P_u is linear for the entire range of normal forces. For the rest of the components, i.e. P_{id}, P_y and P_{cd}, the variation is linear for normal forces higher than about 150 lbf (667 N) and non-linear for normal forces below of that.

The stability analysis of underground openings, design of support systems, mine lay-out, mining sequence and method studies, etc. are performed in terms of stresses. The strength and frictional properties of joints should, therefore, also be expressed in stress terms. Furthermore, the use of stress terms is also required to correlate the shear test results with the results obtained by other laboratory tests, such as uniaxial and triaxial tests.

The theoretical background to calculate the deformation and stress along the lines of contact had been already discussed. Based on those previously discussed equations, the normal stresses, due to the applied normal forces, were calculated. These are, with the results of intermediate calculations, listed in Table 3. The elastic constants, and the specimen dimensions were used for the calculation, are also given in Table 3.

The information given in Figure 26(c) and 26(d) presented anew, in stress terms, in Figure 27. The relationships between the coefficients are also summarized in Figure 27.

Table 3 - Calculated normal stresses for steel specimens with smooth sliding contact lines

P_n, lbf	P_n, N	P_n' N/m	b, m	σ_n, MPa
0.745	3.3	43	0.20×10^{-5}	13.5
41.6	185.1	2,419	1.65×10^{-5}	93.5
83.2	370.1	4,838	2.33×10^{-5}	132.2
166.4	740.2	9,676	3.30×10^{-5}	186.7
249.6	1110.3	14,513	4.04×10^{-5}	228.7
332.8	1479.5	19,340	4.66×10^{-5}	264.2
416.0	1850.5	24,189	5.21×10^{-5}	295.6

$E = 199.9$ GPa
$\nu = 0.269$
$R = 0.019$ m
$L = 0.0765$ m

The second test series was performed on the same specimens set as the first one, but prior to the shear tests the specimens were lubricated with regular machine grease. All tests were conducted along new and fresh contact lines.

The data analyses followed the procedures as had been detailed for the tests of dry condition. The results of the lubricated test series are summarized in Figure 28, where the components of the coefficient of friction and the corresponding shear stress components are presented in function of normal stresses.

A comparison of the results obtained by the two series of tests reveals the effect of lubrication on the coefficient of friction. The lubrication, as expected, reduces the friction. The coefficient of friction values were reduced by about 9%, which is surprisingly low.

For the lubricated condition the values of the static coefficient of friction, μ_{st}, and of the coefficient of friction of deformation, μ_d, are 0.393 and 0.263, respectively, and the ultimate coefficient of friction μ_u is the same as for the dry sliding condition, namely 0.130.

Granite

The yielding shear force values of P_y'', i.e. the mid-value of the shear force bands as shown in Figure 17, are listed in Table 4. It also includes the calculated coefficient of friction values, i.e. the ratios between shear and normal forces. The established parameters obtained by statistical analyses are also given.

The mean values of yielding shear forces, given in table 4, are plotted against the applied normal forces in Figure 29(a). As shown, the data points of the lower normal force range form a curved-line relationship. However, it becomes linear for the higher normal force values. The tangent value of the linear portion found to be 0.962.

The mean coefficient of friction values from Table 15 are plotted in Figure 29(b). The coefficient of friction value for $P_n = 0$ is obtained by extrapolation. The tangent value of 0.962 of Figure 29(a) is represented in Figure 29(b) by a horizontal line, which is the static coefficient of friction value, μ_{st}, of the tested granite. The presented result in Figure 29(b) indicates that the function of the yielding coefficient of friction, μ_y, approaches the value of $\mu_{st} = 0.962$.

Table 4 - Summarized test results for granite specimens with smooth contacts tested by multi-stage procedure

P_n, lbf	TEST LINE	P_y'', lbf	μ_y, P_y''/P_n	P_n, lbf	TEST LINE	P_y'', lbf	μ_y, P_y''/P_n
9.98	1	4.4	0.441	83.2	1	66.6	0.800
	2	6.8	0.681		2	74.0	0.889
	3	8.0	0.802		3	75.9	0.912
	4	9.8	0.981		4	77.7	0.934
	5	7.0	0.701		5	68.5	0.823
	6	5.2	0.521		6	66.6	0.800
Mean Standard Deviation		6.9 1.9 (28%)	0.688 0.194 (28%)	Mean Standard Deviation		71.6 4.9 (7%)	0.860 0.059 (7%)
20.8	1	12.6	0.606	166.4	1	148.6	0.889
	2	15.2	0.731		2	153.6	0.923
	3	16.7	0.803		3	157.3	0.945
	4	18.5	0.889		4	161.0	0.968
	5	15.2	0.731		5	148.0	0.889
	6	13.5	0.649		6	140.6	0.845
Mean Standard Deviation		15.3 2.1 (14%)	0.735 0.102 (14%)	Mean Standard Deviation		151.4 7.4 (5%)	0.910 0.044 (5%)
41.6	1	29.8	0.716	416.0	1	386.7	0.930
	2	33.3	0.800		2	384.8	0.925
	3	35.2	0.846		3	397.8	0.956
	4	37.0	0.889		4	420.0	1.010
	5	32.4	0.779		5	388.5	0.934
	6	31.5	0.757		6	383.0	0.921
Mean Standard Deviation		33.2 2.6 (8%)	0.798 0.062 (8%)	Mean Standard Deviation		393.5 14.0 (4%)	0.946 0.033 (3%)

The previous investigations related to the frictional properties of steel and other rock types, the following relationships were established between the components of friction of the smooth sliding contact lines: $\mu_{st} = \mu_y + \mu_{id}$, $\mu_y = \mu_u + \mu_{cd}$, $\mu_{st} = \mu_u + \mu_d$, $\mu_d = \mu_{id} + \mu_{cd}$, $\mu_{st} = \mu_u + \mu_{cd} + \mu_{id}$. Using these relationships and the facts that for $P_n = 0$, $\mu_{cd} = 0$ and $\mu_y = \mu_u$, it is possible to plot the functions for all other frictional components, as shown in Figure 29(b).

The frictional components plotted against normal stresses, instead of forces, are presented in Figure 30(a). The shear stresses, correspond to the coefficient of friction components of Figure 30(a) are given in Figure 30(b), together with the list of the established relationships.

Indiana Limestone, Sandstone, Diabase and INCO Ore

The coefficient of friction and the shear stress components for the Indiana limestone are plotted in Figure 31, while those information for sandstone are given in Figure 32.

The variations of coefficient of friction and shear stress components for diabase and INCO ore are presented in Figure 33 and Figure 34, respectively.

While discussing the test results obtained for diabase and INCO ore, the "stick and slip" shear mechanism experienced during some of the test runs was also pointed out. The sudden loss of shear strength occured only for the test runs conducted along smooth contact lines at normal stress levels in excess of 100 MPa.

The data obtained by the completed tests are insufficient for arriving at any firm conclusions. Still, the importance of the observed phenomenon deserves a brief discussion.

The results presented in Figure 35 are to be used for this discussion. The graphs in Figure 35(a) belongs to the diabase material. From the recorded P_s versus δ_s graphs, such as Figure 20, an average shear force value of slippage P_{ss} can be established for each of those applied normal force where slippage has occured. Then the coefficient of friction values for stick-slip are $\mu_{ss} = P_{ss}/P_n$.

These coefficient of friction values are plotted in the lower graph of Figure 35(a). Between the calculated data points the variation is assumed to be linear. The corresponding strength values are represented by τ_{ss} in the upper graph of Figure 35(a). It insects the linear ultimate shear stress function of τ_u at the normal stress value of about σ_n = 190 MPa. Logically, for normal stress values higher than this the shear stress values equal to τ_u. Similar results are presented in Figure 35(b) for the INCO ore material.

It is important to note that the "stick and slip" shear mechanism occured only in the case of diabase and INCO ore rock materials, and not for Indiana limestone, sandstone and granite. This behaviour is probably an indication of some properties specific to those material. Further tests on various other rock materials, conducted at elevated stress levels, are justified.

Teflon

The main objective of the laboratory shear test program was to establish the joint strength properties of the various rock types. Steel and teflon specimens were tested to obtain frictional data on materials with near ideal deformation properties. The frictional properties of ideally plastic material were investigated by testing teflon specimens.

Two test series were conducted on teflon material. The specimens of the first series were prepared by lathe turning. The ordinary machine surface roughness provided the cylindrical specimens with smooth contact lines.

Typical test results, obtained for teflon specimens with smooth contact lines, are shown in Figure 36. The graphs include both, the initial single-stage and the multi-stage test runs. Figure 36(a) represents the shear force versus shear displacement graphs, while Figure 36(b) gives the relationship between the normal displacement and shear force.

The teflon is a plastic material, with predominately plastic deformational characteristics. However, at the beginning of loading an elastic deformation phase takes place. Consequently, the graphs resemble to those graphs which were obtained for the steel specimens with smooth contact lines. The graph for the initial test run is with a peak value of shear force, P_{st}. This peak value in shear force is again due to the interlocked minute asperities of sliding contacts. As shown by the graph in Figure 36(a), the initial deformation associated with the peak shear force, is elastic. Consequently, the teflon at that stage behaves elastically. Following the peak, the shear force decreases suddenly to the value of P_e, in the fashion of elastic relaxation. With further displacement, the deformation of minute asperities increasingly continues. Their deformation behaviour becomes first elasto-plastic and ultimately plastic. The sliding shear force value for the transition point from elasto-plastic to plastic behaviour is the yielding shear force P_y'.

The graph obtained for the multi-stage runs also shows slight peak value for each run performed at various applied forces. However, these peak values, in comparison to the peak values of the initial test run, are negligible.

These peak values were regarded as the values of yielding shear forces of the multi-stage procedure, P_y''. Their statistical means, are plotted in Figure 37(a), which also includes the peak shear force values obtained by the initial test runs. The calculated ratios between shear and normal forces, i.e. the values of the coefficient of frictions are plotted in Figure 37(b).

The data spread, expressed by the percentage value of standard deviation, for the teflon found to be considerably larger than those obtained for the steel material, although it is still well below to the usual spread associated with any other shear test method. The reason for the larger data spread is the combination of the less certain capability in the measurements and of the more pronounced effects of the minute asperities in the case of low contact stresses. The uniformly distributed concentrated stresses along the contact lines were substantially lower for the teflon than for the steel specimens. For example, the concentrated stresses associated with an applied normal force of P_n = 416 lbf (1850 N) in the case of steel and teflon specimens were 296 MPa and 13 MPa, respectively.

The information in Figures 37(a) and 37(b) are presented in terms of stresses in Figures 37(c) and 37(d). Due to the uncertainty related to the overwhelming influence of the minute asperities at low normal stresses, and also due to the extremely small value of coefficient of friction, to establish the frictional components of teflon, unlike for the steel and rock materials, it was not possible. The frictional properties of the teflon, therefore, may be defined by its static and yielding coefficient of friction values $\mu_{st} = 0.136$ and $\mu_y = 0.062$, respectively.

The deformation of the minute asperities along the contact lines influences greatly the numerical value of the coefficient of friction. This can be studied by comparing the recorded graphs of the initial test runs, in Figure 38, obtained for the steel and teflon materials under similar test conditions. The surface finish of specimens was the same for both materials.

The general shape of the two graphs is similar. The shear force values, however, for the steel material are much larger. The ruggedness, caused by the minute asperities of contact lines, for the graph of steel material is a dominant feature. For the teflon, however, the similar asperities cause only negligible ruggedness in the graph. The points, with characteristical shear force values (P_{st}, P_e, P_y' and P_s), are equally recognisable in both graphs.

The ratio between the peak or static coefficient of friction of the steel and teflon (Figures 27 and 37) is 0.415/0.136 = 3.05. The ratios for the corresponding points of the two graphs in Figure 38 are: 72.5/23.31 = 3.11, 57.7/18.90 = 3.05, 33.7/10.40 = 3.24, 31.8/8.88 = 3.58.

From the above observations several conclusions can be made. The coefficient of friction is a material property and its value depends on the degree of roughness of the interlocking asperities and the momentary deformation degree of the asperities. The coefficient of friction for the steel is about 3.05 times larger than it is for the teflon. The deformation of the asperities is influenced by the deformational characteristics of the material. The steel and teflon are ideal representatives of elastic and plastic materials, respectively. The initial deformation and relaxation, however, for both materials are elastic. This is perhaps the reason why the ratios for P_{st} and P_e shear forces are so close to the value of 3.05.

With the increasing shear displacement the plastic deformational characteristic becomes more dominating and the ratios for P_y' and P_s change to 3.24 and 3.58, respectively. The different degree of ruggedness of the graphs is the result of the different degrees of deformation of the minute asperities, governed by the deformation characteristics of the two materials.

The teflon specimens of the second test series were prepared with thread-like minute asperities which resulted continuously interlocking mechanism between the asperities along the contact lines. The threads were produced by lathe turning, cut to a depth of 0.01 inch (0.25 mm) by using a 90° cutting-tool, producing 16 threads per inch.

Typical recorded test data are presented in Figure 39. Figures 39(a) and 39(b) are the recorded graphs of the initial test run at an applied normal force of P_n = 332.2 lbf (1480 N), representing the relationships between shear force and shear displacement, and between shear force and normal displacement, respectively. For the same contact lines, the recorded graphs of the multi-stage test results are shown in Figures 39(c) and 39(d), representing the variation of shear force with respect to shear displacement, and the relationship between shear force and normal displacement, respectively.

The influence of the deformation status of the interlocking asperities on the coefficient of friction had already been, repeatedly, emphasized. This important information can be, perhaps, most convincingly concluded from the data of Figure 39.

In order to provide the most informative picture, in Figure 39(a) the graph of the initial test run obtained with smooth sliding contact (from Figure 36(a)) is also reproduced by broken line. The comparison of this graph with the recorded graph of the initial test run of Figure 39(a), reveals the effects of the thread-like asperities on the frictional properties of teflon. Furthermore, information can be gained on the variation of these effects, as influenced by the deformation status of the simulated asperities.

Firstly, due to the asperities, the shear forces were increased by about five times. This increase equally holds for any characteristical points of the graphs (i.e., P_{st}/P_{st} = 5.38, P_e/P_e = 5.52, P_y'/P_y' = 4.81 and P_s/P_s = 4.89). The deformation characteristic of the rising leg for the smooth sliding contact lines is elastic. The plastic deformation character of the teflon, however, comes into play even during this initial loading phase, as indicated by the larger angle of inclination of the rising leg. The elastic behaviour, however, is also present as indicated by the straightness of the rising leg. The shear displacement of the rising leg can be interpreted as the total deformation of the interlocking thread-like asperities which resulted from both elastic and plastic deformation of these asperities.

The combined effect of plasticity and elasticity on the shear force variation can also be seen from the mechanism of asperity disengagement. The recorded graph in Figure 39(a) shows two general patterns for this mechanism. A complete cycle of shear force variation of the pattern, dominant for the lower displacement range, is indicated by points A-B-C-D-A'. A cycle of the higher shear displacement range is marked by K-L-M-N-O-P-K'.

The rigid body analyses of both cycles are given in Figure 40. Must remember that the explanatory figures are correct only with respect to the position of the asperities relative to each other. Asperity deformation, which is especially significant in case of teflon, is ignored. Nevertheless, the analysis provides explanations on the reasons behind the significant variations in the shear force values.

At point A, under the combined effect of the applied normal force and the prevailing shear force which has the value of A, the asperities are completely interlocked.

Due to the continuously maintained shearing deformation of the interlocked asperities takes place. This deformation is entirely elastic. The displacement in the explanatory figure B is to be regarded as elastic deformation and not an actual shear displacement, as being shown. Shear force B is equivalent to the peak strength of the interlocking asperities, for the deformed asperity condition which prevailes at that specific shear displacement value.

At the instant of reaching the peak strength, while the shear displacement continuous, a relaxation of the asperities' material takes effect. Due to the relaxation the shear force drops to the value of C. The relaxation is elastic.

The further shearing results a plastic reshaping of the deformed asperity tips, while they are being disengaged. The associated shear force value is D.

Following the disengagement the shearing on the down-slope faces of the thread-like asperities takes place. Consequently, the shear force drops to the value of A'. A further reshaping of the asperity tips follows. Based on the shape of the relevant graph portion, the associated deformation is plastic.

A similar step-by-step analysis can be performed for the second typical shear force cycle in Figure 40. It would, however, result only unnecessary repeats. The discussion, therefore, is to be restricted to the differences of the two cycles.

The difference is caused by the mode of deformation of the asperities which had already been deformed by the numerous repeated cycles of the preceding shear displacement. Beginning at point K the initial deformation respond is elastic. However, at point L some reshaping of the previously deformed asperity takes place. This reshaping is indicated by the plastic relaxation between points L and M. The reshaped asperities, having now full contacts between the sloping faces of matching thread-like asperities, will then deform elastically until the shear force value of N is reached. Shear force N is equivalent to the peak value of the interlocking asperities. Beyond Point N, the mode of deformation, therefore, the pattern of change in the shear force value follows the form of changes between the points of B and A' of shear force cycle A - A'.

Figure 39 contains even further information with respect to the interplay between the asperity deformation and the frictional values. As shown by Figure 39(c), because the asperities were deformed by the initial test run, i.e. Figure 39(a), the multi-stage test runs are without peak shear strength values. Although the asperities undergone considerable previous deformation cycles, their effects on shear force variation remained dominating. Each cycle reflects the interplay between the prevailing condition of asperity deformation and the magnitude of acting forces.

Figures 39(b) and 39(d) reveal that the normal displacements were exclusively contraction. From the comparision of the two recorded normal displacement graphs, it can be concluded that about half of the deformation, occured during the initial test run, was permanent.

The summarized test results are presented in Figure 41, in terms of stresses. The steeply sloping primary portion of τ_{st} function can apparently be replaced by the linear function with the slope angle of $45° + \emptyset_{st}$, where, $i = 45°$ is the inclination of the thread-like asperities and $\emptyset_{st}$ is the angle of static frictional sliding obtained by the test series of smooth sliding contact lines.

From the coefficient of friction functions in Figure 41(b) it is evident that the two lines will join at a normal stress level somewhat higher than the upper level of the test series. The continuous decrease of coefficient of friction can be anticipated, until the value is reduced to $\mu_{st} = 0.136$, and then to $\mu_y = 0.062$, and finally to the value of the ultimate coefficient of friction μ_u. Due to the extremely low coefficient values of the teflon, the measurement accuracy became an impediment in establishing the value of μ_u.

SHEAR PROPERTIES ALONG CONTACT LINES WITH SIMULATED ASPERITY

Steel Specimens

The shear mechanism along contact lines with simulated large asperity is detailed previously in connection with Figure 23. The presented discussion had provided explanatory information only with respect to the mechanism of shearing. Still further analysis is required to interpret the meaning of the tests results and to express them in terms of coefficient of friction.

This analytical procedure relies on the method of interpretation established for smooth contact lines.

In Figure 42(a) the recorded graph obtained for steel specimens with large single asperity sheared in Case A direction. The graph in Figure 42(b) is recorded for the initial test run conducted on steel specimens with smooth contact lines. The surface finish and the applied normal force were identical for both cases. The comparison of the two graphs should, therefore, reflect those differences which are attributable completely to the large asperity.

As previously discussed, the shear displacement of the peak shear force (i.e. P_2 in Figure 42(a)) for the test graph obtained in Case A direction, is the sum of the elastic deformation of two elements. Caused by the shear force application, both the large asperity itself and the minute asperities on the sloping faces are deformed simultaneously. Having much smaller volume the yield load of the interlocking minute asperities is reached first, which is given the shear force value of $P_{1.5}$ at the kink point of the rising leg. The elastic deformation of the large asperity contact tip is continued then until the yield load of the contact tip itself is reached at the shear force value of P_2.

The value of $P_{1.5}$ is the peak shear force what the interlocking minute asperities on the sloping face can sustain. As it should, this shear force has the same value (within the range of experimental errors) as of the peak shear force P_{st} obtained for the minute asperities of smooth contact lines (Figure 42(b)). Therefore, shear force $P_{1.5}$ is to be identified by the symbol of $\bar{P}_{stma}$, where the bar refers to the test series with single large asperity, subscripts of st are to recognize the identity of the static or peak shear forces and the subscripts of ma are to refer to the minute asperities which define this shear force value.

The result of $P_{st} = \bar{P}_{stma}$ is important to verify that the peak shear force of smooth sliding contact is associated with the elastic deformation of the minute asperities. The finish of the sloping face of the large asperity and the smooth sliding contacts was identical, therefore, the two independent tests, conducted at identical normal forces, resulted the same peak shear force values, as far as the minute asperities are concerned.

The further shear force application causes further elastic deformation of the contact tips of the asperity. The rate of deformation increases, as indicated by the increased angle of inclination from the horizontal. The peak shear force is P_2 which is the yield load of the contact tips. This peak shear value is analogous with the peak shear value of smooth contact lines, P_{st}, therefore, $P_2 = \bar{P}_{st}$, where the bar refers again to the test data of the single large asperity series.

Following the peak the shear forces suddenly decrease, due to the elastic relaxation. The amount of decrease is about the same for both graphs. The analogy between shear forces P_3 and $\bar{P}_e$ can be easily recognized, therefore, $P_3 = \bar{P}_e$.

The shear force plateau, which is signaling the transition point between the elasto-plastic and the plastic deformation of the asperities, can readily be recognized. This shear force level is analogous with yielding shear force of the smooth sliding contact, P_y', it is, therefore, designated as $P_4 = \bar{P}_y$.

The asperity deformation is a function of the shear displacement. Since the shear displacement for Point 5 is the same as the total displacement of the smooth sliding contact, a similar degree of asperity deformation can be assumed for both cases. Therefore, $P_5 = \bar{P}_s$.

The shear force value of $P_{5.5}$ marks the mid value between the shear forces of P_5 and P_6. It is identified as $\bar{P}_m$. It designates the inflection point on the descending S shaped leg of the graphs which signifies the elastic relaxation of the large asperity. There is no equivalent point exist on the graph of the smooth contact line test. The angle of inclination from horizontal of the relaxation curve is the same as for the rising curve, but with negative sign.

Shear force P_6 corresponds to the ultimate deformation conditions of the point contacts. It refers to the minimum value of shear force which is required to maintain continuous sliding of the steel material when the sliding contacts are perfectly smooth. The ultimate shear force value, $\overline{P}_u$, can be determined by test series with single large asperity. The equivalent value, i.e. the same value, in the case of smooth sliding contact test series, could only be achieved if the specimens used were long enough to allow sufficiently large displacement necessary to attain the asperity deformation of perfectly smooth contact lines. The required specimen length, to achieve the condition of $P_s = \overline{P}_u$, however, would be impractical.

The selection of the discussed points of the recorded graph was based on the assumption that they are important in analysing the test results in order to make conclusions with respect to the effects of a large asperity on frictional properties. The relative importance of these points are being now investigated and evaluated.

The shear stress values of the identified points are summarized in Table 5, where the coefficient of friction values are also calculated. The shear force values listed in Table 5 are plotted in Figure 43. This presentation reveals that the variation of shear forces follows the same pattern for all the identified points, except $P_{1.5}$ values. For the lower normal force values $P_{1.5} < P_{5.5}$, however, they are equal for the normal force values above 250 lbf (1112 N).

The variations of coefficient of friction values with normal stress are presented in Figure 44. These variations are based on the coefficient friction values listed in Table 5 and are labelled by the previously established terms of designation (Figure 42). The corresponding shear stresses are plotted in Figure 45. The additional information contained in Figures 44 and 45 will be discussed later.

In order to investigate the effects of the large asperity, the shear stress difference values were plotted in Figure 46. These shear stress difference values were calculated by substracting the shear stress values of the smooth contact lines (Figure 27) from the analogous shear stress values of the large asperity (Figure 45).

The main difference between the two test series is the inclination angle of the shear path, which are 23.7° and 0° for the asperity and for the smooth contact line, respectively. The shear stress associated with the $\alpha_A = 23.7°$ inclined shear path is: $\tau = \tan \alpha_A \sigma n = 0.438 \sigma_n$.

Table 5 - Summarized test results for Case A test series performed on steel specimens with large asperity

P_n	$P_{1.5}$	$\mu_{1.5}$	P_2	μ_2	P_3	μ_3	P_4	μ_4	P_5	μ_5	$P_{5.5}$	$\mu_{5.5}$	P_6	μ_6
16.6	3.7	0.223	34.2	2.060	25.9	1.560	24.1	1.452	22.2	1.337	13.0	0.783	7.4	0.446
33.3	11.1	0.333	59.2	1.778	46.3	1.390	42.6	1.279	38.9	1.168	29.6	0.889	14.8	0.444
49.9	16.7	0.335	75.9	1.521	59.2	1.186	55.5	1.112	48.1	0.964	31.5	0.631	13.0	0.261
66.6	18.5	0.278	87.0	1.306	81.4	1.222	66.6	1.000	55.5	0.833	40.7	0.611	14.8	0.222
83.2	29.6	0.356	107.3	1.290	92.5	1.112	85.1	0.980	70.3	0.845	55.5	0.667	20.4	0.245
166.4	61.1	0.367	193.4	1.163	180.4	1.084	159.1	0.956	112.9	0.678	70.3	0.422	24.1	0.145
249.6	103.6	0.415	279.4	1.119	248.9	0.997	228.5	0.915	164.7	0.660	101.8	0.408	31.5	0.126
332.8	127.7	0.383	347.8	1.045	314.5	0.945	290.5	0.873	222.0	0.667	131.4	0.395	40.7	0.122
416.0	159.1	0.382	410.7	0.987	386.7	0.930	347.8	0.836	277.5	0.667	168.4	0.405	46.3	0.111

Therefore, would the inclined shear path the only influencing factor of the large asperity, then the shear stress differences in Figure 46 should coincide with $\tau = 0.438\ \sigma_n$ value. However, the presented data show entirely different picture. The shear stress differences of $\bar{\tau}_{st} - \tau_{st}$, $\bar{\tau}_e - \tau_e$ and $\bar{\tau}_y - \tau_y$ are all higher than the value defined by the inclined shear path. The data points are seemingly positioned within a relatively narrow band which is more or less parallel to the slope defined by $\tau = 0.438\ \sigma_n$.

The shear difference values of $\bar{\tau}_s - \tau_s$ show, however, a different pattern. For the normal stress values larger than 60 MPa, it departs the other curves and gradually approaches the linear relationship of inclined shear path.

The above patterns of variations can be related to the deformation of the asperity contact tips. The deformation of the asperity associated with the shear force value of $\bar{P}_s$ (Figure 42) is considerably larger than the deformations connected to the other values (i.e. $\bar{P}_{st}$, $\bar{P}_e$ and $\bar{P}_y$). Therefore, the corresponding shear stress difference, $\tau_s - \tau_s$, value should expectantly be the closest to the linear relationship. One must remember that $\tau = 0.438\ \sigma_n$ function is applicable only for the sliding of a rigid body on an inclined plane, i.e., no deformation is considered. The variation pattern of shear stress difference value of $\bar{\tau}_s - \tau_s$ indicates that theoretically, at a sufficiently high normal stress value, the degree of deformation will attain the condition of rigid body slidings. This condition will necessarily coincide with the degree of deformation required for a perfectly smooth sliding contact, i.e. complete deformation and ultimate coefficient of friction, μ_u.

Because the deformation associated with the shear forces of $\bar{P}_{st}$, $\bar{P}_c$ and $\bar{P}_y$ are much smaller, it logically follows that the corresponding shear difference values are further away from the linear relationship of the inclined shear path.

There are other important information that can be concluded from Figure 46. It had been deduced in connection with Figure 42 that the shear force values of P_{st} and $\bar{P}_{stma}$ are equal. Therefore, the data points for the $\bar{\tau}_{stma} - \tau_{st}$ shear difference values should lay on the abscissa. They are, instead, positioned on a straight line parallel to the abscissa at -10 MPa. This consistant vertical shift is due to the difference in the conditions of the two independent test series.

Shear stress value of $\bar{\tau}_m$ corresponds to the inflection point on the elastic relaxation curve in Figure 42. Although, there is no equivalent value in the case of smooth contact line test, the shear stress difference values of $\bar{\tau}_m - \tau_{st}$ were calculated and plotted in Figure 46. The obtained curved line joins the constant value of $\bar{\tau}_{stma} - \tau_{st} = -10$ for the normal stresses larger than 260 MPa. The linear function of $\tau = 0.438\ \sigma_n$ is tangent to the curved line at the origin.

So far the interplay between the asperity deformation and the shear stresses was investigated. For the characteristic points of the recorded graphs the condition and the degree of deformation and then the relationship between the deformation and shear stresses were established. The questions, that which one of these characteristic points provides the data which are essential, and also useful, in determining the frictional properties of the simulated joint were not yet answered.

The following analysis is based on the information presented in Figure 45, which is the graphical representation, in stress terms, of the data listed in Table 5. The subscripts refer to the characteristic points as were defined in Figure 42. In Figure 45 there several linear function, are also shown by broken lines. Function τ_{st}, reproduced from Figure 27, is the stress relationship for the peak, or static, shear stress for the smooth sliding contact lines.

Each of the functions given by solid lines can be taken as a strength envelope, applicable to the prevailing deformation condition of the asperity for the particular characteristic point. The question is: which one of these envelopes can be regarded, in the sense customary in rock mechanics investigations, as the failure envelope of the joint simulated by the test series.

To decide, the principle developed in connection with rock joint investigation is used [7]. There, the conclusion was that the steeply sloping primary portions of the failure envelopes are approximately equal to $\emptyset + i$. The inclination of the secondary portions of the failure envelopes are approximately equal to $\emptyset_r$. The definition of these terms are:

> $\emptyset$ = the angle of frictional sliding resistance. The appropriate value for practical problems can apparently be obtained after large displacements have occured along macroscopically smooth and flat but microscopically irregular (i.e., unpolished) wet surfaces.

i = the angle of inclination of the failure surfaces with respect to the direction of application of the shearing force.

ϕ_r = the angle of residual shearing resistance of materials which initially were partly or completely intact. It is obtained from the asymptotic minimum values of shear strength following large displacements.

The angle of inclination in our case is $i = \alpha_A = 23.7°$. Actually, neither the frictional sliding resistance angle (ϕ) nor the residual shearing resistance angle (ϕ_r), which would entirely fulfill the above definitions, is available. However, the frictional constants, established for the smooth sliding contact lines, do have close similarities. These constants from Figure 27 are: $\mu_{st} = 0.415$ ($\phi_{st} = 22.5°$), and $\mu_u = 0.130$ ($\phi_u = 7.4°$).

In accepting the validity of the above $i + \phi$ approximation principle, two straight lines were drawn in Figure 45, one with the slope angle of $23.7° + 22.5° = 46.2°$, the other with $23.7° + 7.4° = 31.1°$. The third line has a slope angle of ($i + \phi_y$). It is the straight line fit of the slightly curved line plot which was obtained by adding to $i = 23.7°$ the angle values of μ_y in Figure 27.

Based on the results presented in Figure 45 the following information can be concluded:

(a) the $\bar{\tau}_{st} / \sigma_n$ curve represents the relationship between the normal stress and the peak shear stress. From the previous discussions it is evident that the peak shear stress, $\bar{\tau}_{st}$, is the yielding stress of the elastically deformed asperity contact tips. Therefore, the $\bar{\tau}_{st} / \sigma_n$ curve can be regarded as the yield strength envelope of the asperity contact tips. The equivalent normal and shear forces are required to initiate shear displacement.

(b) the $\bar{\tau}_e / \sigma_n$ curve represents the post-yield stress condition of the asperity contact tips, immediately after the yield. Therefore, the curve can be regarded as the post-yield strength envelope of the asperity contact tips.

(c) the $\bar{\tau}_y / \sigma_n$ curve reflects the stress conditions associated with the transition of elasto-plastic deformation of the contact tips to plastic deformation. It can be regarded as the lower yield strength envelope of the asperity contact tips.

(d) all of these envelopes are strength envelopes, expressing the stress conditions which prevail for the specific deformation phases of the asperity contact tips. The failure envelope criteria of rock joint investigation, however, does not apply to these envelopes. Their steeply sloping primary portions cannot be approximated by neither possible linear τ / σ_n functions.

(e) the description of a failure envelope seamingly fits for $\bar{\tau}_s$ / σ_n curve. Its steeply sloping primary portion is approximately equal to (α_A + ϕ_{st}). This is applicable for the normal stress values of up to 80 MPa. For normal stress values higher than this, the $\bar{\tau}_s$ / σ_n curve deviates from the straight line, first rapidly and then gradually, in such a fashion that with the increasing normal stresses its slope angle approaches the value of (α_A + ϕ_u). Therefore, it can be concluded that $\bar{\tau}_s$ / σ_n curve is the peak failure envelope for the simulated large asperity. The stress conditions of the curve refer to the maximum degrees of asperity deformations which were attained at the point where the sliding on the inclined seat is completed. The deformation of asperity is permanent plastic, with some elastic component which relaxes suddenly at the instant of the total asperity disengagement.

(f) the stress condition at the instant of the total disengagement is represented by the $\bar{\tau}_u$ / σ_n curve. These stress data refer to the ultimate degree of asperity deformation when the perfectly smooth sliding contact of the asperity tips is attained. Therefore, the $\bar{\tau}_u$ / σ_n curve represents the residual failure envelope for the simulated large asperity.

(g) for the test condition defined by the kink on the rising leg of a Case A test graph (see Figure 42) the stress condition is represented by the $\bar{\tau}_{stma}$ / σ_n curve. It had been already established that the shear force corresponding to the kink point is equal to the peak shear force of the smooth sliding contact lines, i.e. $\bar{P}_{stma} = P_{st}$. The consistent difference between the two values is due to the different conditions of the two tests. This shadow of difference is the result of the dissimilarity between

$\vec{\tau}_{stma} / \sigma_n$ and τ_{st} / σ_n functions in Figure 45. As had been concluded, the kink is due to the elastic deformation of the minute asperities of the inclined seat of the large asperity. Consequently, the $\vec{\tau}_{stma} / \sigma_n$ curve represents the envelope of the sliding resistance which is exerted by the minute asperities of the inclined seat. It represents only a passing, intermediate stage of asperity deformation and only in the case of low angle of inclination.

(h) for the inflection point of the descending leg of the test graph the stress relationships are defined by $\vec{\tau}_m / \sigma_n$ curve. From the definition follows that this curve is positioned at mid-values between $\vec{\tau}_s / \sigma_n$ and $\vec{\tau}_u / \sigma_n$ curves. For the higher normal stress values it merges with the $\vec{\tau}_{stma} / \sigma_n$ curve.

The presented conclusions can be made from Figure 44, as well, where the values of the coefficient of friction components and their variation with normal stresses are plotted.

The analyses of Case B test data provided similar results. The differences in the results are attributable always to the geometrical differences of the large asperity with respect to the shear directions of Case A and Case B.

Granite

The shear mechanism had already been analysed in connection with Figure 25. The analysis also included comparison between the shear mechanism for the steel and the granite specimens. The dissimilarities in shear mechanism, caused by the different properties of the two materials, were identified through the detailed analysis of the test graphs. To establish the frictional properties of the granite joint simulated by the test specimens, the procedure as detailed previously for the steel was followed.

The shear stress values of the identified points (Figure 25) are summarized in Table 6, where the coefficient of friction values are also calculated. The shear force values listed in Table 6 are plotted in Figure 47.

Table 6 - Summarized test results for Case A test series performed on granite specimens with large asperity

P_n	P_2	μ_2	P_5	μ_5	$P_{5.5}$	$\mu_{5.5}$	P_7	μ_7	P_6	μ_6
1.664	68.8	41.386	48.1	28.906	35.2	21.154	22.2	13.341	6.7	4.026
4.16	76.2	18.317	65.5	15.745	40.7	9.784	19.2	4.615	10.4	2.500
9.98	96.2	9.639	75.9	7.605	53.7	5.381	37.0	3.707	20.3	2.034
20.8	140.6	6.760	111.0	5.337	64.8	3.115	35.2	1.692	18.5	0.889
41.6	205.4	4.938	177.6	4.269	122.1	2.935	79.6	1.913	48.1	1.156
83.2	290.5	3.492	262.7	3.157	185.0	2.224	136.9	1.645	101.8	1.224
166.4	462.5	2.779	392.2	2.397	292.3	1.757	210.9	1.267	155.4	0.934
416.0	999.0	2.401	880.6	2.117	621.6	1.494	462.5	1.112	373.7	0.898

The variation of coefficient of friction values with normal stress are presented in Figure 48. These curves represent the best fit curved lines drawn on the calculated values listed in Table 6. The shear stress functions shown in Figure 49 are based on the coefficient of friction curves of Figure 48.

In order to define the failure envelope let us go back to the analysis of the shear mechanism in Figure 25. As discussed, the continuous shear displacement along the sloping contact faces is accompanied mainly by the crushing of minute asperities. The crushing of the large asperity earnestly begins at Point 5. The shear force P_5 is large enough to initiate the break of that volume of the asperity which is defined by the still existing contacts of the interlocking asperity sections.

The continuous crushing of the asperity is characterized by an S shaped unloading curve, with the inflexion point at Point 5.5 and the lower end at Point 7. The shear force of $P_{5.5}$ represent a mid shear strength value between the maximum value of P_5, associated with the initiation of break, and the minimum value of P_7. The complete asperity disengagement occurs at Point 6.

From the previous discussions it is apparent that function $\tau_{5.5}$ represents the shear stress values falling between the shear stress values for the initiation of asperity break, τ_5, and the minimum value of shear stress, τ_7, associated with the broken asperity. Therefore, function $\tau_{5.5}$ represents average values, and is to be regarded as the failure envelope of the asperity.

Function τ_6 marks the stress condition of complete asperity disengagement. It represents the lowest shear stress values, associated with the asperity. It prevailes when the broken asperity slides along the smooth contact lines of the specimen surface. Function τ_6 is to be regarded as the residual strength envelope of the broken asperity.

The granite material had been tested extensively to determine the strength and deformation properties [8]. The test program included 74 conventional triaxial tests. The confining pressure of these tests varied between 3.5 and 55 MPa. The results of these triaxial tests are presented in Figure 50. The obtained stress relationships define the peak strength envelope, τ_{tc}, as established by the conventional triaxial test method.

One of the objectives of the Rock Properties and Support Systems Project is to establish standard procedures for laboratory testing required to characterize and classify mine rocks. The standard procedure development work had resulted the multi-stage triaxial testing technique. The proposed procedure require to test three specimen by multi-stage triaxial technique.

The required three specimens were prepared from the same drill core as the specimens which were used in the series of confined shear tests. The multi-stage triaxial tests resulted two strength envelopes, namely, the peak strength envelope, τ_{tp}, and the residual strength envelope, τ_{tr}. These results are presented in Figure 51.

The various τ / σ_n functions, which were obtained by various testing methods, are summarized in Figure 52(a). Their definitions are:

$\tau_{5\cdot5}$ = peak failure envelope of the asperity, obtained by confined shear test method on specimens with single large asperity;

τ_{tc} = peak failure envelope of cylindrical specimens, obtained by conventional triaxial test method;

τ_{tp} = peak strength envelope of cylindrical specimens, obtained by multi-stage triaxial test method;

τ_6 = residual strength envelope of the broken asperity, obtained by confined shear test method on specimens with single large asperity;

τ_{tr} = residual strength envelope of cylindrical specimens, obtained by multi-stage triaxial test method.

τ_{st} = peak (static) strength envelope, obtaine by confined shear test method on specimens with smooth sliding contact lines;

τ_u = ultimate strength envelope, deduced from the test results obtained by confined shear test method on specimens with smooth sliding contact lines;

The remarkable closeness of the strength envelopes obtained by triaxial and by confined shear test methods provides a sound proof of the reliability and accuracy of the test data obtained. Consequently, it is proven that the confined shear testing concept and related techniques may be applied to establish the shear properties of joints with asperities.

The ultimate goal of the laboratory tests is to determine the peak and residual strength envelopes of the rock mass. Figure 52(a) summarizes the strength envelopes which are applicable either for the rock substance or for the joint. From these strength envelopes the one must be selected which will provide an adequately safe design.

Two basic principles are followed in the selection. Firstly, each section of the design envelopes is to be based on the strength envelope with the lowest value within that section. Secondly, the non-linear sections of the envelopes are to be approximated by linear segments.

The peak and residual strength envelopes of the investigated type of granite rock mass are presented in Figure 52(b). The peak strength of the rock mass in case of normal stresses between 0 and 80 MPa is controlled by the strength of the rock substance (τ_{tp}). For the normal stress range of 80-160 MPa it is governed by the failure strength along the joints ($\tau_{5.5}$).

The residual strength of the rock mass, for the normal stress magnitudes form 0 to 80 MPa is given by the peak shear strength along the smooth joints (τ_{st}). For the normal stresses between 80 to 160 MPa the residual strength of the broken substance, that is either τ_6 or τ_{tr}, which should be the same, although they were established by entirely different methods.

The remarkable agreement of the peak strength envelopes must also be pointed out. Although, the testing methods were different, the basic test conditions were the same for all the three tests. Consequently, the methods should yield the same results.

The strength envelope for the theoretical rock mass with perfectly smooth joint contacts is the ultimate strength envelope, τ_u.

The equations of the recommended design envelope segments for a granite rock mass are:

Peak strength:

if $0 \leq \sigma_n < 80$ $\qquad \tau_p = 1.56\ \sigma_n + 35$
if $80 \leq \sigma_n \leq 160$ $\qquad \tau_p = 0.89\ \sigma_n + 90$

Residual strength:

if $0 \leq \sigma_n < 80$ $\tau_r = 0.96\ \sigma_n$
if $80 \leq \sigma_n \leq 160$ $\tau_r = 0.52\ \sigma_n + 35$

Diabase

The details of diabase test and analysis procedures were reported previously [9]. Figure 53 presents the summary of the results. The various strength envelopes are given in Figure 53(a). The linear τ_{st} and τ_u envelopes were obtained for the diabase specimens with smooth contact lines. The curved line envelopes of τ_{tc} and τ_r are the peak and residual strength envelopes, respectively, for the diabase rock substance, determined by triaxial test methods of an independant test program [10].

The meanings and the significances of τ_5, $\tau_{5.5}$ and τ_7 were discussed previously in connection with the granite testing. The function of $\tau_{5.5}$ represents the peak failure envelope of the asperity. At the time of diabase testing the confined shear test method was still under development. The shear forces for the complete asperity disengagement (Point 6) were not yet recorded. Therefore, in Figure 53(a) can be shown only the triaxial residual strength envelope, τ_{tr}.

The peak and residual strength envelopes of a diabase rock mass are given in Figure 53(b). In case of normal stresses between 0 and 80 MPa, the peak strength of the rock mass is controlled by the strength of rock substance (τ_{tc}). For the normal stress range of 80-200 MPa it is governed by the failure strength of joints ($\tau_{5.5}$).

The residual strength of the rock mass for the normal stress magnitudes of 0 to 80 MPa is given by the peak shear strength along the smooth joints (τ_{st}). For normal stresses between 80 and 200 MPa the residual strength envelope is defined by the residual strength of the rock substance (τ_{tr}).

The strength envelope for a rock mass, with joint contacts assumed to be perfectly smooth, is the ultimate strength envelope, τ_u.

The segments of the recommended design envelopes of a diabase rock mass are defined by the following equations:

Peak strength:

if $0 \leq \sigma_n < 80$ $\tau_p = 1.41\ \sigma_n + 55$
if $80 \leq \sigma_n \leq 200$ $\tau_p = 0.52\ \sigma_n + 126$

Residual strength:

if $0 \leq \sigma_n < 80$ $\tau_r = 1.06\ \sigma_n$
if $80 \leq \sigma_n \leq 200$ $\tau_r = 0.34\ \sigma_n + 55$

Indiana Limestone

The strength envelopes of the Indiana limestone, established by the various testing programs, are summarized in Figure 54(a). One particular characteristics of the Indiana limestone is reflected by the results of the traditional triaxial tests [11]. As can be seen the difference between the peak and residual strength envelopes (τ_{tc} and τ_{tr}) is negligible. Specimens broken under triaxial test conditions, subject to the prevailing stresses, were recompacted and consequently they regained their strength almost to the point of original values. Continuous load application resulted further compaction of the test specimens with very little reduction, or in some cases even gain, in strength.

Similarly to the diabase, the shear forces for the complete asperity disengagement were missed by the test procedure used at the time of testing. Therefore, the residual shear strength envelope of the joint (τ_6) is not available. Due to the unusual behaviour of the Indiana limestone, the residual strength of the joint, unlike the other rock types, cannot be based on the residual strength envelope of rock substance, which was obtained by the traditional triaxial testing method (τ_{tr}).

Instead, an additional information is used in determining the residual strength envelope of an Indiana limestone jointed rock mass. The shear stress envelope of τ_{ext} shown in Figure 54(a) was established by the extension triaxial test method. No significant recompaction of specimens occurs during this type of test, therefore, τ_{ext} function can be regarded as the residual strength envelope of the Indiana limestone rock substance.

Furthermore, the constant coefficient of friction value, indicated by the plateau of the τ_7 function, signifies a limiting condition. It is being interpreted as the shear stress function for the complete asperity disengagement. Since, in comparison with τ_{ext}, the plateau has the lower shear stress values, it is assumed that the beginning of the upper segment of the residual strength envelope coincides with this plateau. It then merges with τ_{ext} function for the higher normal stresses. The first segment of the residual strength envelope is defined by the peak strength of the smooth contact lines (τ_{st}).

The first segment of the peak strength envelope is determined by both the peak strength envelope of rock substance (τ_{tc}) and the failure strength envelope of the simulated asperity ($\tau_{5.5}$). The second segment is governed by the triaxial peak strength evelope of rock substance (τ_{tc}).

The equations of the segments of the strength envelopes, recommended to use for design purposes, as shown in Figure 54(b) are:

Peak strength:

if $0 \leq \sigma_n < 45$ $\quad \tau_p = 0.97\ \sigma_n + 12$
if $45 \leq \sigma_n \leq 120$ $\quad \tau_p = 0.3\ \sigma_n + 42$

Residual strength:

if $0 \leq \sigma_n < 15$ $\quad \tau_r = 1.11\ \sigma_n$
if $15 \leq \sigma_n \leq 120$ $\quad \tau_r = 0.32\ \sigma_n + 12$

CONCLUSIONS

The method described in this report represents a novel testing technique, equally suitable for determining the shear strength of smooth joints and joints with asperity.

The cylindrical specimens required for the tests are prepared from ordinary diamond-drill cores. Since diamond drilling is the most common sampling technique, drill cores representing the rock formations to be investigated are usually readily available. Subsequent specimen preparation work is minimal.

The same specimen set of four cores can be used for several (up to nine) shear tests, which are performed at various applied normal forces. This eliminates the usual variation in shear properties from specimen to the next. Also, the number of specimens, required to establish the shear strength properties of joints for a specific rock formation, is greatly reduced.

The test apparatus, incorporating methods for normal and shear force application, represents a self-adjusting self-contained system. This ensures that the normal forces are automatically equalized, and that the applied shear force is concentric. Thus, complete force and displacement control is inherent in the system design.

The three equal normal forces are applied along the three equally spaced contact lines of the central sliding core. This method of load application creates confined test conditions. Therefore, it reproduces the actual field conditions of the rock mass around an underground opening.

The shearing occurs along the contact lines of the cylindrical specimens. Therefore, uncertainties, associated with the continuous variations in the magnitude of the actual contact areas during the tests (so characteristic of other shear test methods), are eliminated.

Furthermore, since shearing does take place along the contact lines, the test results thus obtained are only affected by the variation in roughness along the one-dimensional contact lines. Consequently, the results more closely reflect the true frictional properties of the tested material. The influence of the sheared surface quality variations, unlike other shear test methods, is essentially eliminated.

The novel test principle effectively utilizes the inherent geometrical features of the system. The applied normal loads produce concentrated normal stresses along the contact lines of the cylindrical specimens. Therefore, shear tests can be conducted at much greater normal stress levels than has been possible with any other type of shear test method.

Combination of these advantages resulted in a shear test procedure that yields a large quantity of highly reliable and consistent test data.

Based on the reliable and consistent test data thus obtained, it is seemingly possible to evolve a new data analysis method. With this new method of analysis, in turn, it is seemingly possible to identify and separate the major shear components.

The properly analysed results of the joint properties tests can also be correlated with the uniaxial and triaxial test data. Consequently, all the major strength and deformation properties of the rocks can be interlinked.

On the basis of the defined interrelationships between the strength properties of the joints and of the rock substance, the shear strength of a jointed rock mass can be established. Both the peak and the residual strength envelopes of a jointed rock mass can be defined, and made practical use of the laboratory test results in the design and stability analysis of underground openings.

In view of its simplicity, the test apparatus is highly versatile. Not only can it be used in a laboratory press, but also it can be used in a portable and simple test frame at the actual mine sites. Normal and shear forces can be provided by hand operated hydraulic pumps. The necessary amount of specimen preparation can also be achieved at the mine sites.

Even though the test apparatus, used for the tests described in this report, was only an in-house-made prototype, it performed very well indeed. The normal displacement measuring device constitutes the only exception. However, the test data analysis procedure proved that measurement of normal displacement is only useful, but not essential. There is, therefore, little need for any modification of the prototype test apparatus.

ACKNOWLEDGEMENT

A considerable number of illustrations was necessary to adequately convey the new testing concept and the procedures used in analysing the data. They were prepared by J. Folta. Her excellent work is greatly appreciated.

The lengthy manuscript with the complex tables was typed by C.D. Baxter. Her accurate and excellent work is highly praised.

Sincere appreciation is also due to B. Gorski for his excellent and untiring efforts in first producing the test apparatus, and then assisting with the tests.

REFERENCES

1. Gyenge, M. "Laboratory test requirements for post-failure strength properties of rocks"; Division Report MRP/MRL 82-33(TR); CANMET, Energy, Mines and Resources Canada; 1982.

2. Gorski, B. "The design and operation of a stiff triaxial assembly for post-failure rock property testing"; Division Report MRP/MRL 82-81(TR); CANMET, Energy, Mines and Resources Canada; 1982.

3. Stimpson, B. "A suggested technique for determining the basic friction angle of rock surfaces using core"; Int. J. Rock Mech Min Sci; 18; 63-65; 1981.

4. Gorski, B. "A multi-shear apparatus"; Division Report MRP/MRL 84-44(TR); CANMET, Energy, Mines and Resources Canada; 1984.

5. Timoshenko, S. and Goodier, J.M. "Theory of elasticity"; Engineering Societies Monographs, Second Edition, International Student Edition; pp 381-382; McGraw-Hill Book Co. Inc.; New York; 1951.

6. Nam P. Suh and H.C. Sin, "The genesis of friction"; Wear; 69; pp. 91-114; Elsevier Sequois S.A., Lausanne, Switzerland; 1981.

7. Patton, F.D. "Multiple modes of shear failure in rock"; Proc. 1st Congr. ISRM; Vol. 1. pp 509-513; Lisbon; 1966.

8. Jackson, R. "Summary of mechanical properties of Lac Du Bonnet and Eye-Dashwa specimens"; Division Report MRP/MRL 84-85(TR); CANMET, Energy, Mines and Resources Canada, 1984.

9. Gyenge, M. "Confined shear test method to establish the frictional and strength properties of jointed rocks"; Division Report MRP/MRL 85-62(INT); CANMET, Energy, Mines and Resources Canada, 1985.

10. Shimotani, T. "Evaluation of testing procedures for minimizing rock sample requirement"; Division Report MRP/MRL 83-19(INT); CANMET, Energy, Mines and Resources Canada; 1983.

11. Bétournay, M. and Shimotani, T. "Triaxial properties of Indiana limestone"; Division Report ERP/MRL 83-99(TR); CANMET, Energy, Mines and Resources Canada; 1983.

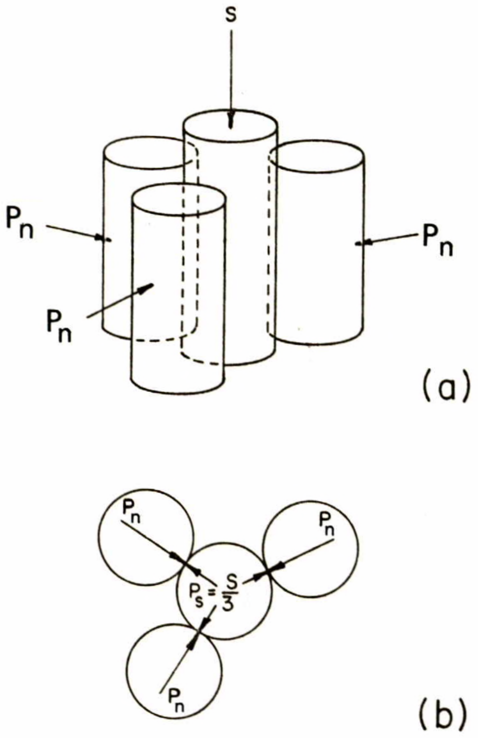

Fig. 1 - Principle of confined shear test method; (a) isometric view of specimen set, (b) top view of specimen set.

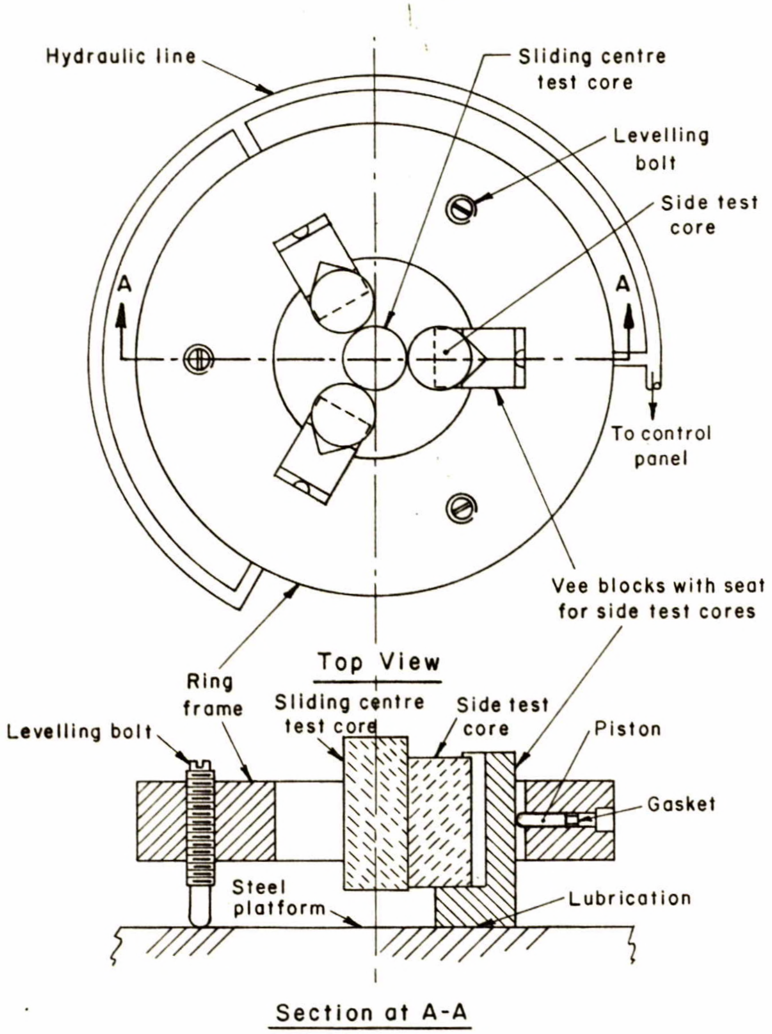

Fig. 2 - Test apparatus; (a) top view, (b) section.

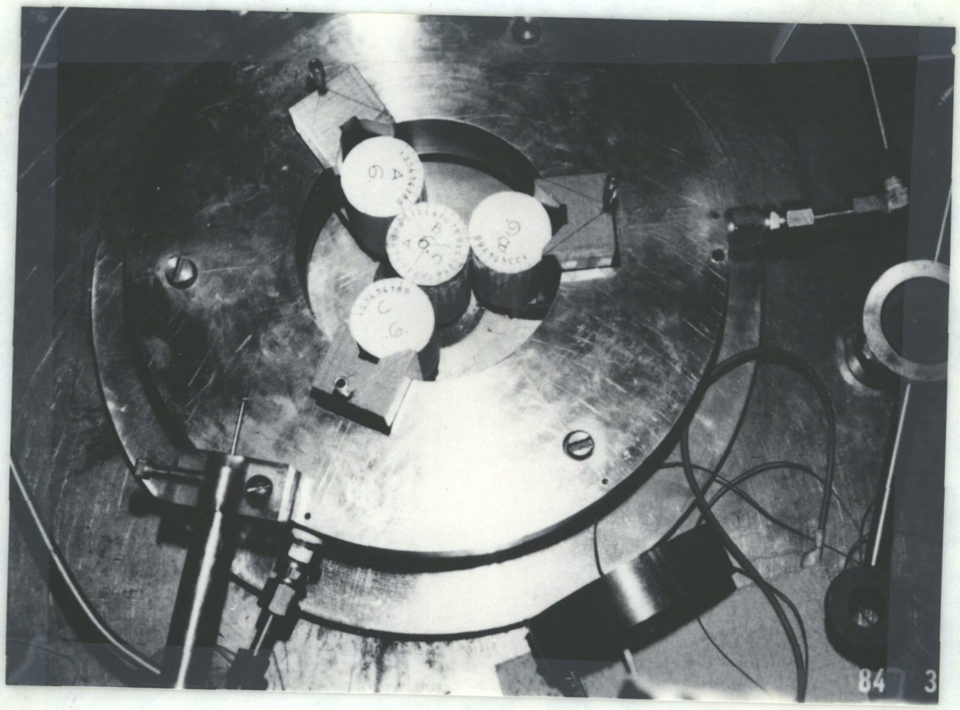

Fig. 3 - Photograph of test apparatus with specimen cores and with device to measure normal displacement.

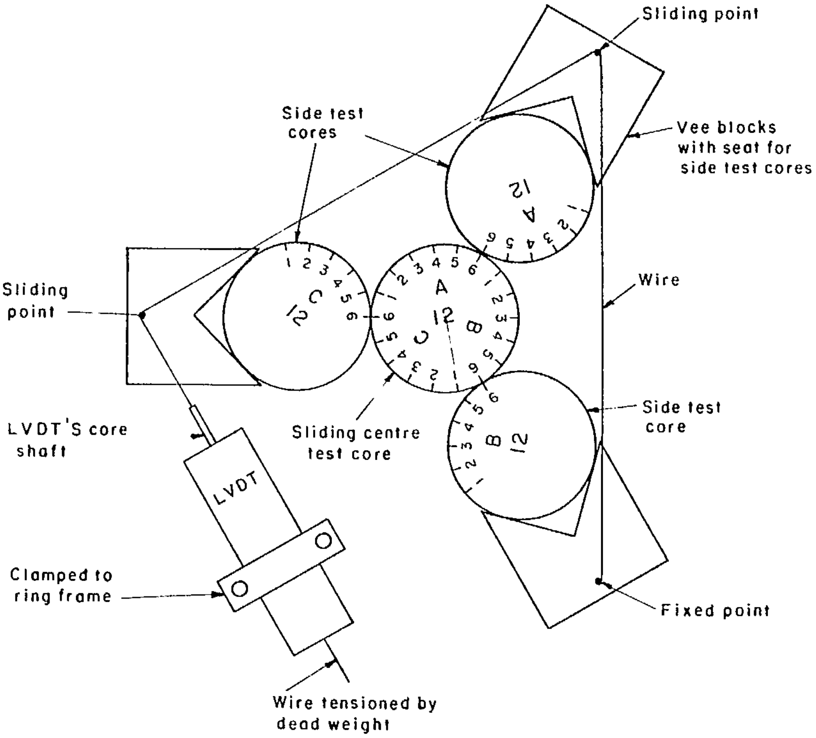

Fig. 4 - Arrangement for measurement of normal displacement

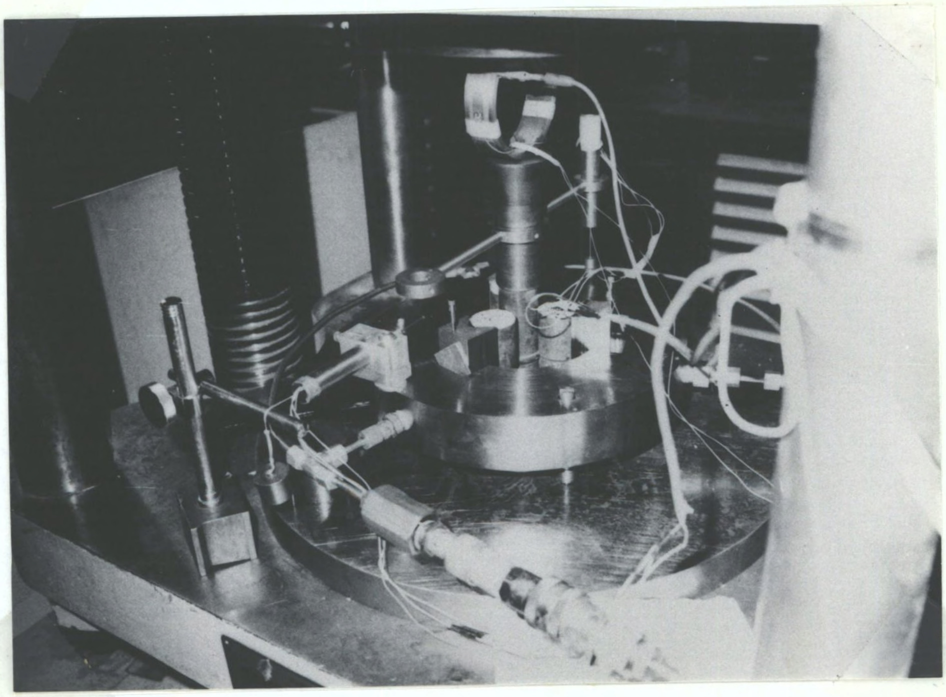

Fig. 5 - Test set-up in conjunction with the laboratory press.

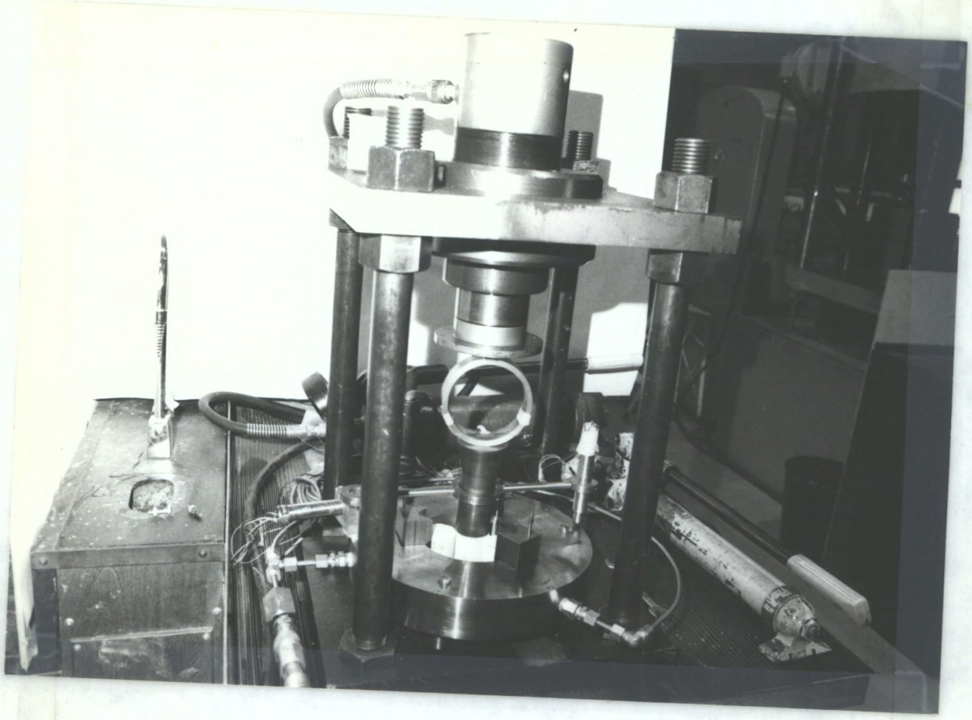

Fig. 6 - Test set-up in conjunction with a portable field press.

Fig. 7 - Surface grinding in machinist-lathe.

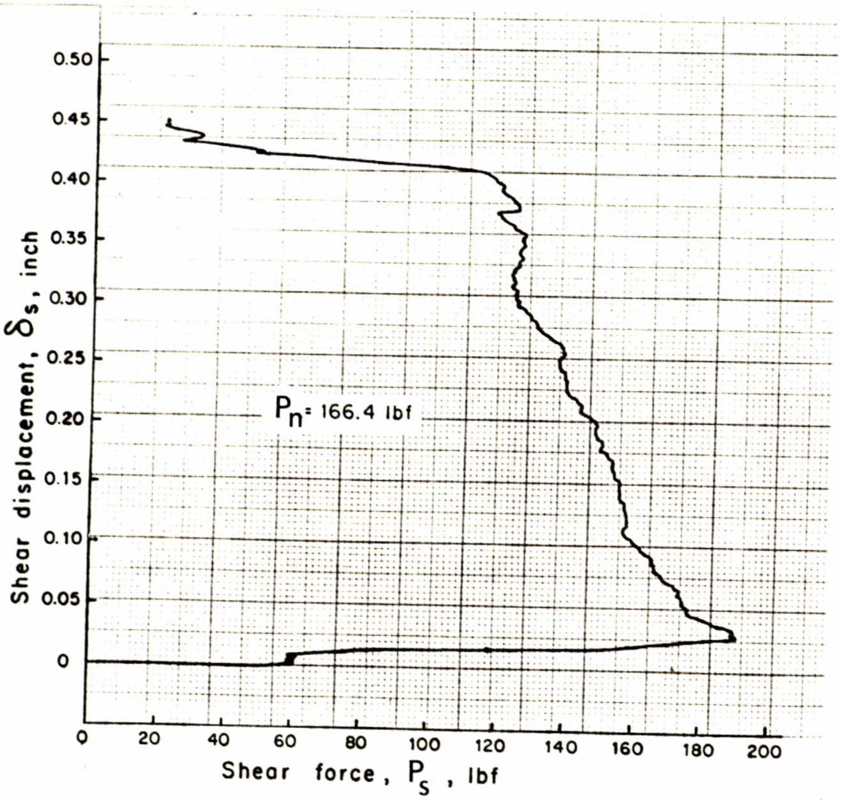

Fig. 8 - Record of test result obtained for steel specimen set with large single asperity.

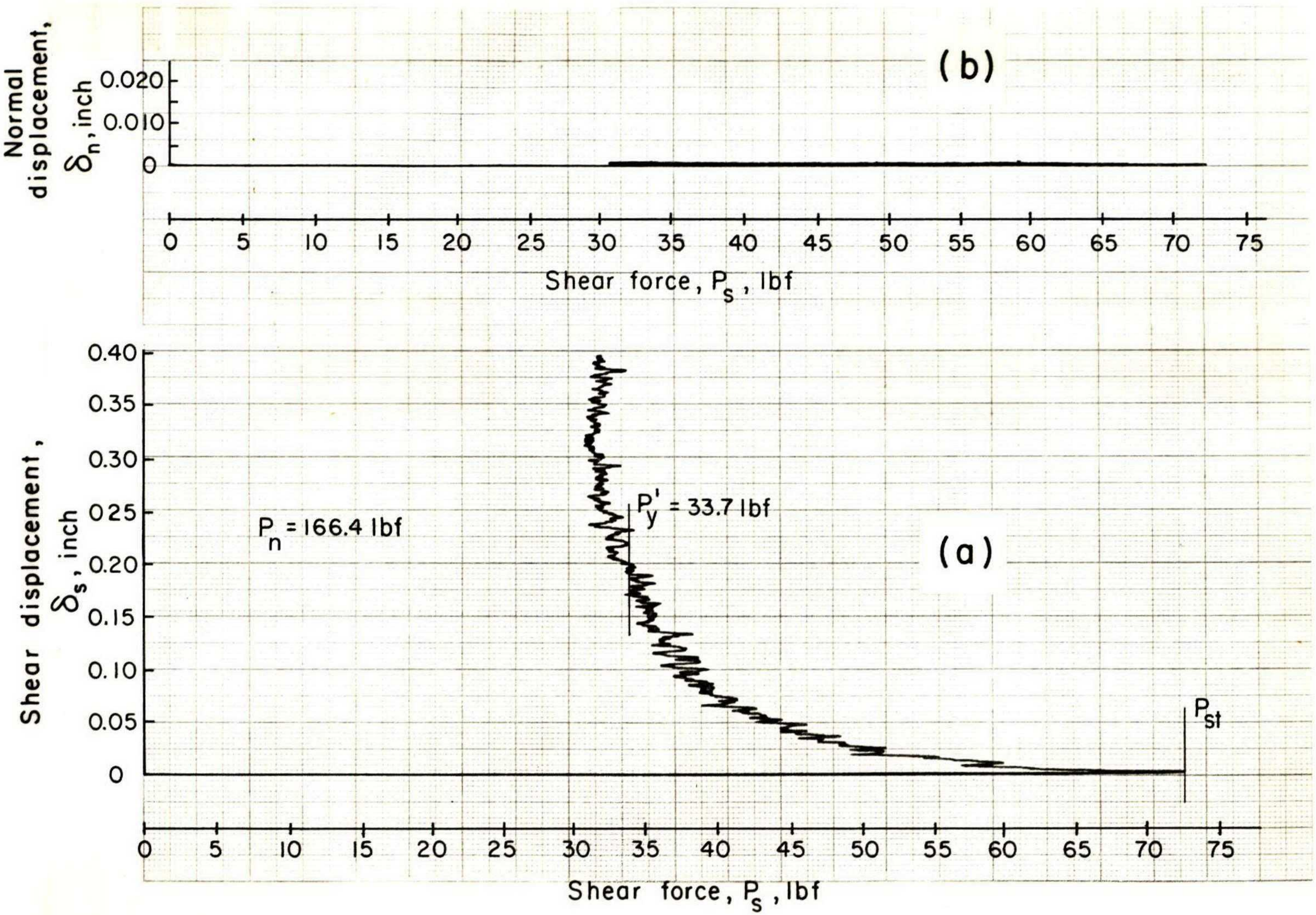

Fig. 9 Records of test results obtained by the initial test run on smooth specimen set; (a) shear force versus shear shear displacement, (b) shear force versus normal displacement.

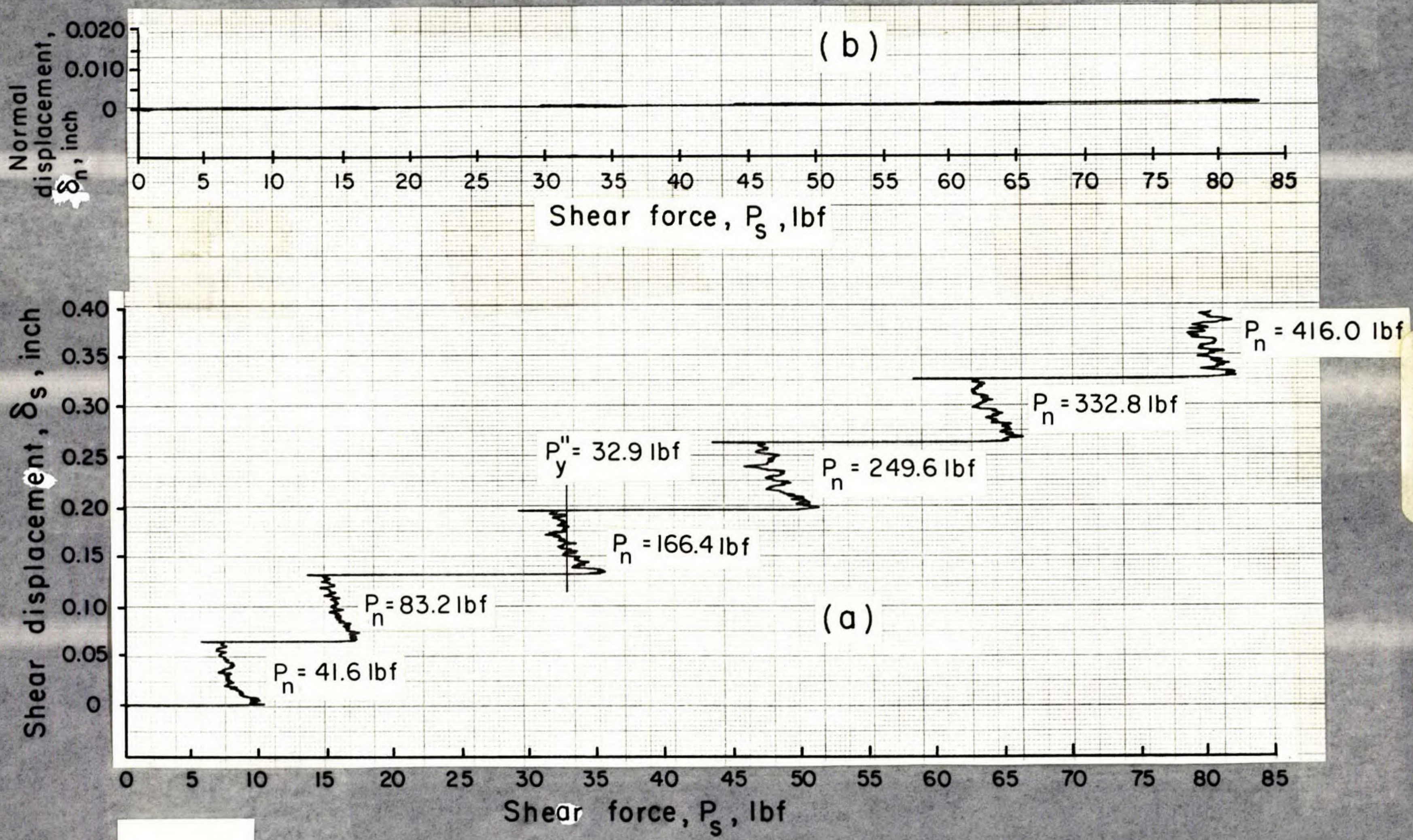

Fig. 10 - Records of test results obtained by multi-stage procedure on smooth steel specimen set; (a) shear force versus shear displacement, (b) shear force versus normal displacement.

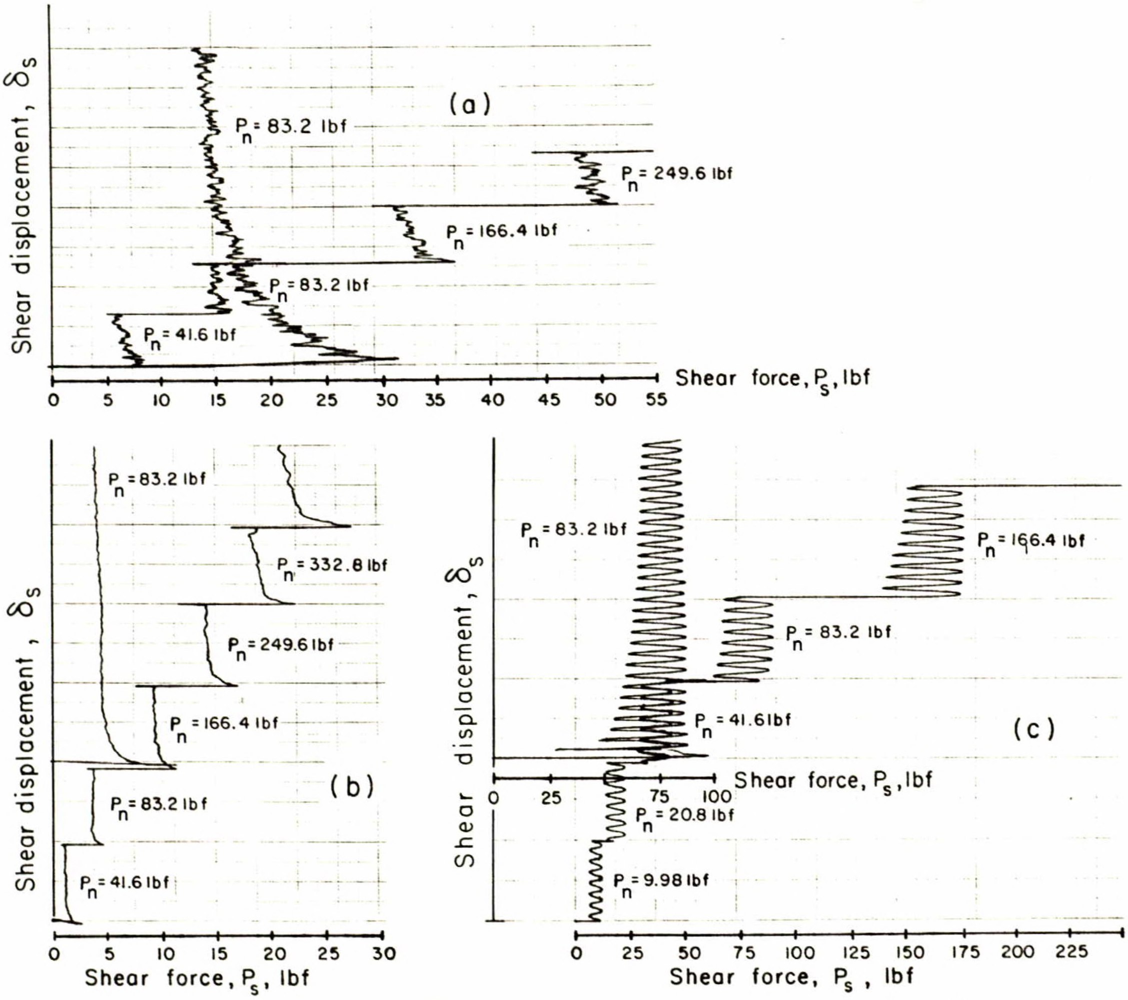

Fig. 11 - Typical test results obtained for various materials; (a) steel, (b) teflon, (c) granite.

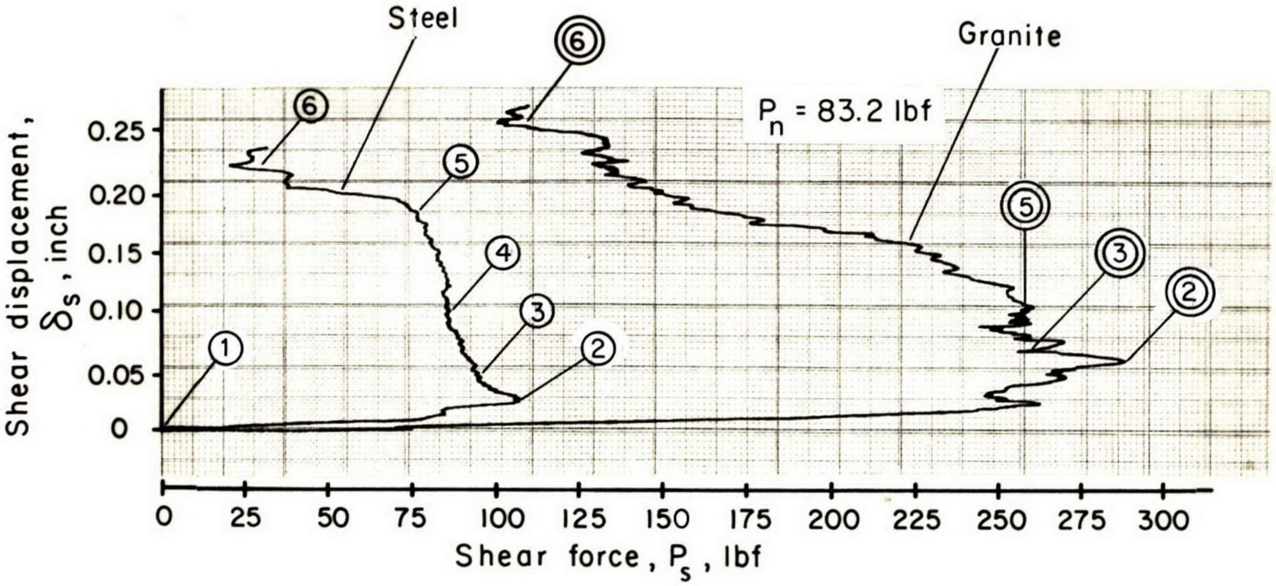

Fig. 12 - Typical test results obtained for steel and granite specimen sets with large single asperity sliding contacts.

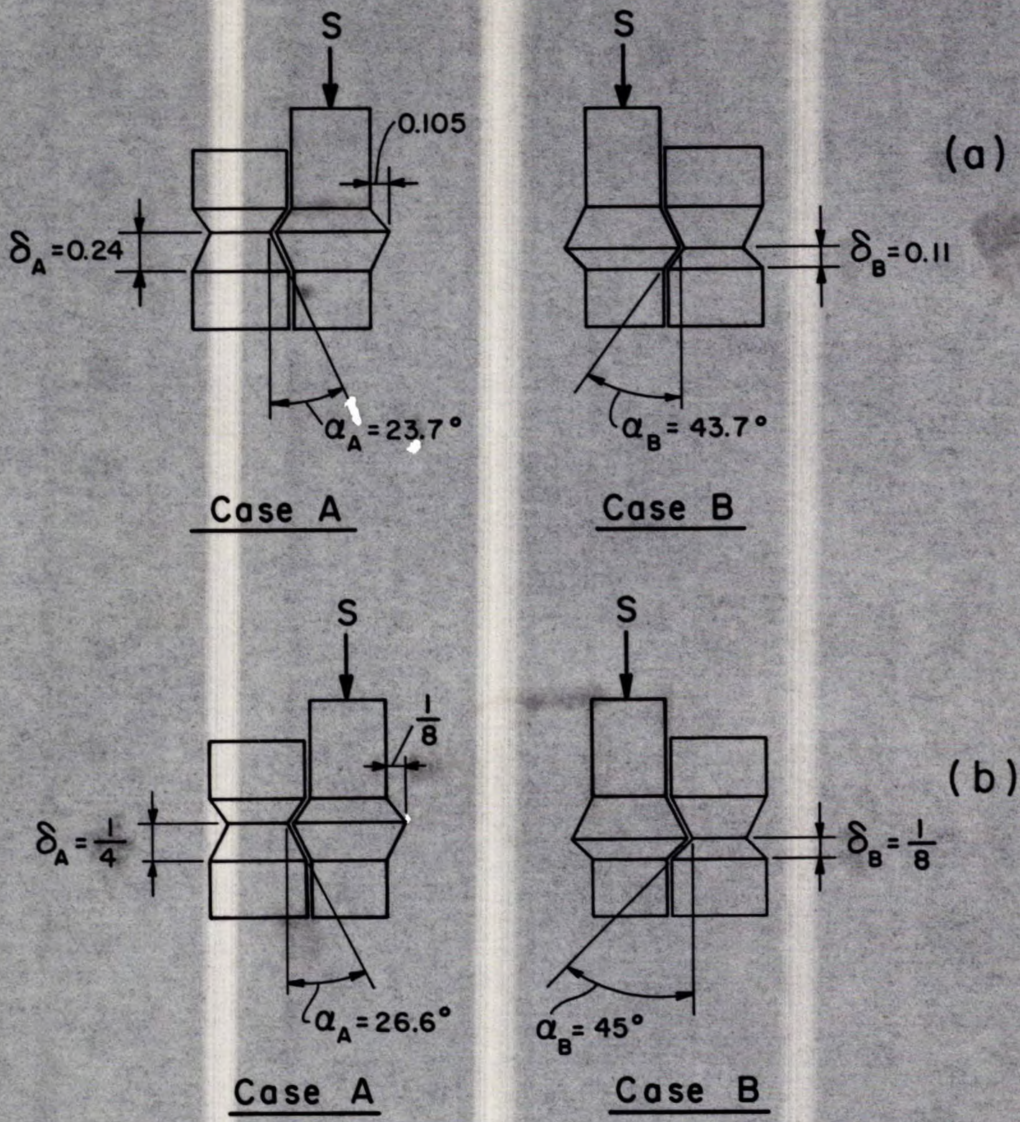

Fig. 13 - Dimensions of the simulated large single asperity and the directions of shearing; (a) for steel specimens, (b) for granite specimens

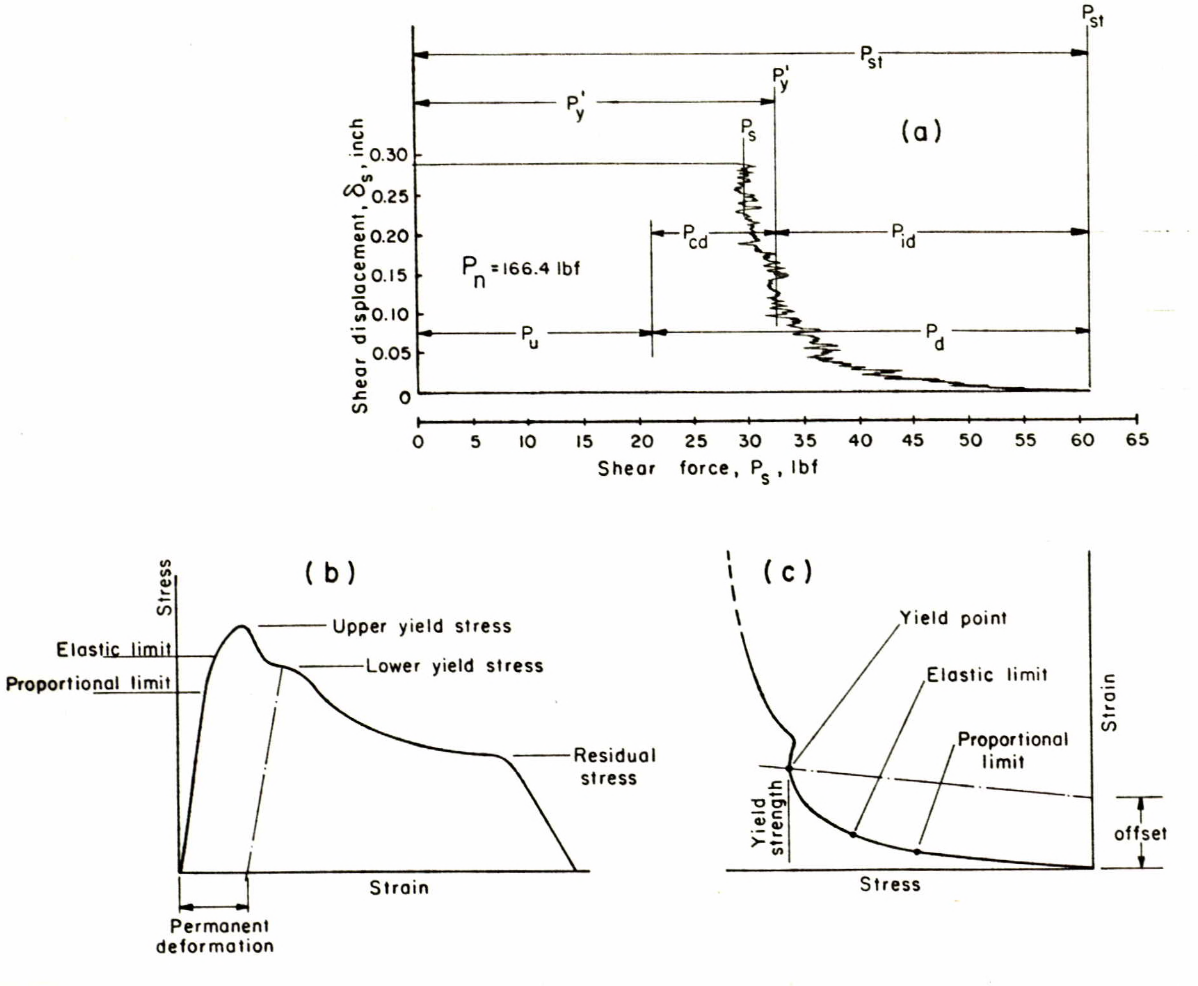

Fig. 14 - Essential relationships based on the shear test data; (a) recorded graph of shear test data, (b) typical complete stress-strain curve, (c) stress-strain curve for conventional steel testing.

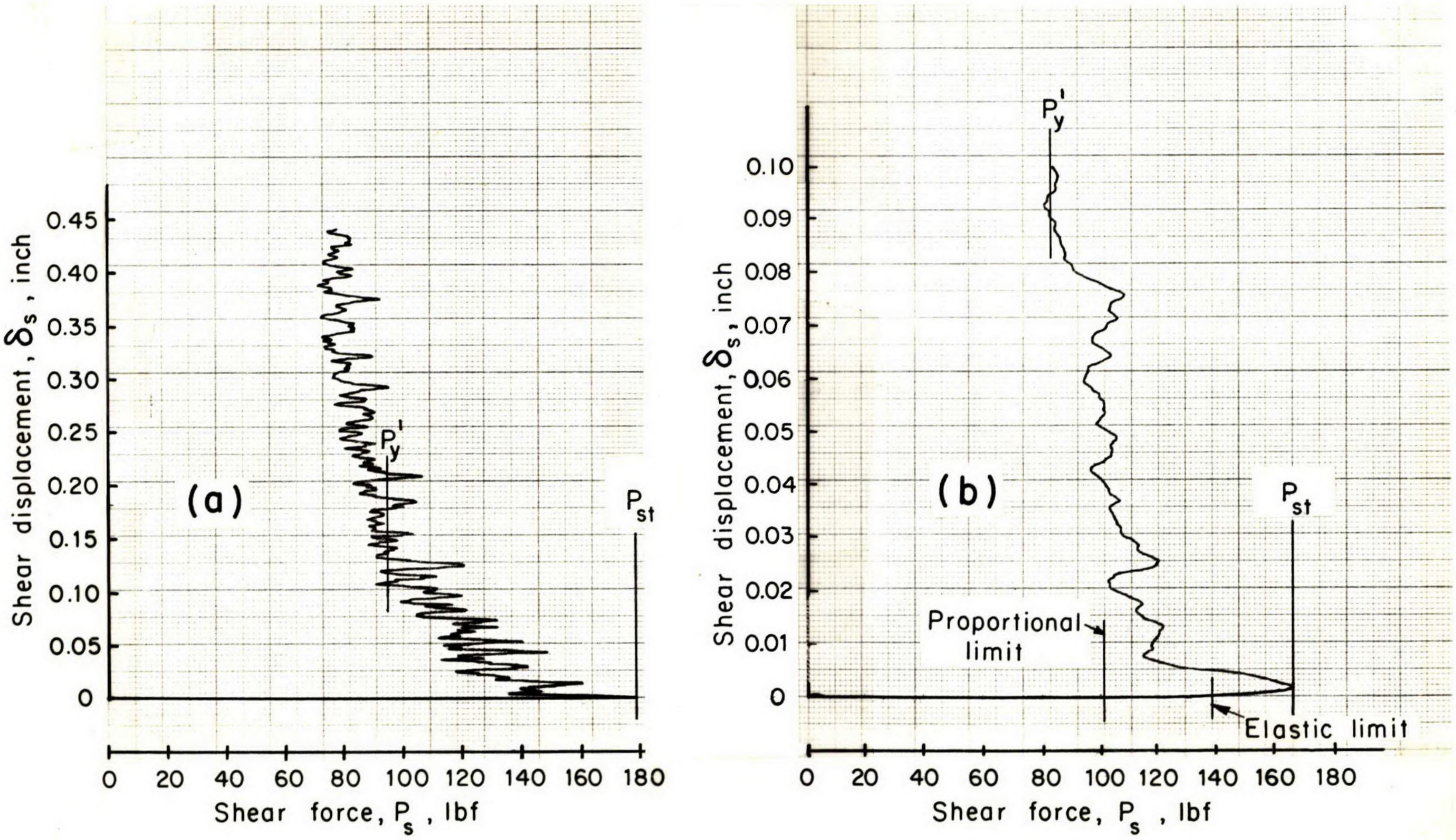

Fig. 15 - Shear test data of two tests with different scale of shear displacement; (a) 5.1×10^{-3} inch/div., (b) 1.02×10^{-3} inch/div.

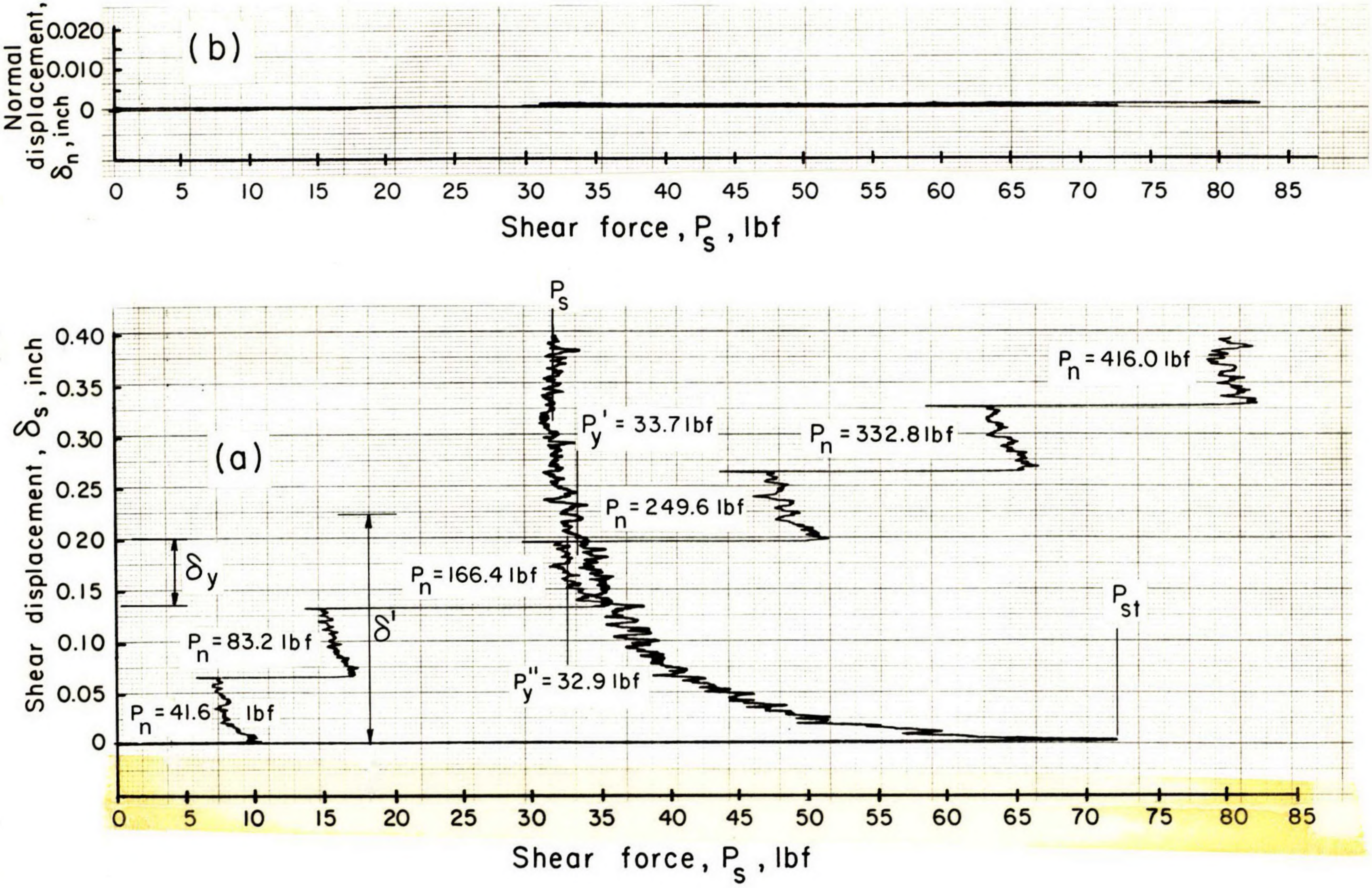

Fig. 16 - Recorded graphs of the initial and multi-stage test runs; (a) shear force versus shear displacement, (b) shear force versus normal displacement.

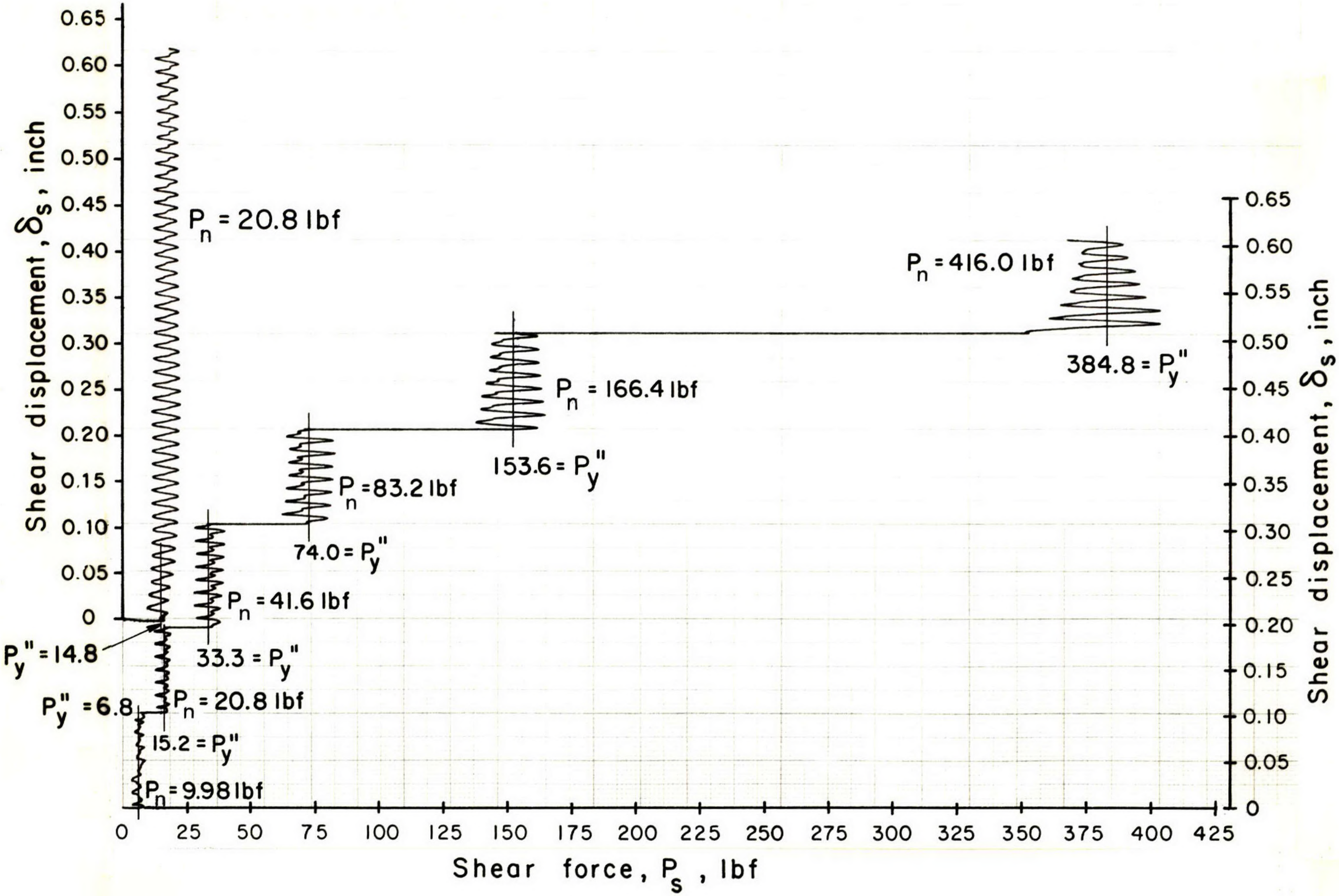

Fig. 17 - Recorded graphs of the initial and multi-stage test runs for granite specimens with smooth sliding contact lines

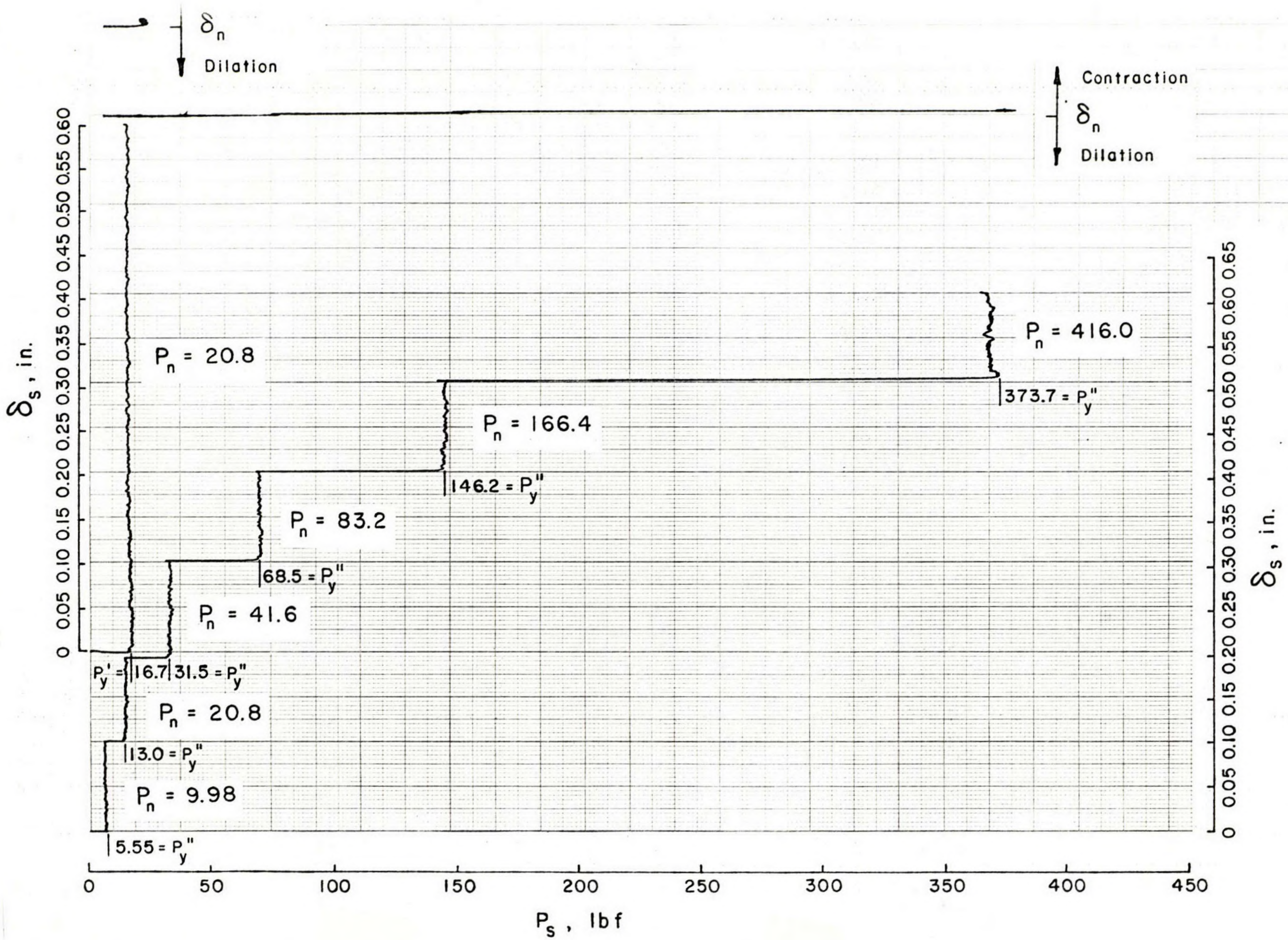

Fig. 18 - Recorded graphs of the initial and multi-stage test runs for sandstone specimens with smooth sliding contact lines.

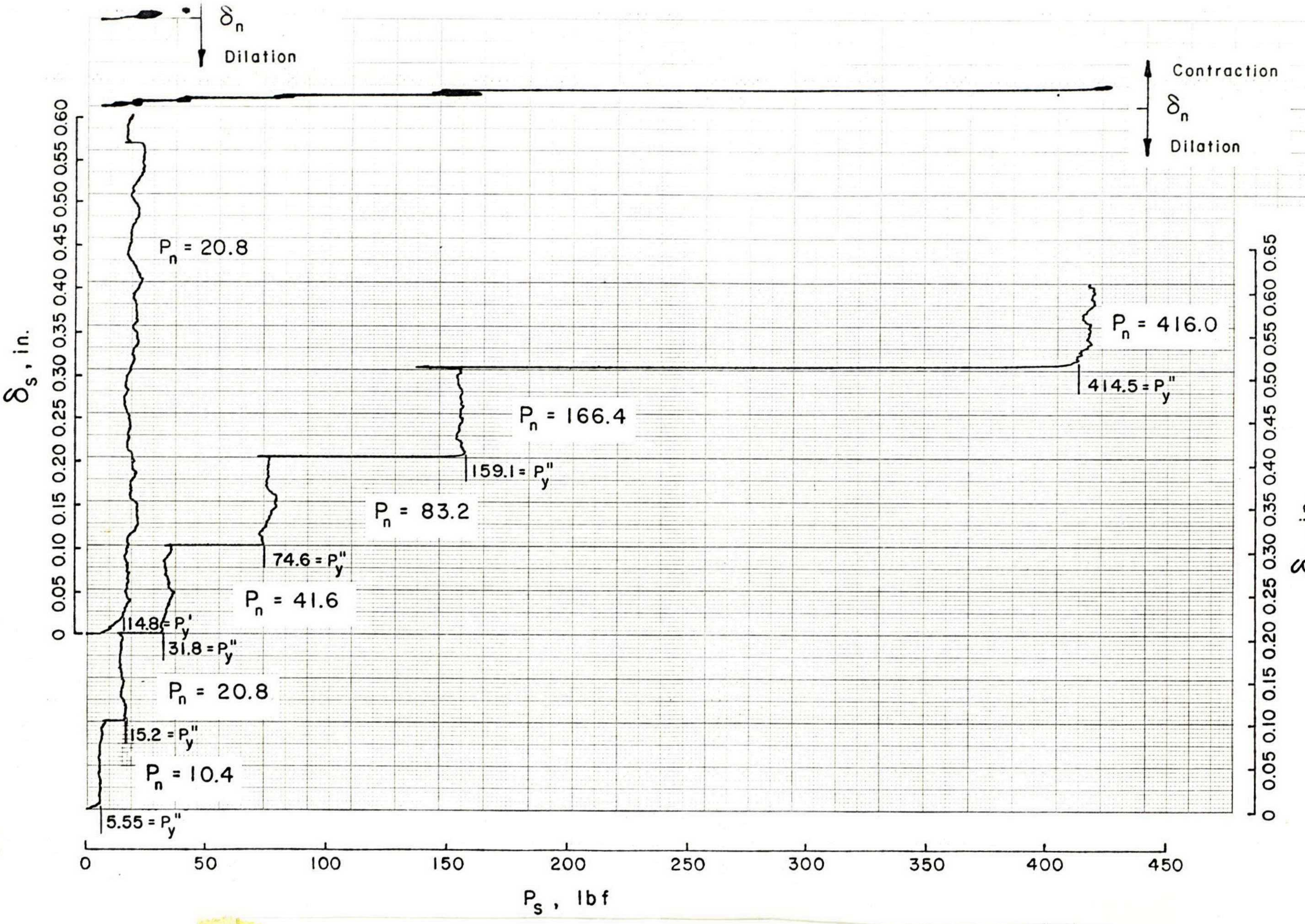

Fig. 19 - Recorded graphs of initial and multi-stage test runs for Indiana limestone specimens with smooth sliding contact lines.

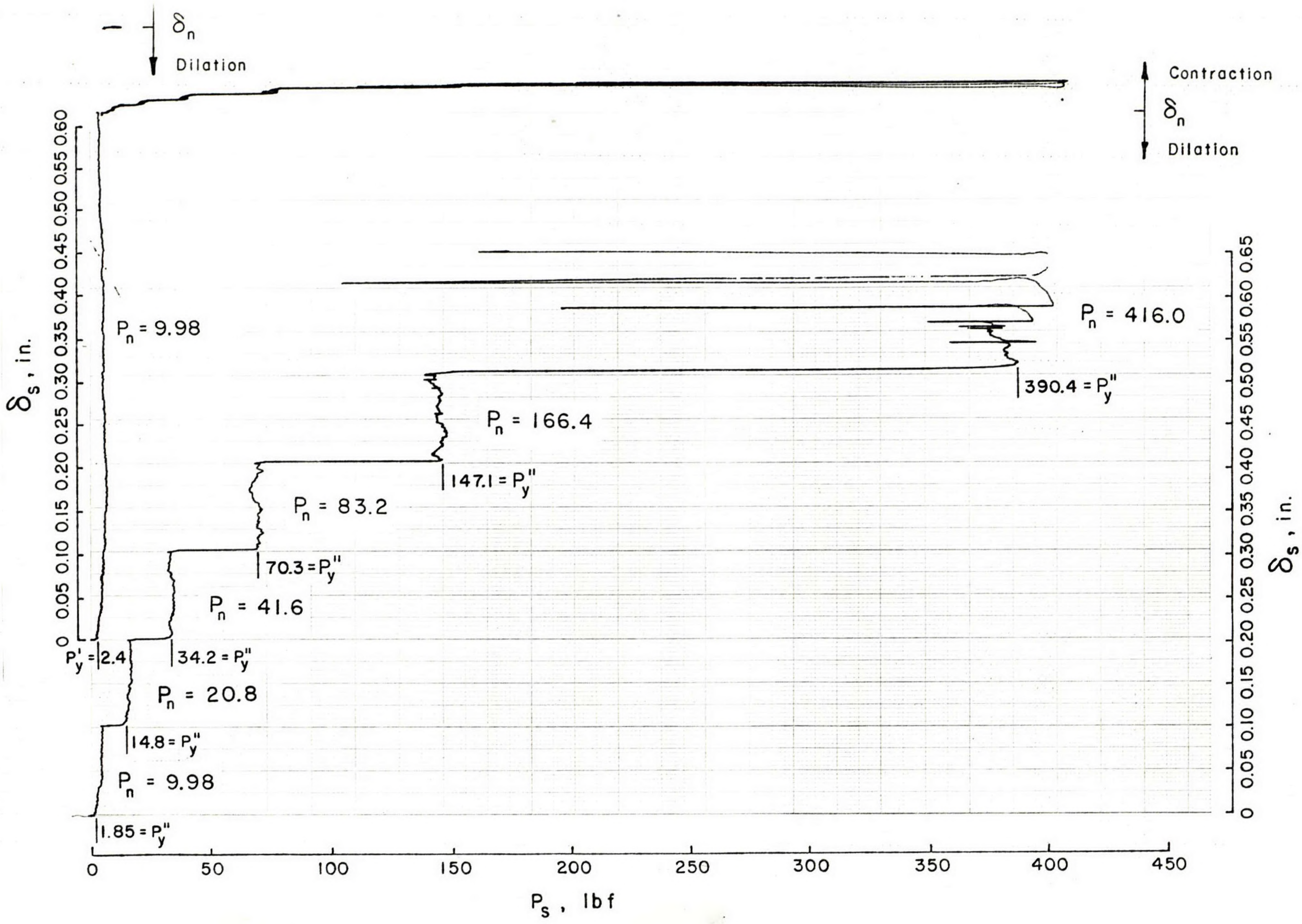

Fig. 20 - Recorded graphs of the initial and multi-stage tests runs for diabase specimens with smooth sliding contact lines.

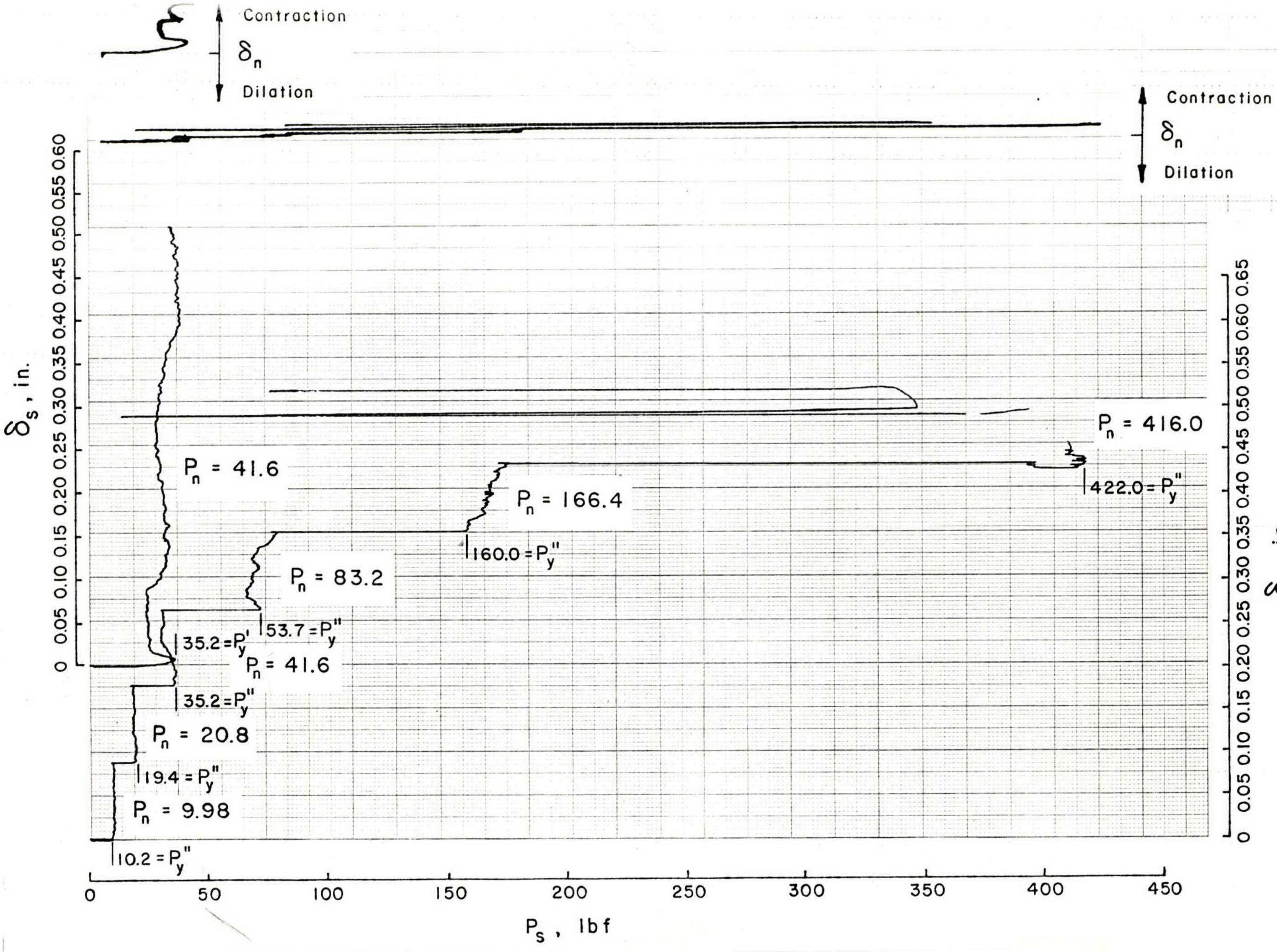

Fig. 21 - Recorded graphs of the initial and multi-stage test runs for INCO ore specimens with smooth sliding contact lines.

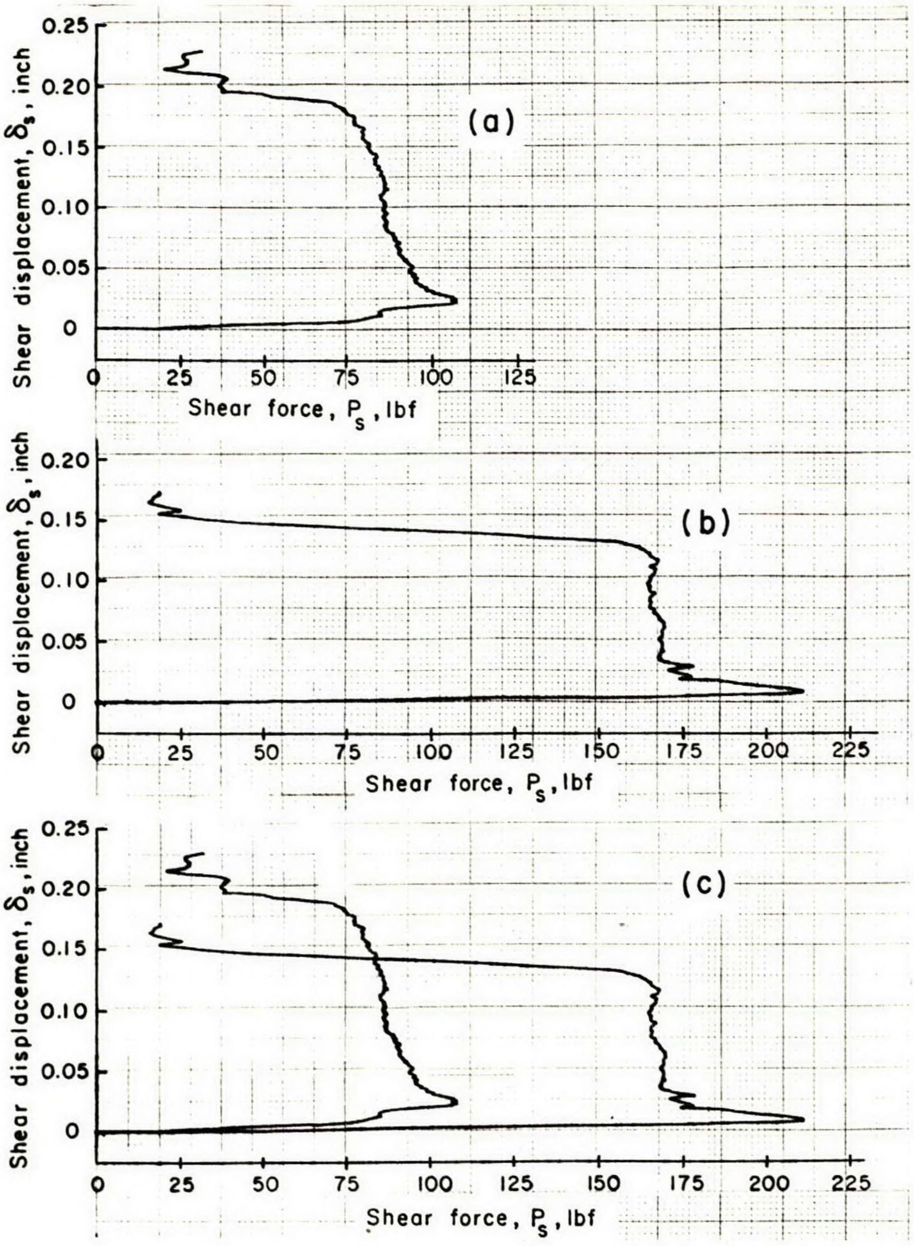

Fig. 22 - Typical records of shear tests conducted on steel specimens with large single asperity; (a) shear direction Case A; (b) shear direction Case B, (c) graphs are superimposed by repeated photocopy exposure method.

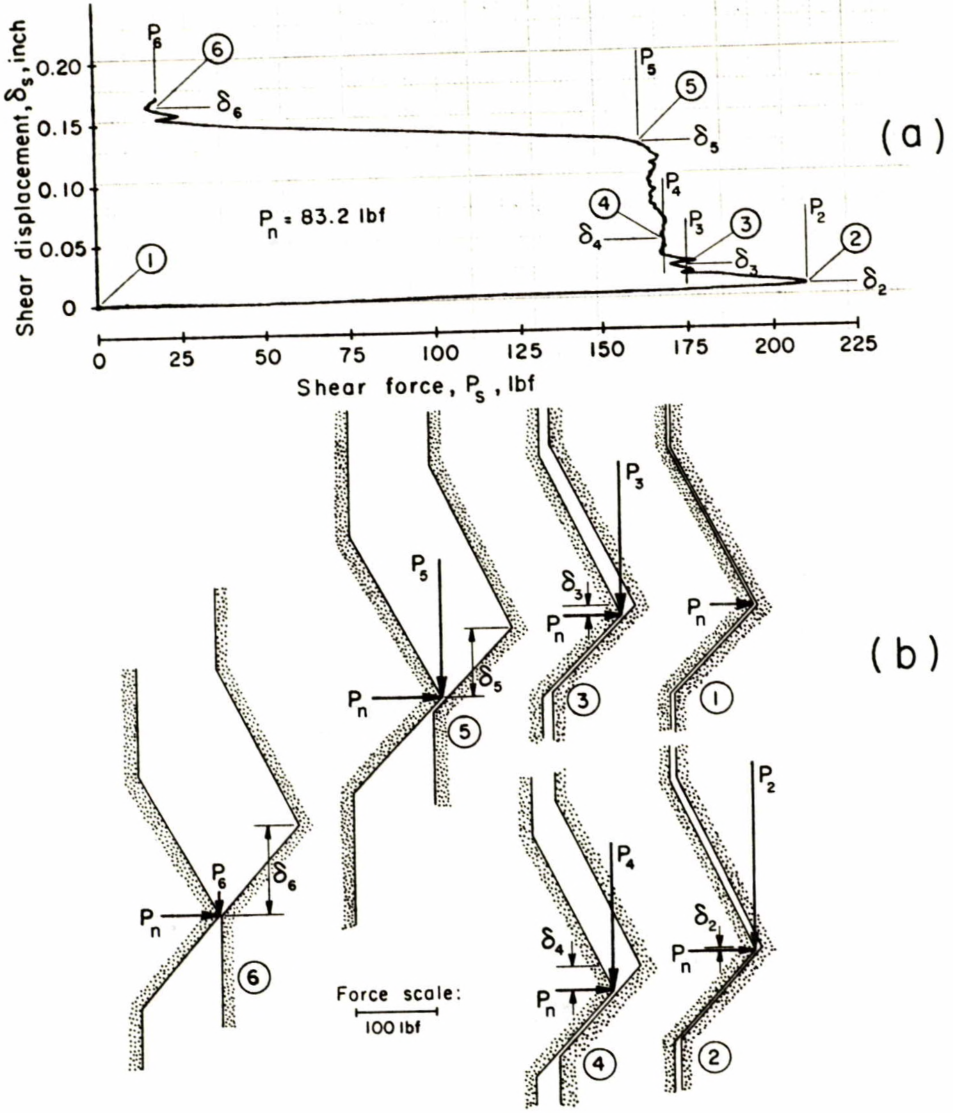

Fig. 23 - Detailed analysis of a Case B test run performed on steel specimens with single large asperity; (a) recorded test graph, (b) rigid body demonstration.

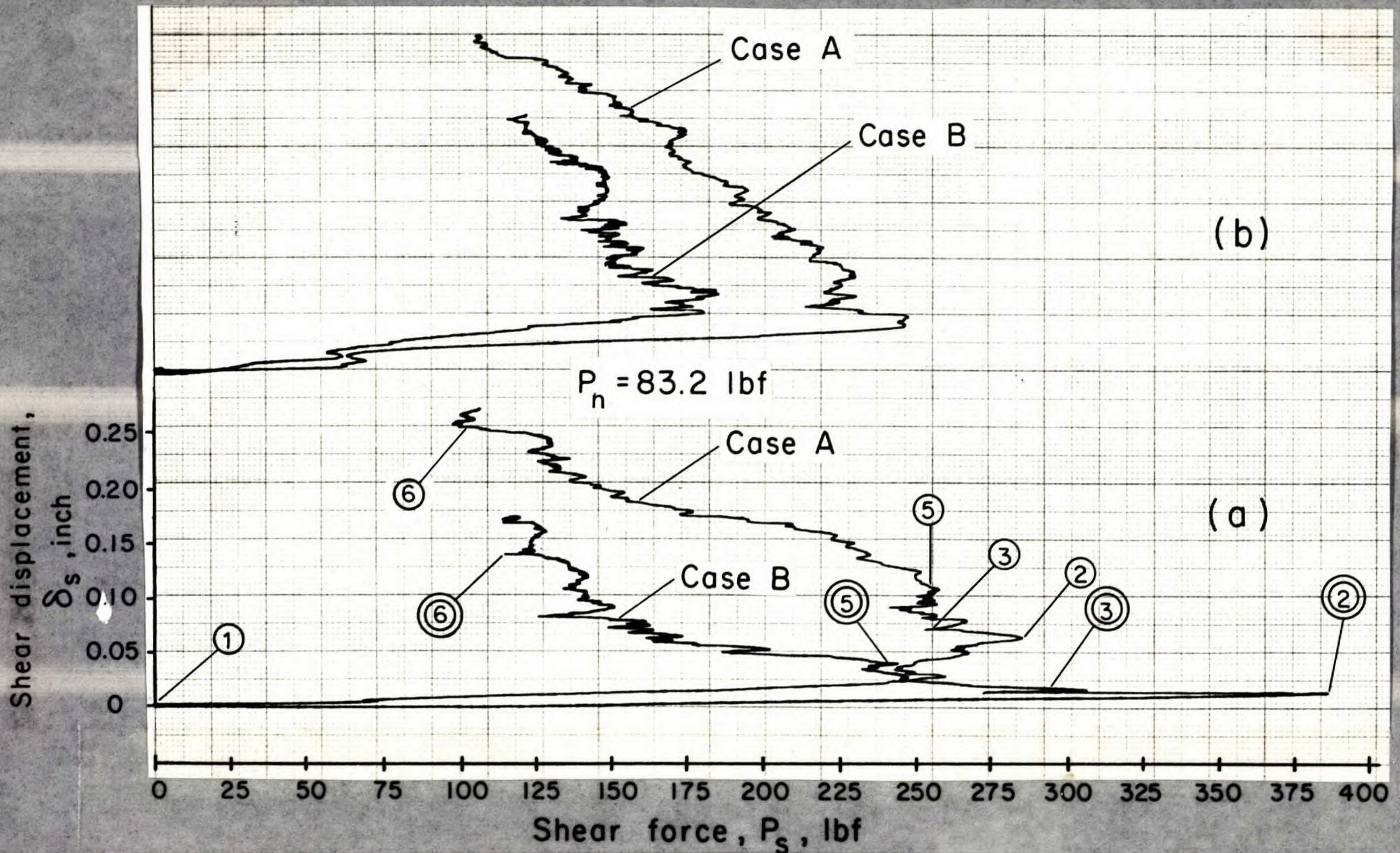

Fig. 24 - Comparison of test graphs obtained for granite tested in shear directions Case A and Case B; (a) first test runs, (b) repeated test runs.

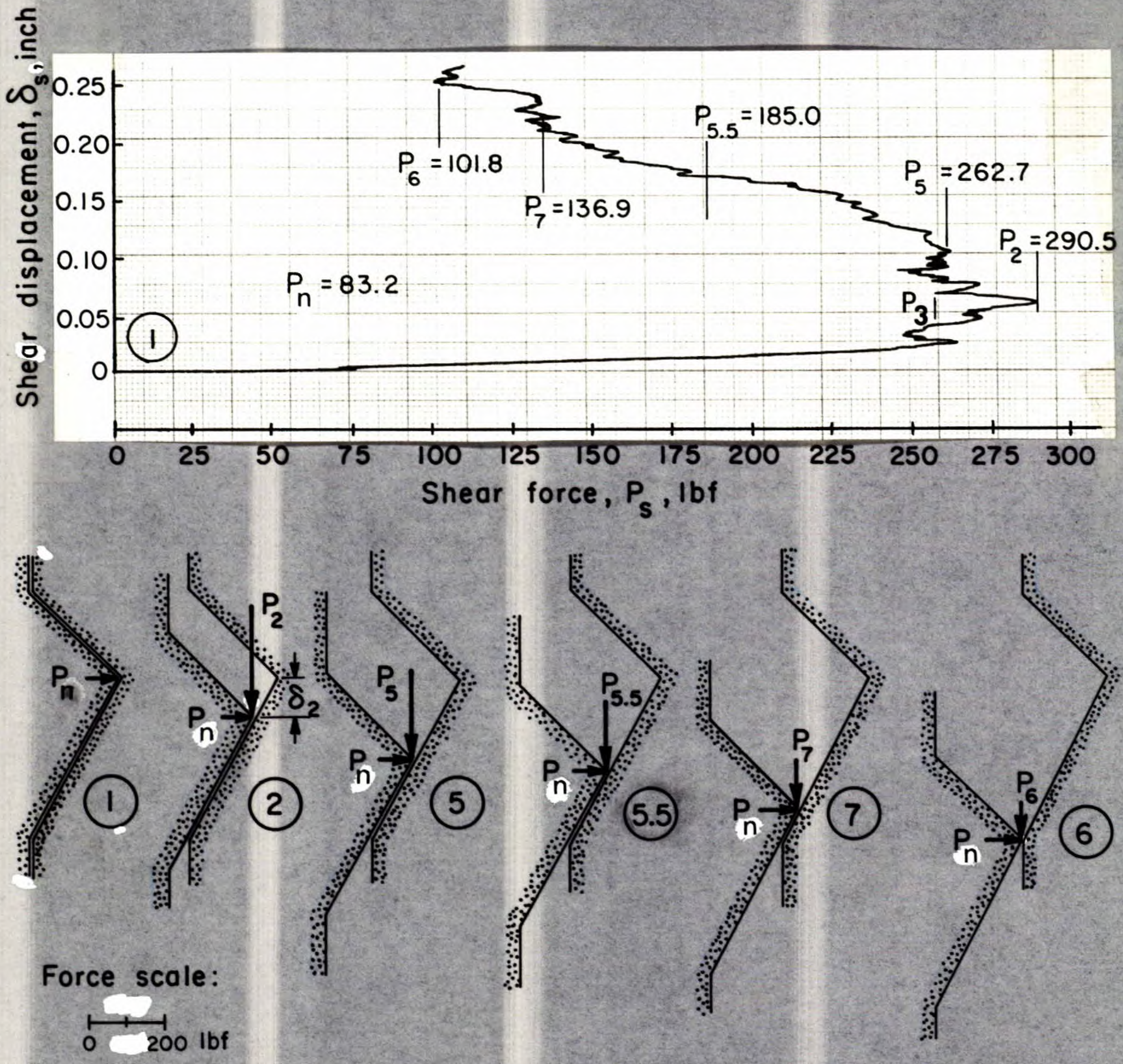

Fig. 25 - Detailed analysis of a test run performed on granite specimens with single large asperity tested in shear direction Case A.

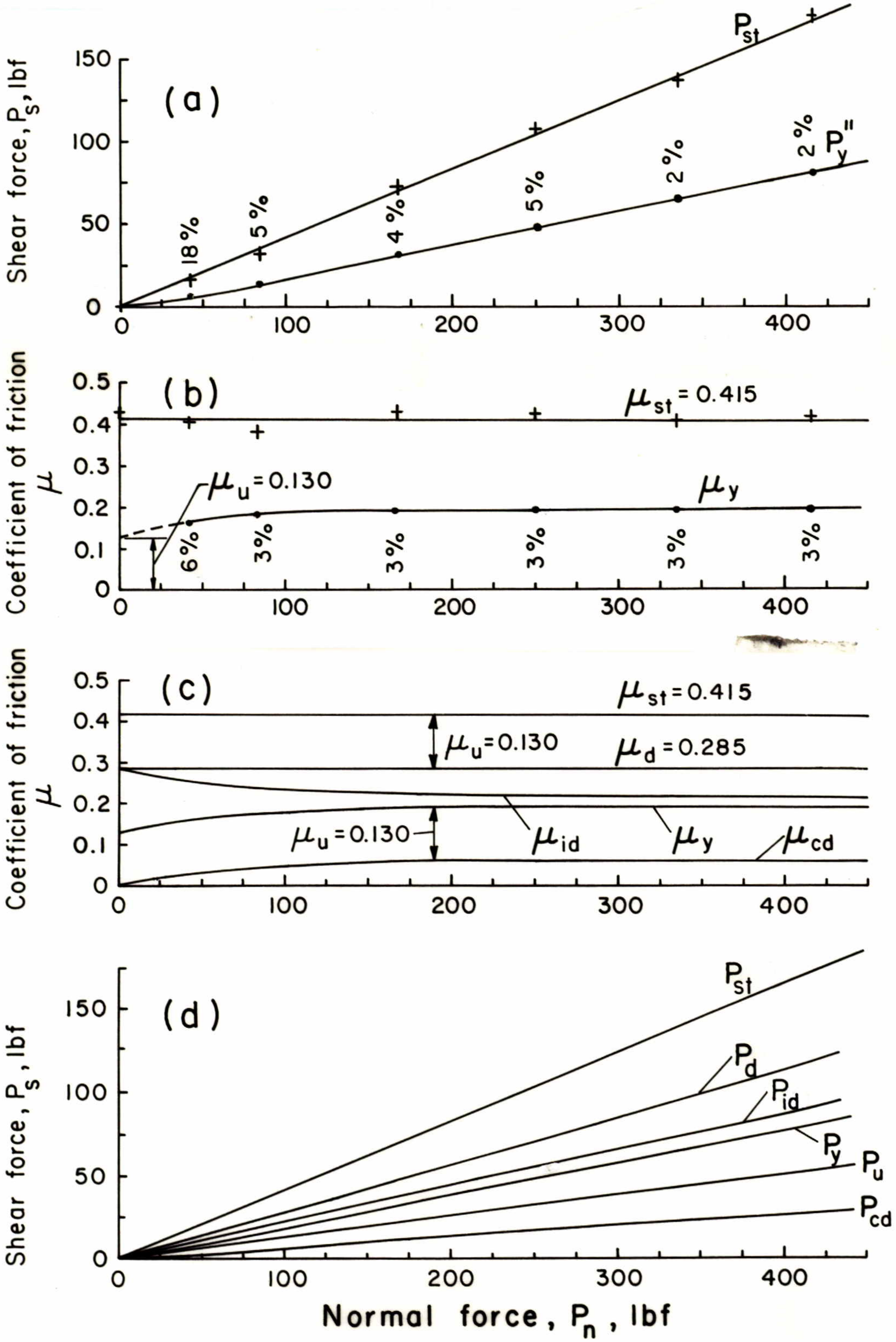

Fig. 26 - Variation of the shear force and coefficient of friction components for steel specimens with smooth sliding contact lines tested in dry condition; (a) measured shear forces, (b) calculated coefficients from measurements, (c) components of coefficients, (d) components of shear forces.

$$\mu_{st} = \mu_y + \mu_{id} \qquad \tau_{st} = (\mu_y + \mu_{id})\,\sigma_n$$

$$\mu_y = \mu_u + \mu_{cd} \qquad \tau_y = (\mu_u + \mu_{cd})\,\sigma_n$$

$$\mu_{st} = \mu_u + \mu_d \qquad \tau_{st} = (\mu_u + \mu_d)\,\sigma_n$$

$$\mu_d = \mu_{id} + \mu_{cd} \qquad \tau_d = (\mu_{id} + \mu_{cd})\,\sigma_n$$

$$\mu_{st} = \mu_u + \mu_{cd} + \mu_{id} \qquad \tau_{st} = (\mu_u + \mu_{cd} + \mu_{id})\,\sigma_n$$

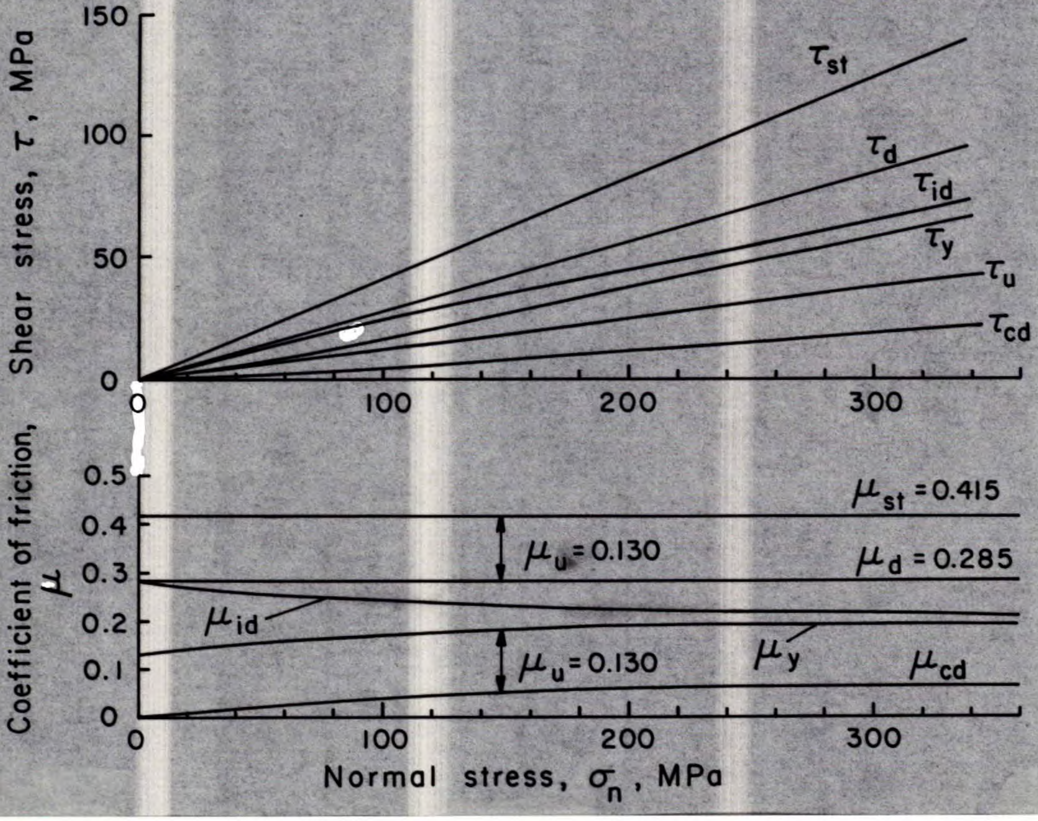

Fig. 27 - Coefficient of friction components versus normal stress and shear stress components versus normal stress for steel specimens with smooth sliding contact lines tested in dry condition.

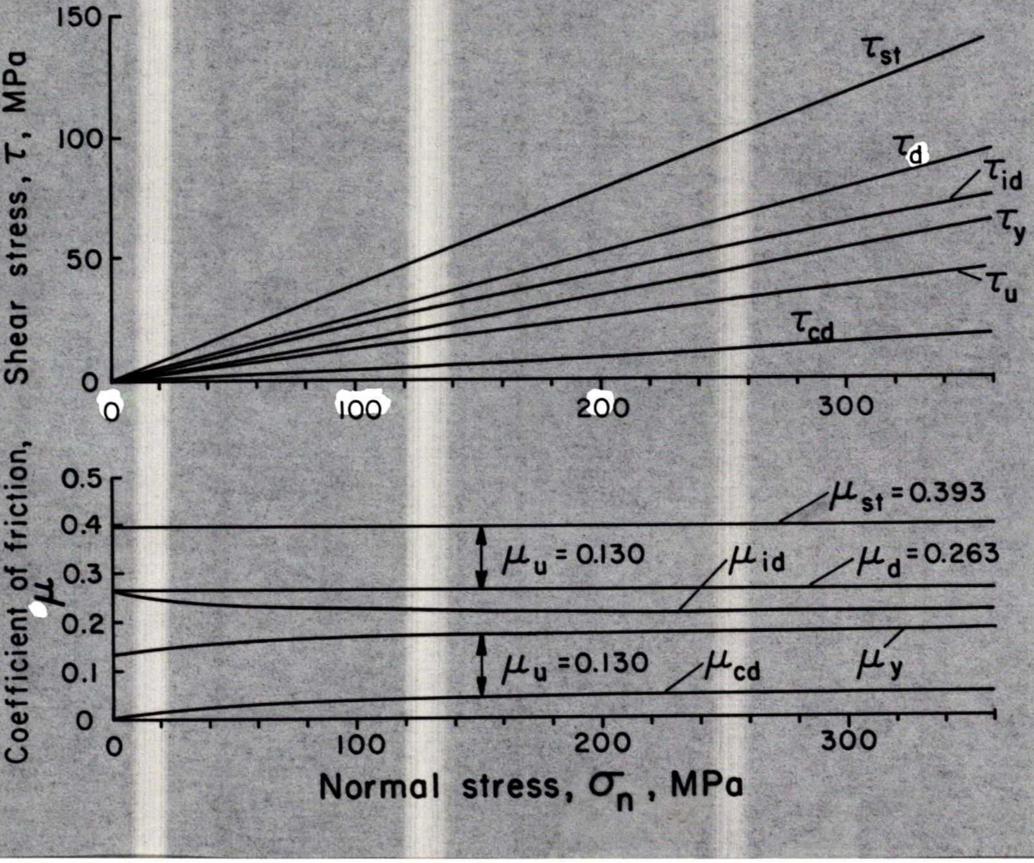

Fig. 28 - Coefficient of friction components versus normal stress and shear stress components versus normal stress for steel specimens with smooth sliding contact lines tested in lubricated condition.

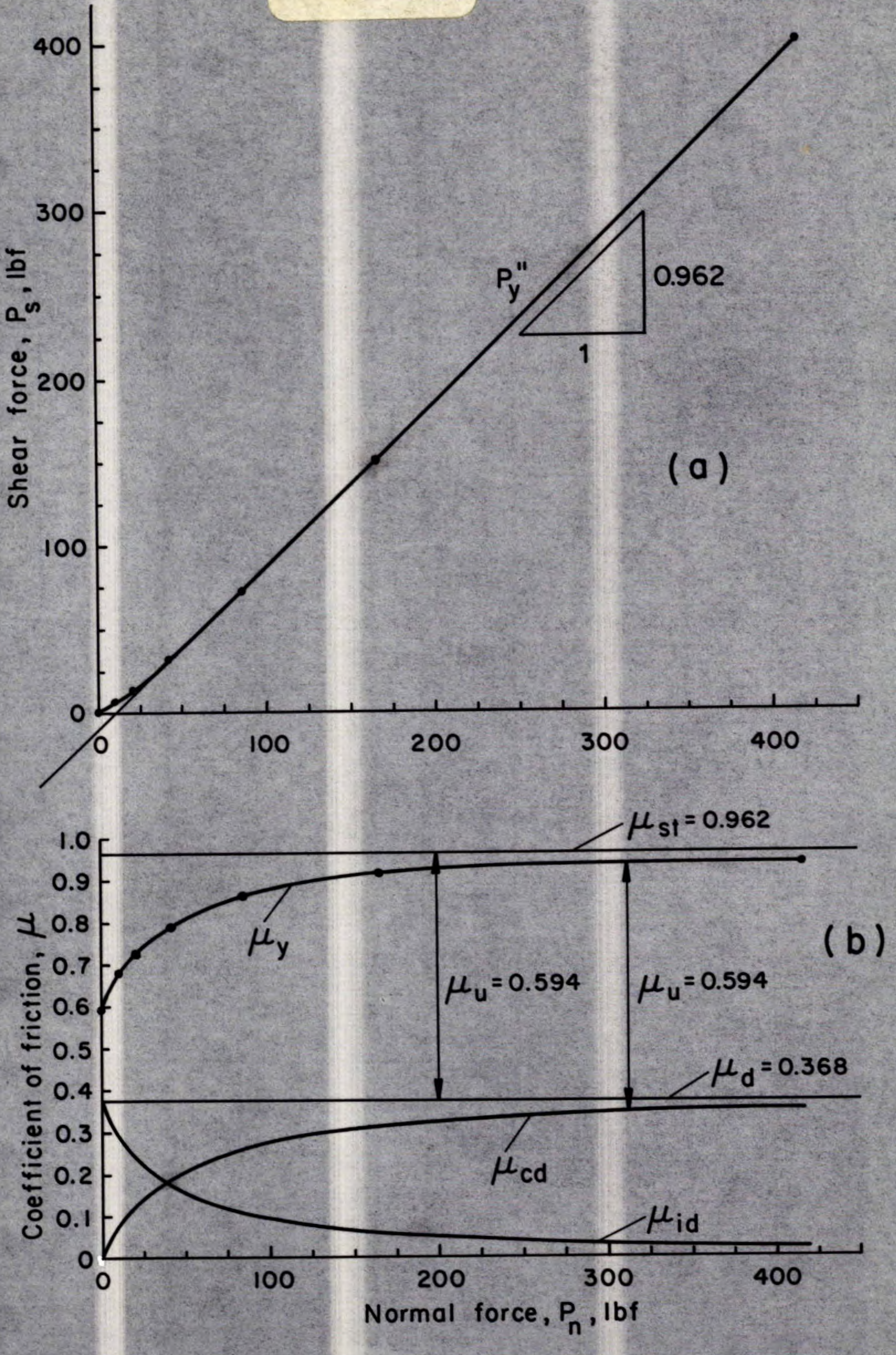

Fig. 29 - Variation of shear force and coefficient of friction components for granite specimens with smooth sliding contact; (a) mean value of measured shear force, (b) components of coefficient of friction.

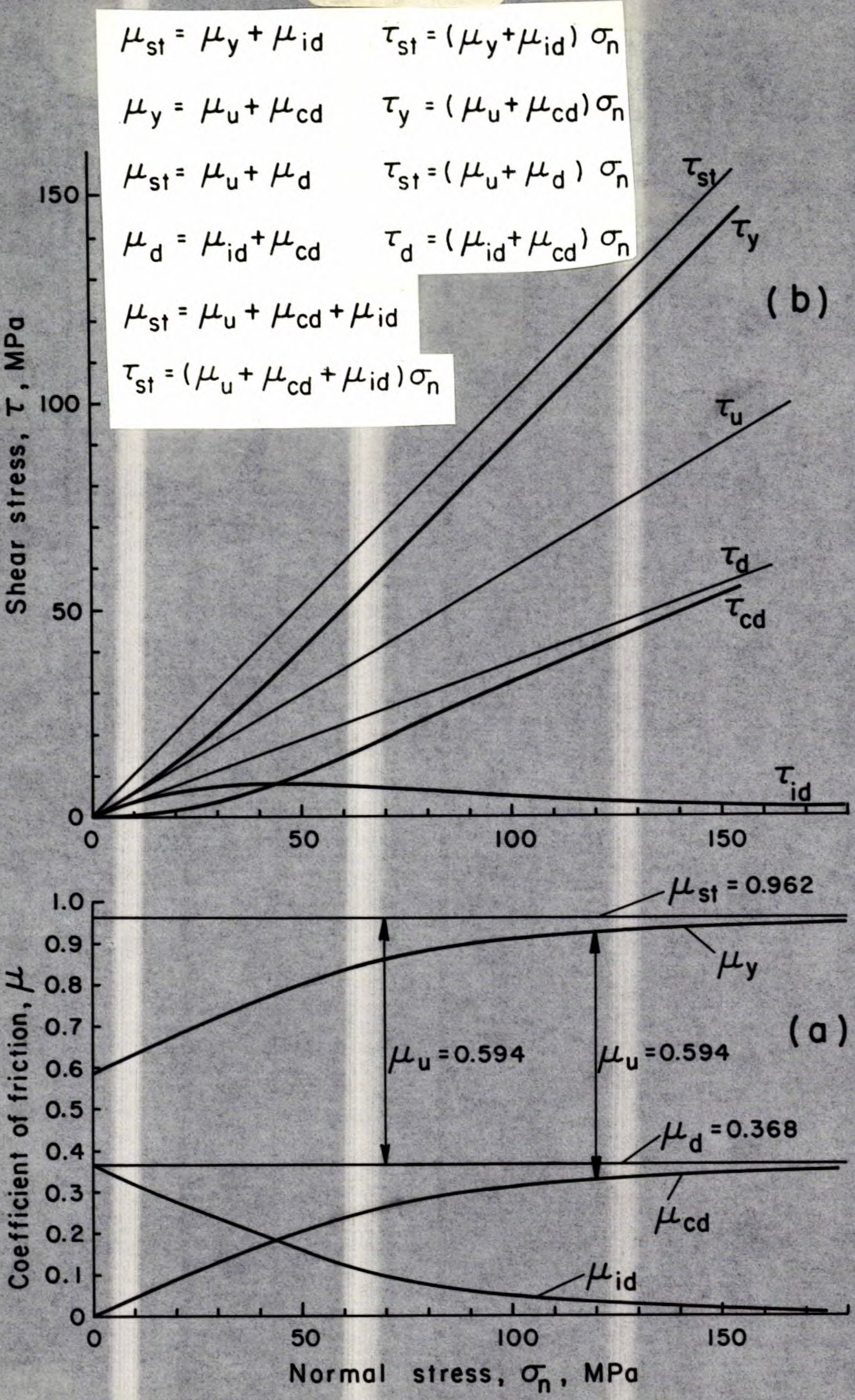

Fig. 30 - Variation of coefficient of friction and shear stress components for granite specimens with smooth sliding contact; (a) coefficient of friction components versus normal stress, (b) shear stress components versus normal stress.

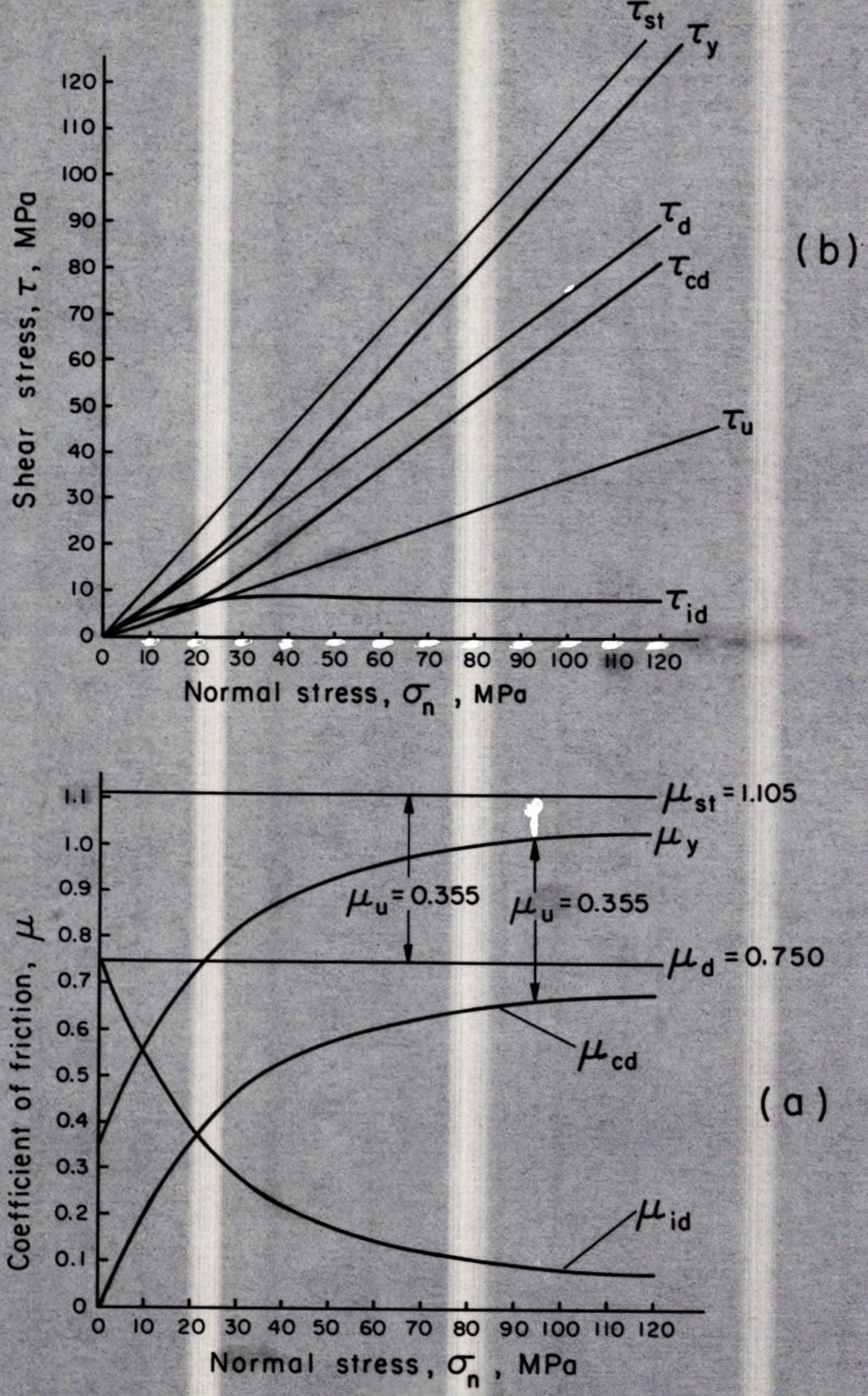

Fig. 31 - Variation of coefficient of friction and shear stress components for Indiana limestone specimens with smooth sliding contact; (a) coefficient of friction components versus normal stress, (b) shear stress components versus normal stress.

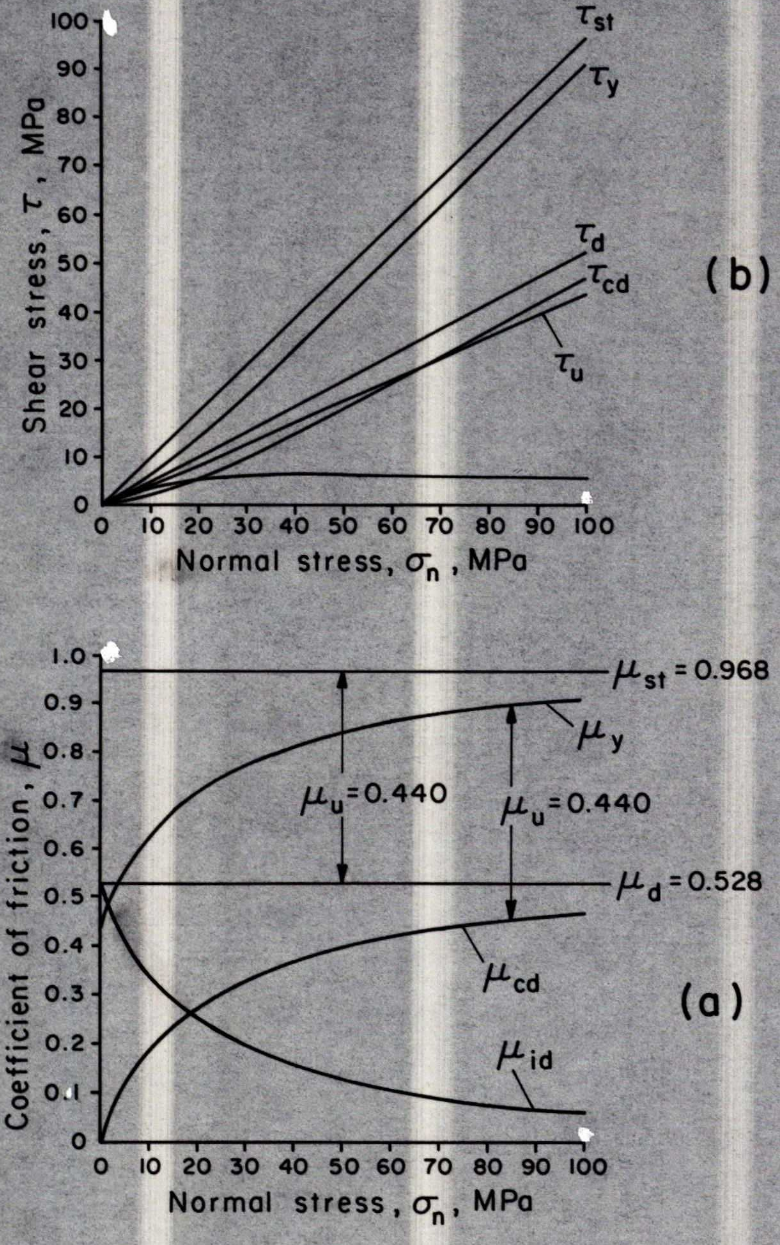

Fig. 32 - Variation of coefficient of friction and shear stress components for sandstone specimens with smooth sliding contact; (a) coefficient of friction component versus normal stress, (b) shear stress components versus normal stress.

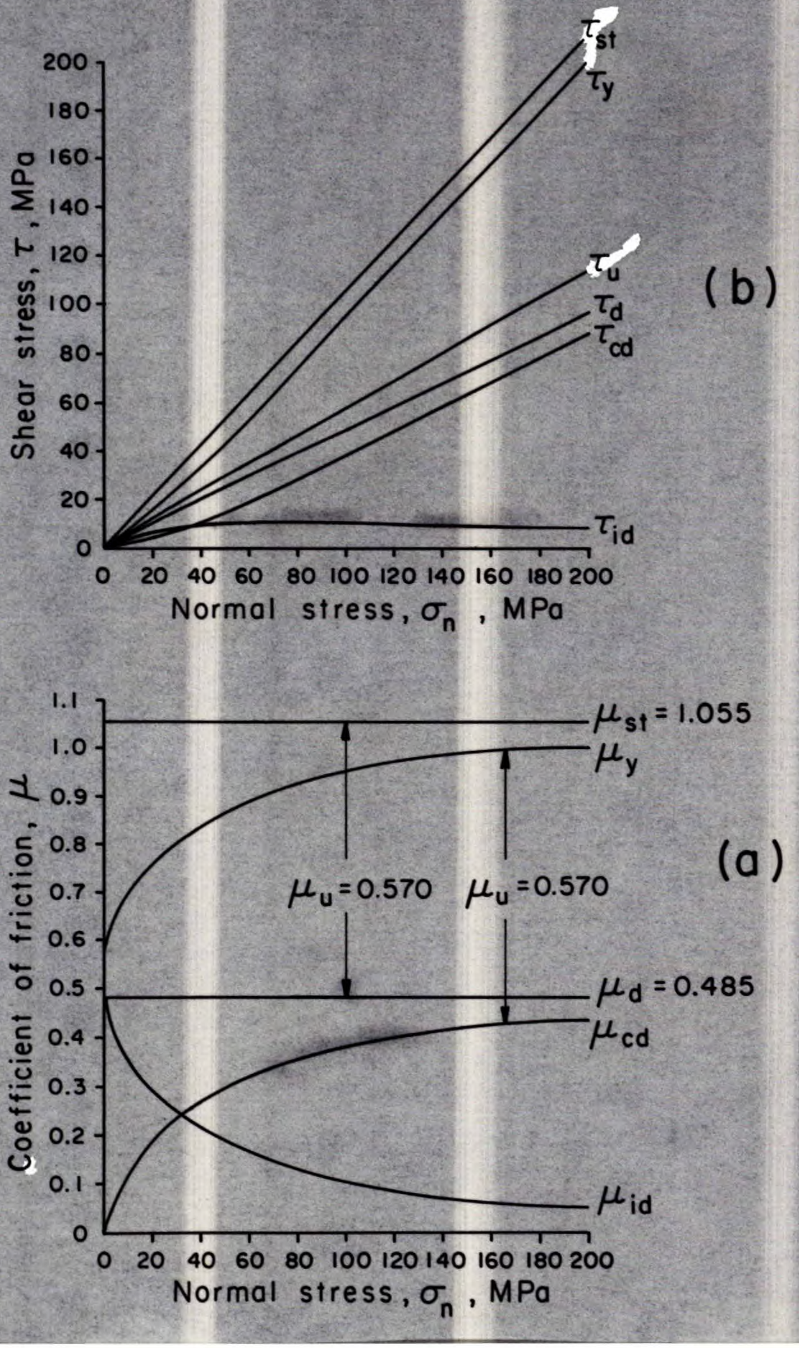

Fig. 33 - Variation of coefficient of friction and shear stress components for diabase specimens with smooth sliding contact; (a) coefficient of friction components versus normal stress, (b) shear stress components versus normal stress.

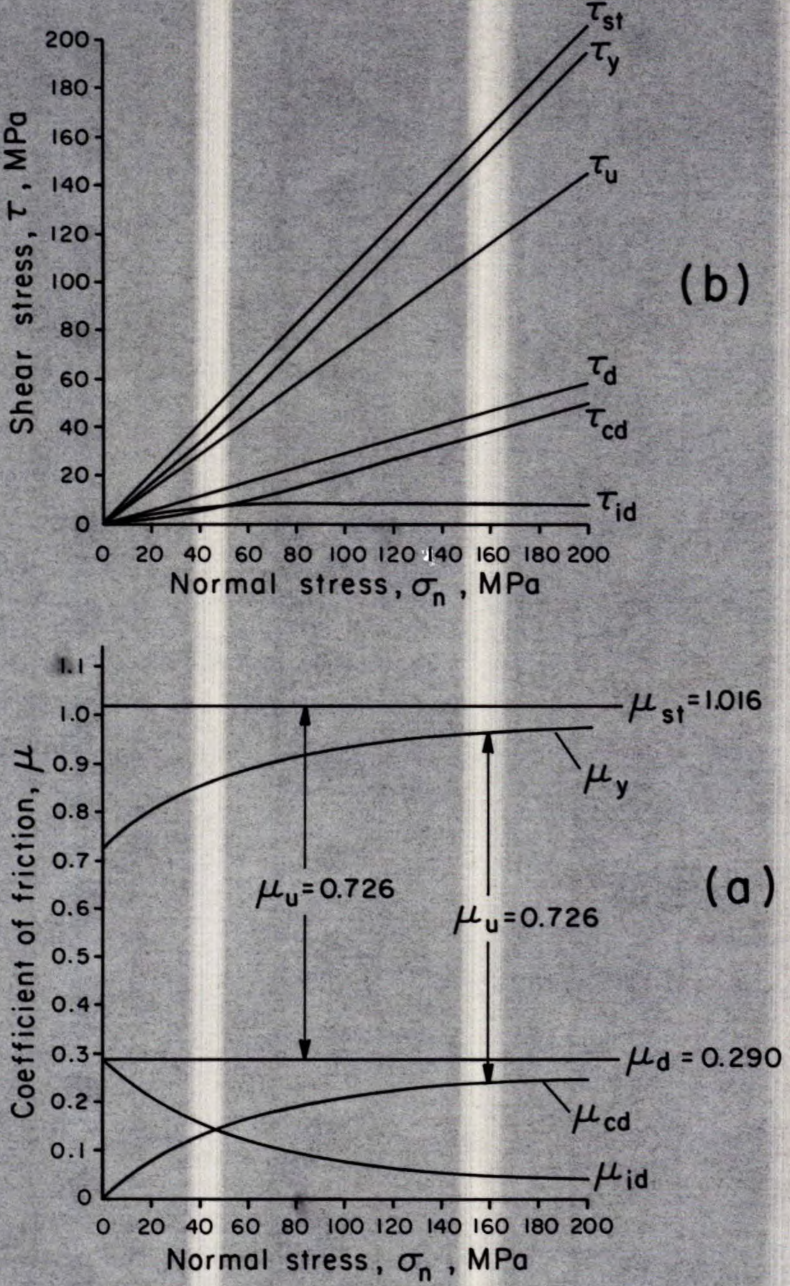

Fig. 34 - Variation of coefficient of friction and shear stress components for INCO ore specimens with smooth sliding contact; (a) coefficient of friction components versus normal stress, (b) shear stress components versus normal stress.

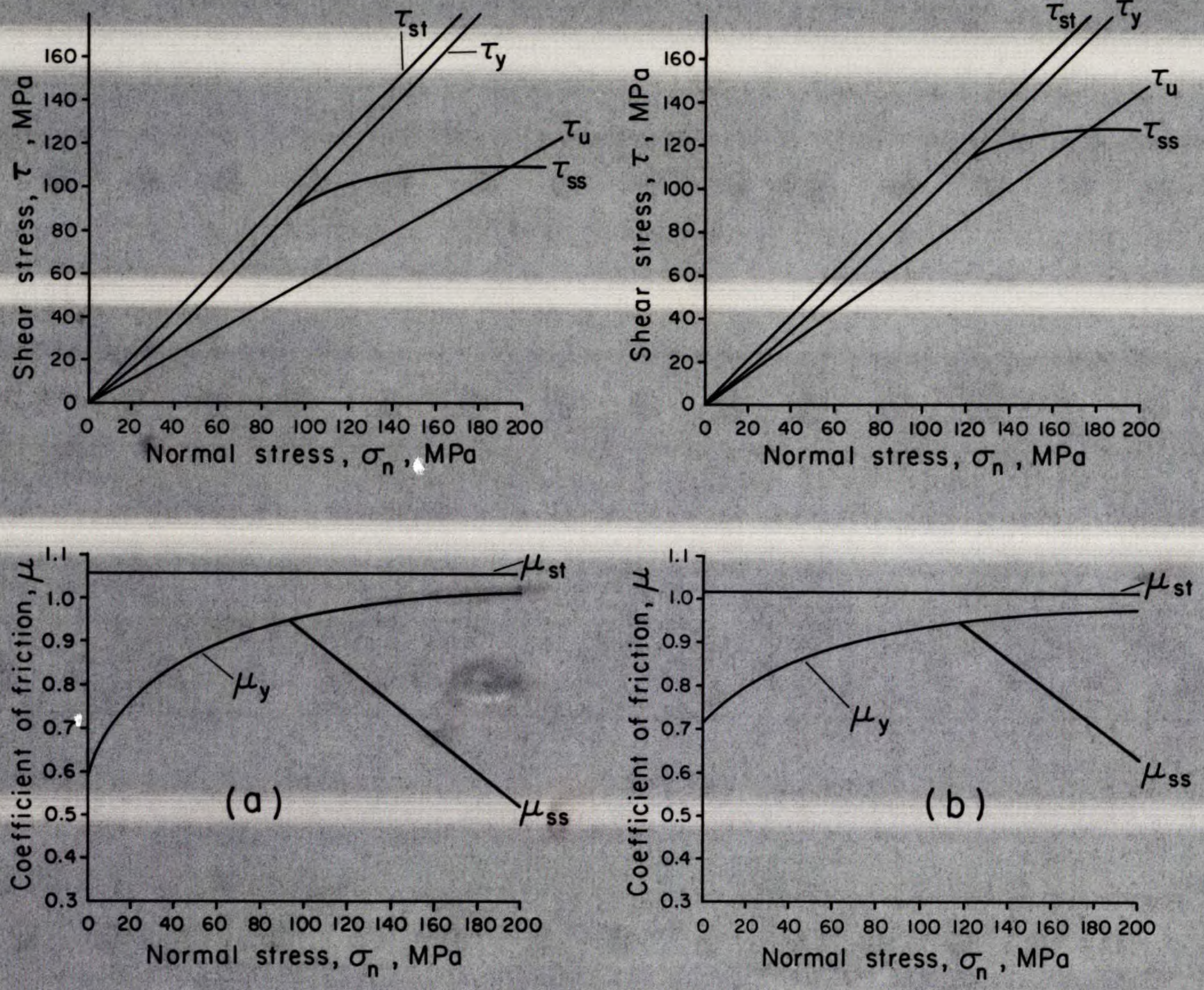

Fig. 35 - Sudden loss of shear strength along smooth contact lines; (a) diabase, (b) INCO ore.

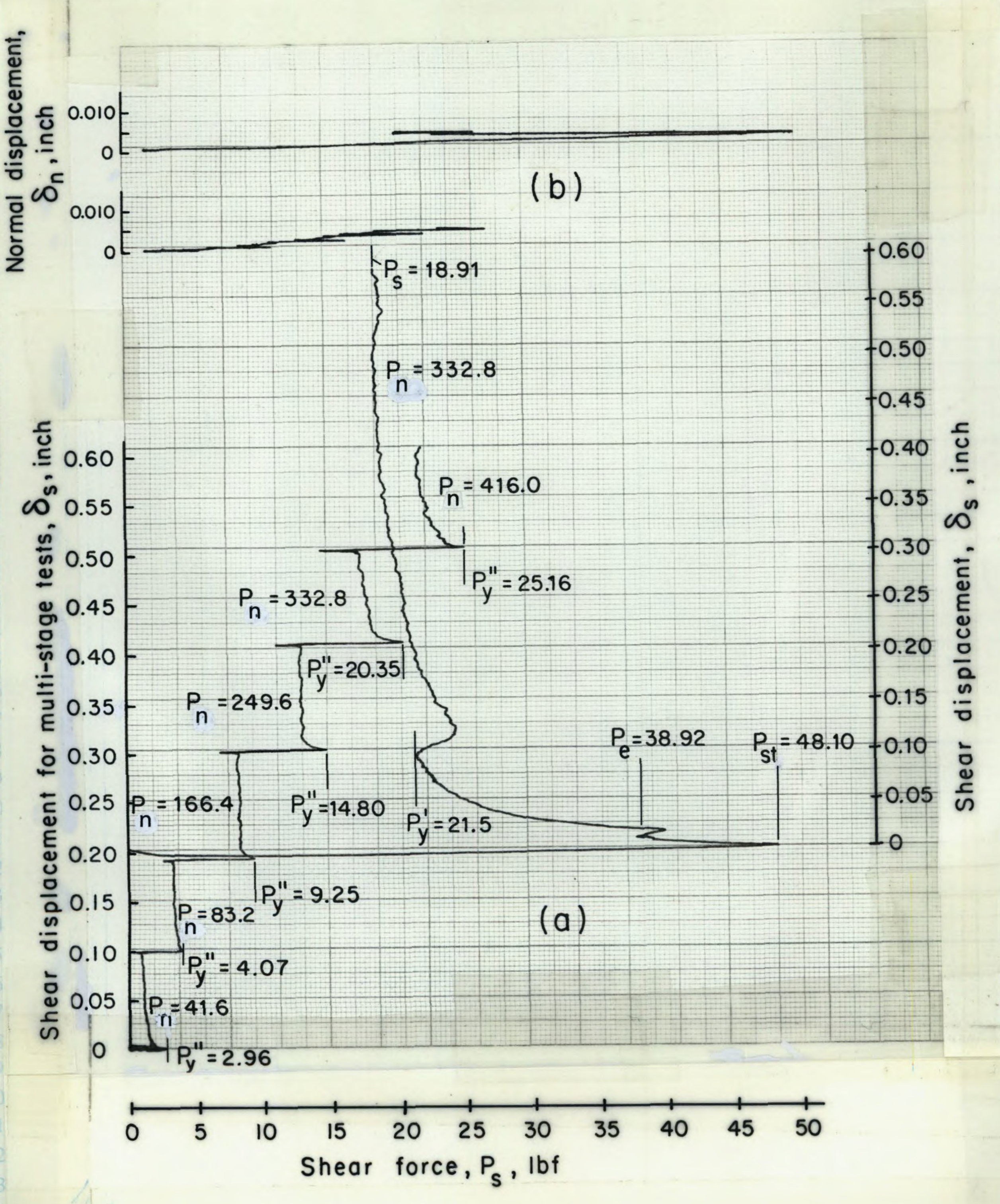

Fig. 36 - Recorded graphs of the initial and multi-staged test runs for teflon specimens; (a) shear force versus shear displacement, (b) shear force versus normal displacement.

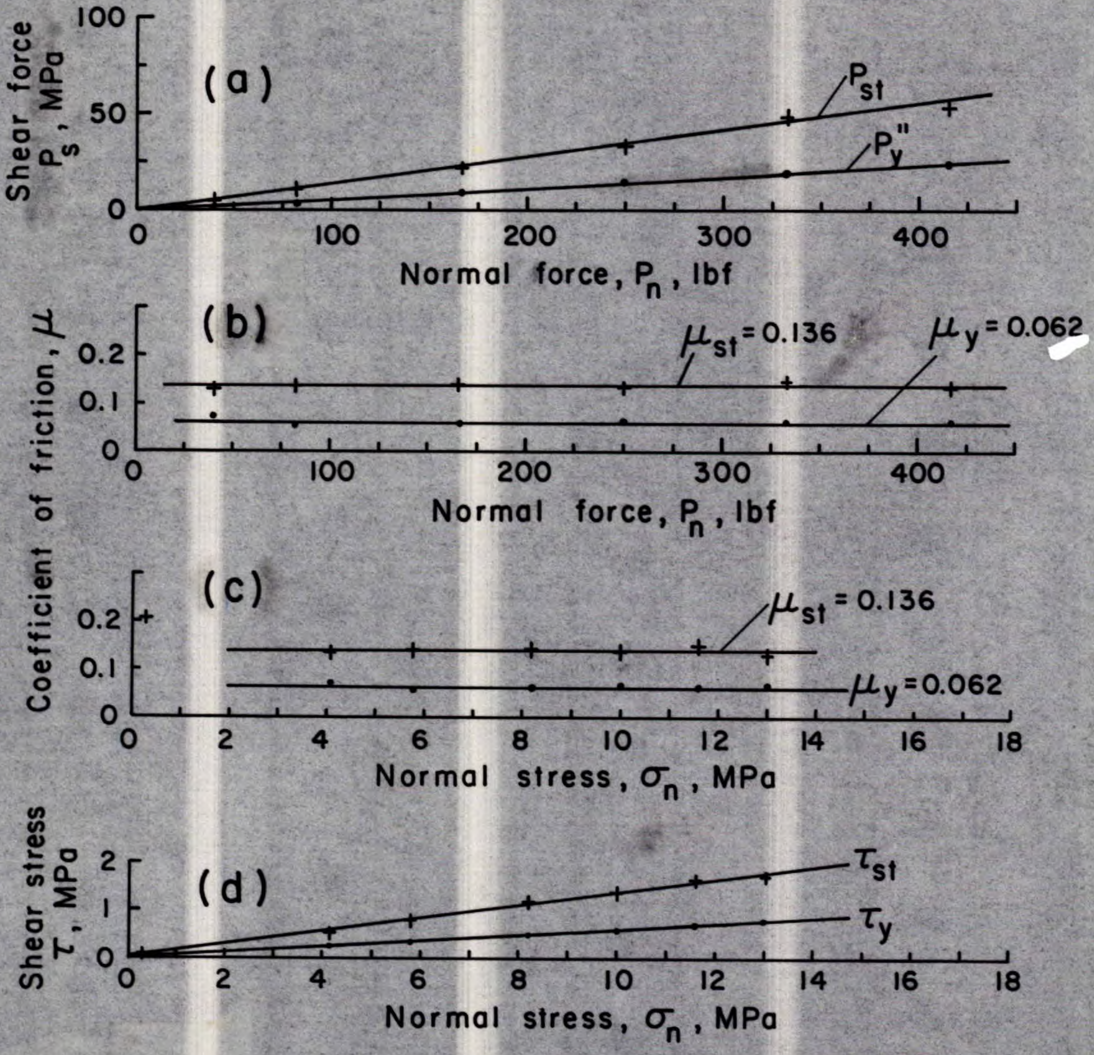

Fig. 37 - Variation of shear force and coefficient of friction components for teflon specimens wit smooth sliding contact; (a) measured shear force, (b) coefficients calculated from measurements (c) coefficients versus normal stresses, (d) shear stresses versus normal stresses.

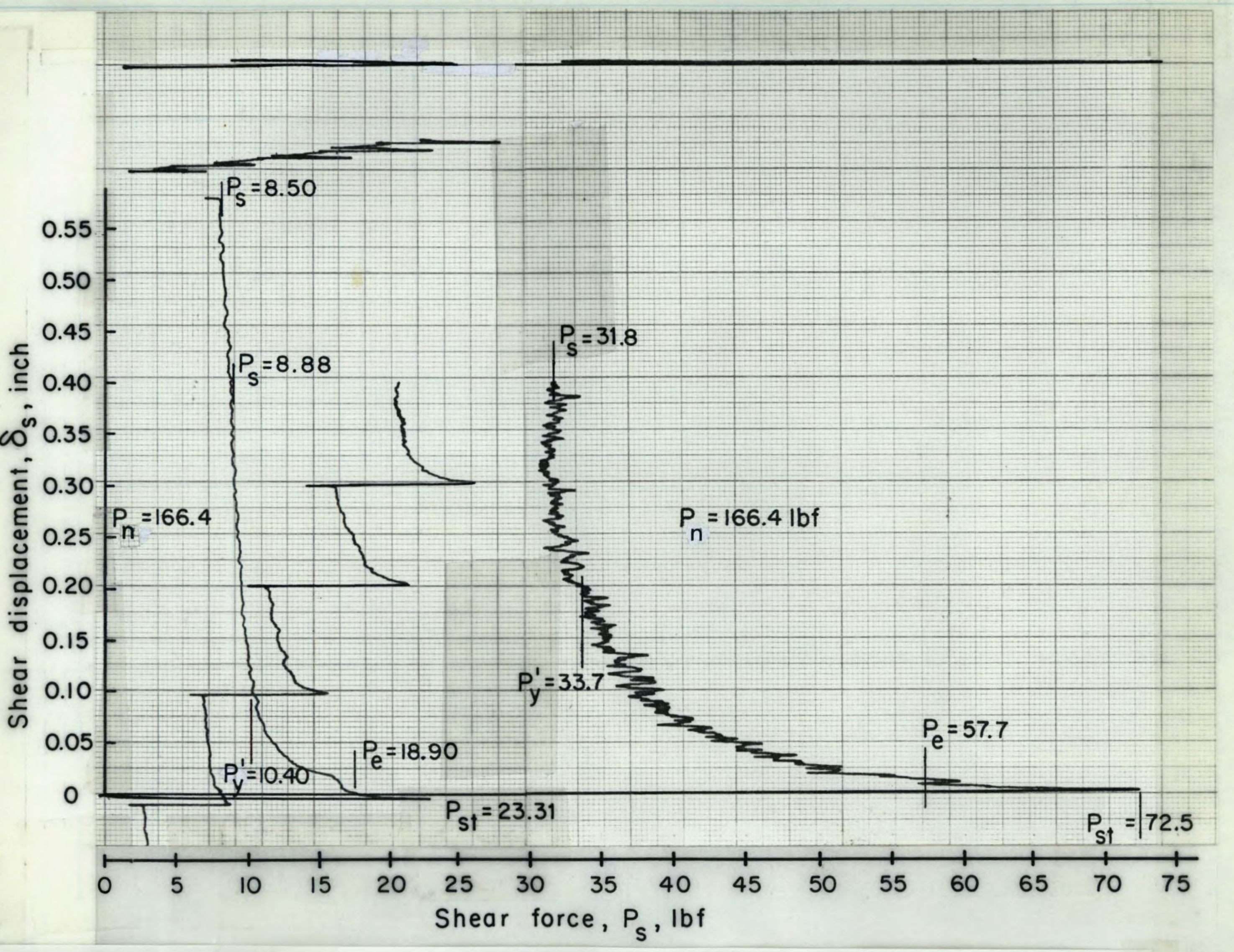

Fig. 38 - Comparison of test results for teflon and steel materials.

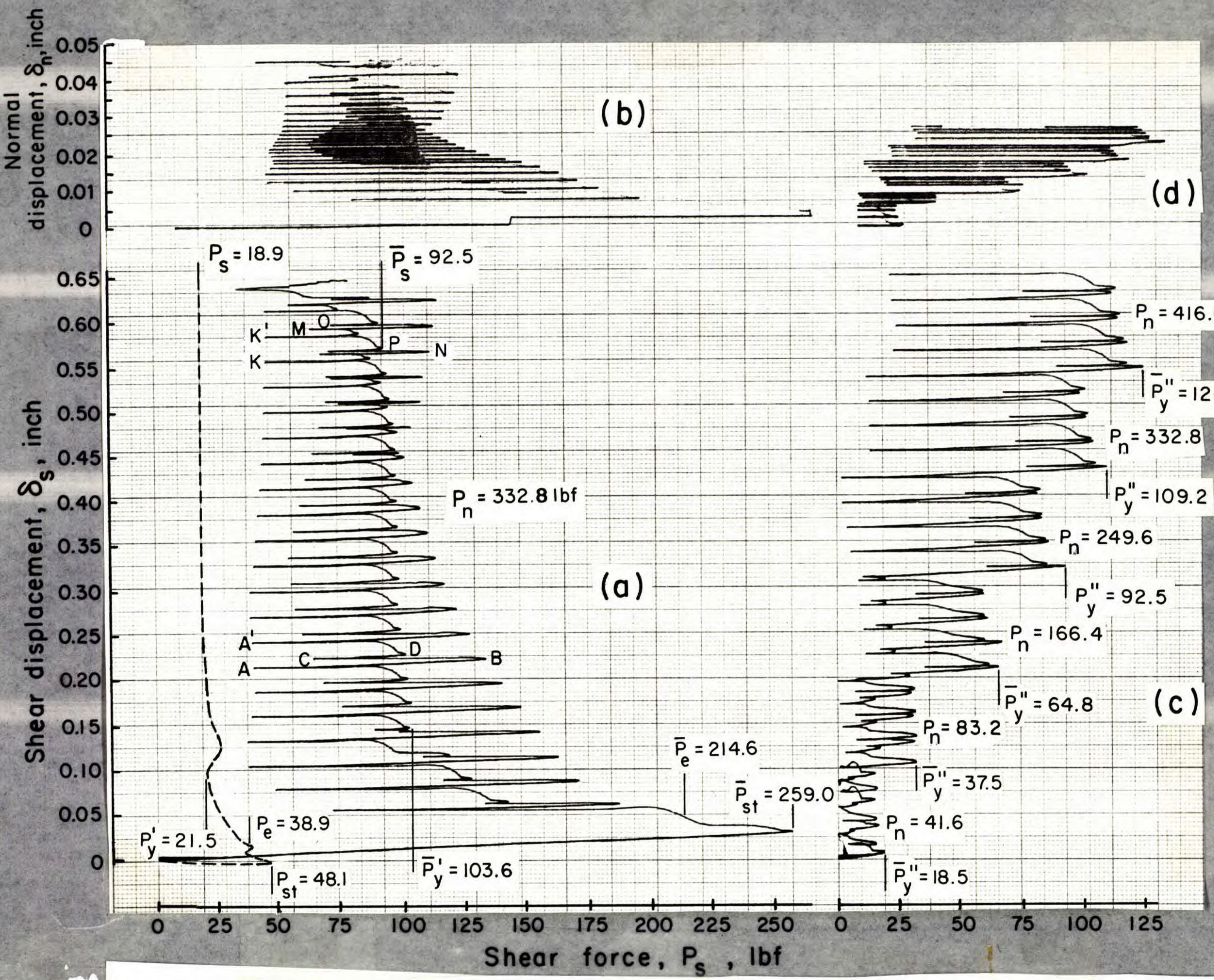

Fig. 39 - Recorded graphs of the initial and multi-stage test runs for teflon specimens with thread-like simulated asperities; (a) initial run shear force versus shear displacement, (b) initial run shear force versus normal displacement, (c) multi-stage shear force versus shear displacement, (d) multi-stage shear force versus normal displacement.

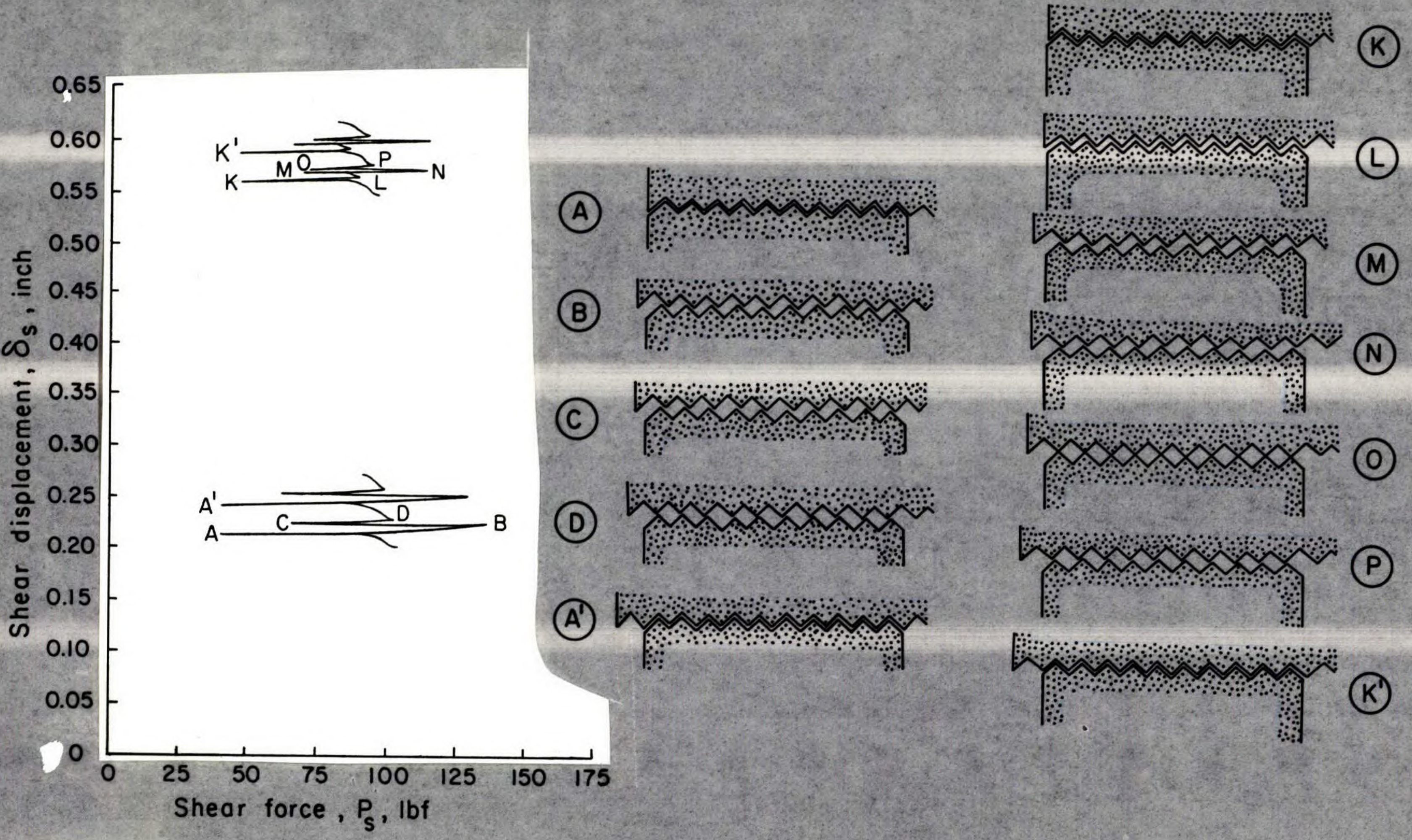

Fig. 40 - Detailed analysis of shear force variation cycles of an initial test run on teflon specimens with thread-like simulated asperities.

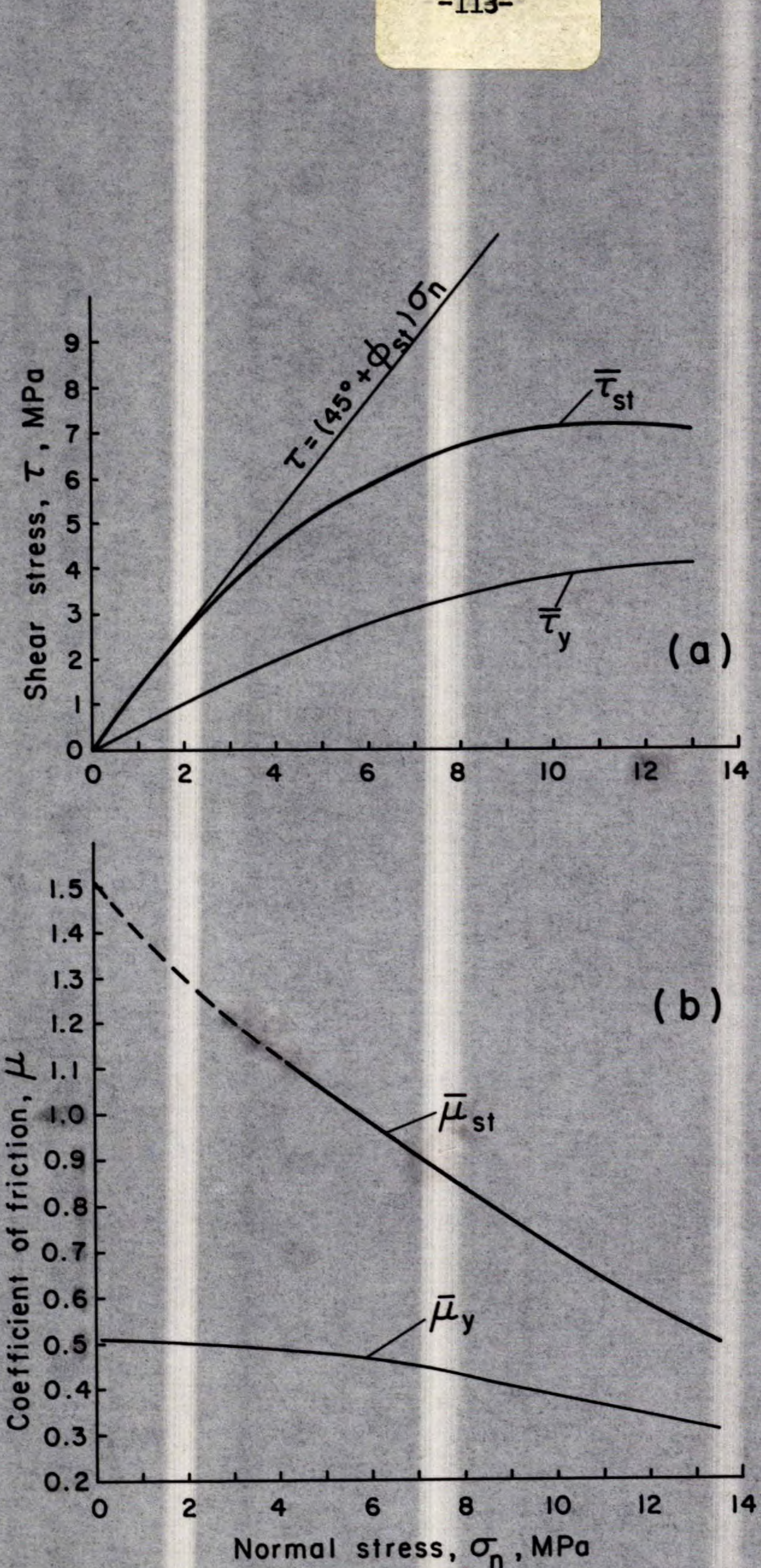

Fig. 41 - Variation of shear stress and coefficient of friction values for teflon specimens with thread-like simulated asperities; (a) shear stress versus normal stress, (b) coefficient of friction versus normal stress.

50

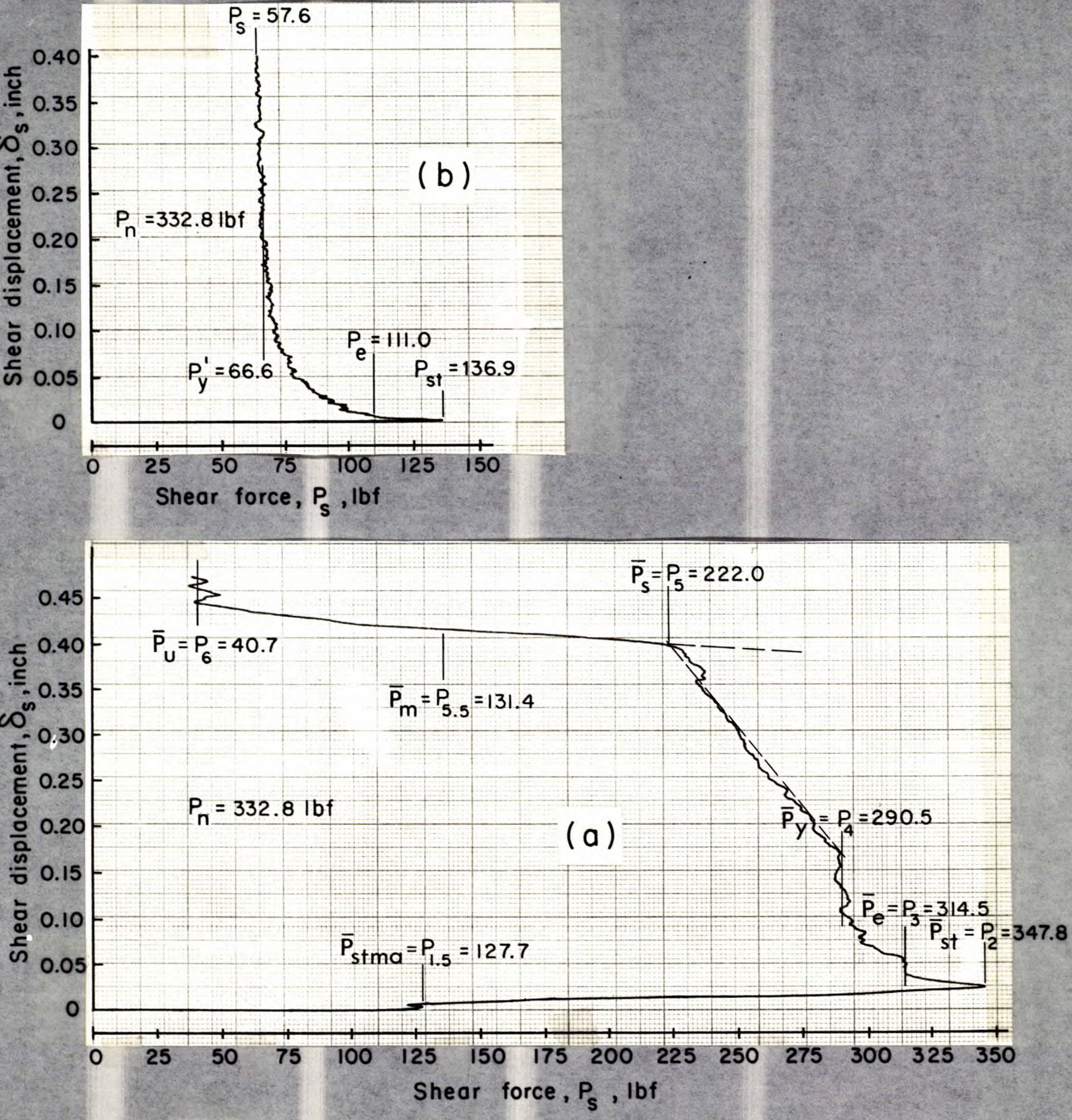

Fig. 42 - Analysed example of a Case A test run on steel specimens; (a) recorded graph for large single asperity, (b) recorded graph for smooth sliding contact lines.

23

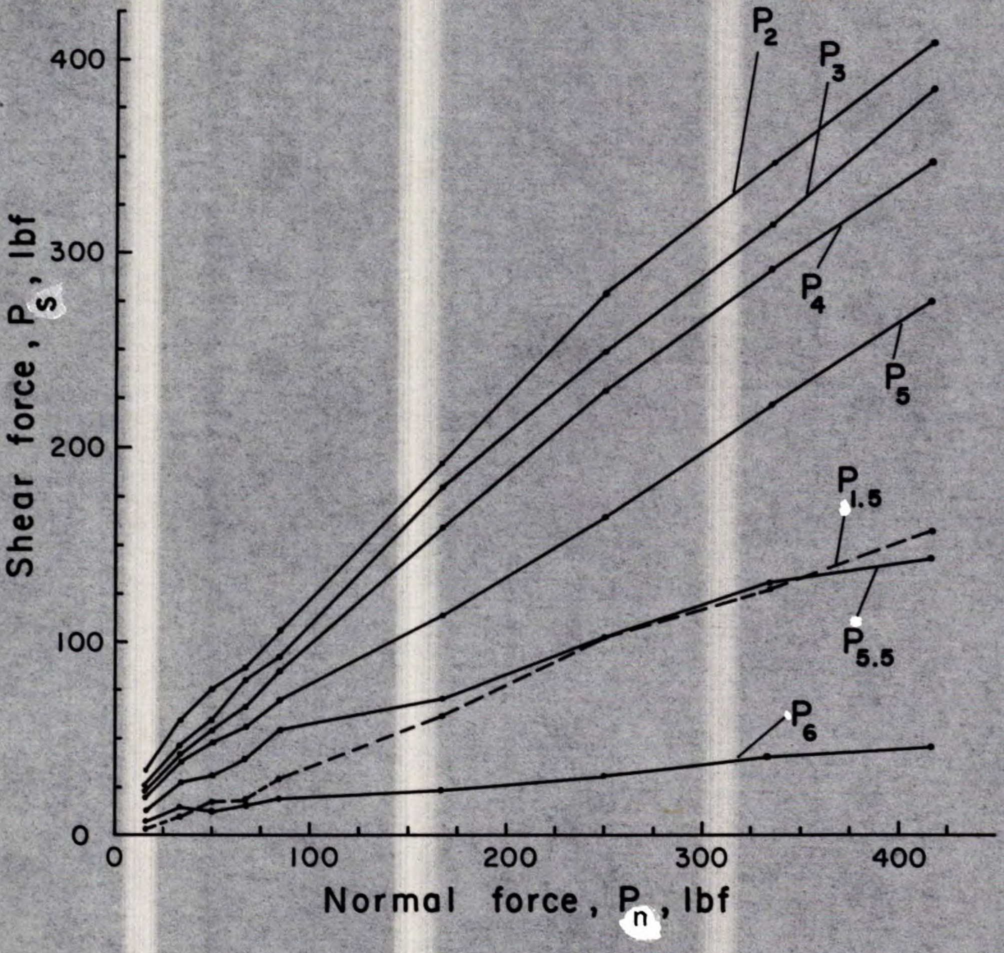

Fig. 43 - Variation of shear forces with applied normal forces for the Case A test series performed on steel specimens with large asperity.

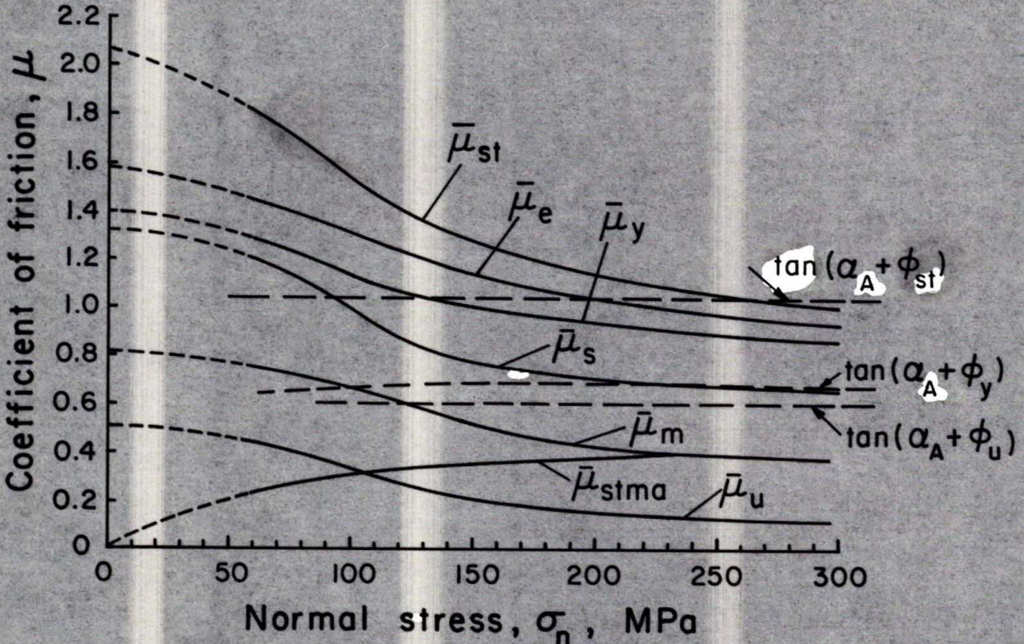

Fig. 44 - Coefficient of friction versus normal stress for Case A test series on steel specimens with large asperity.

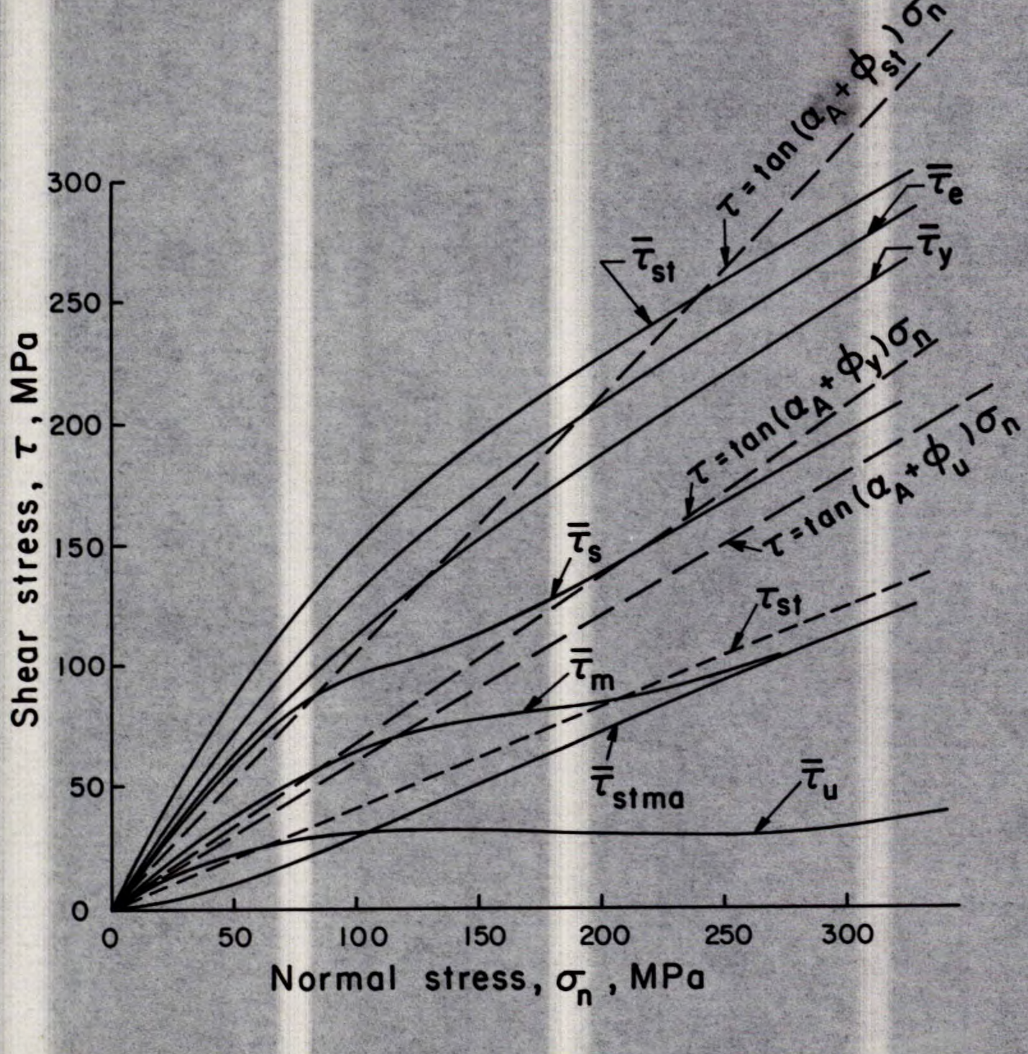

2

Fig. 45 - Shear stress versus normal stress for Case A test series on steel specimens with large asperity.

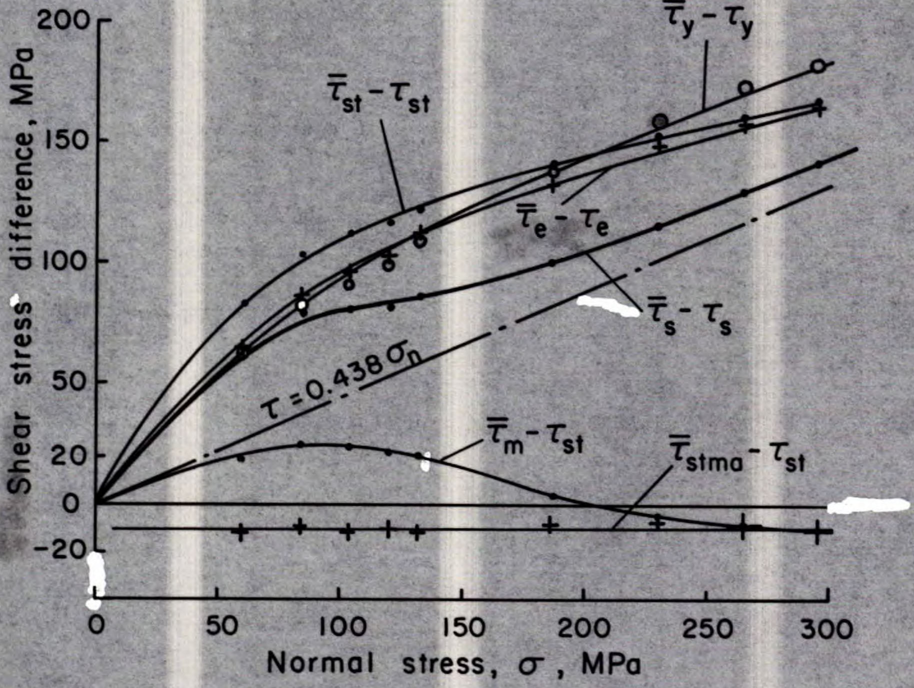

Fig. 46 - Shear stress difference values versus normal stresses, between Case A and smooth contact line test series on steel specimens with large asperity.

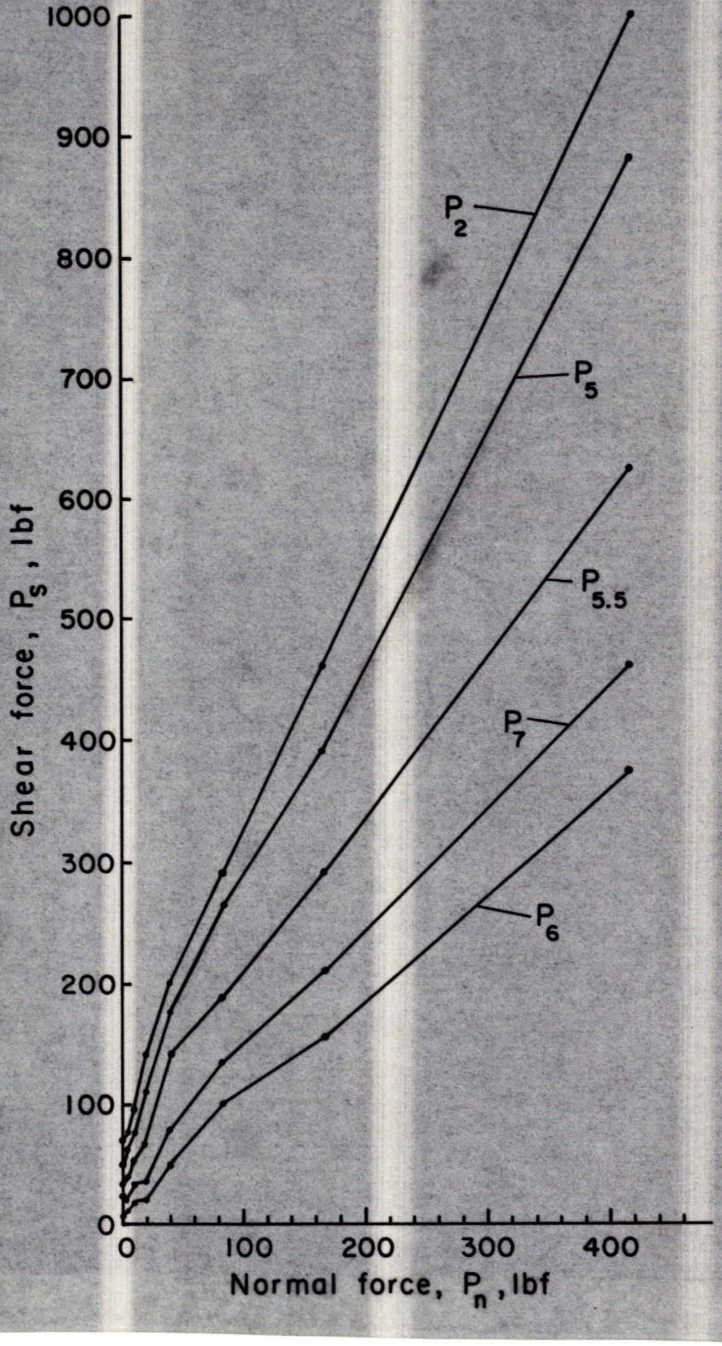

Fig. 47 - Variation of shear force with applied normal forces for the Case A test series performed on granite specimens with single large asperity.

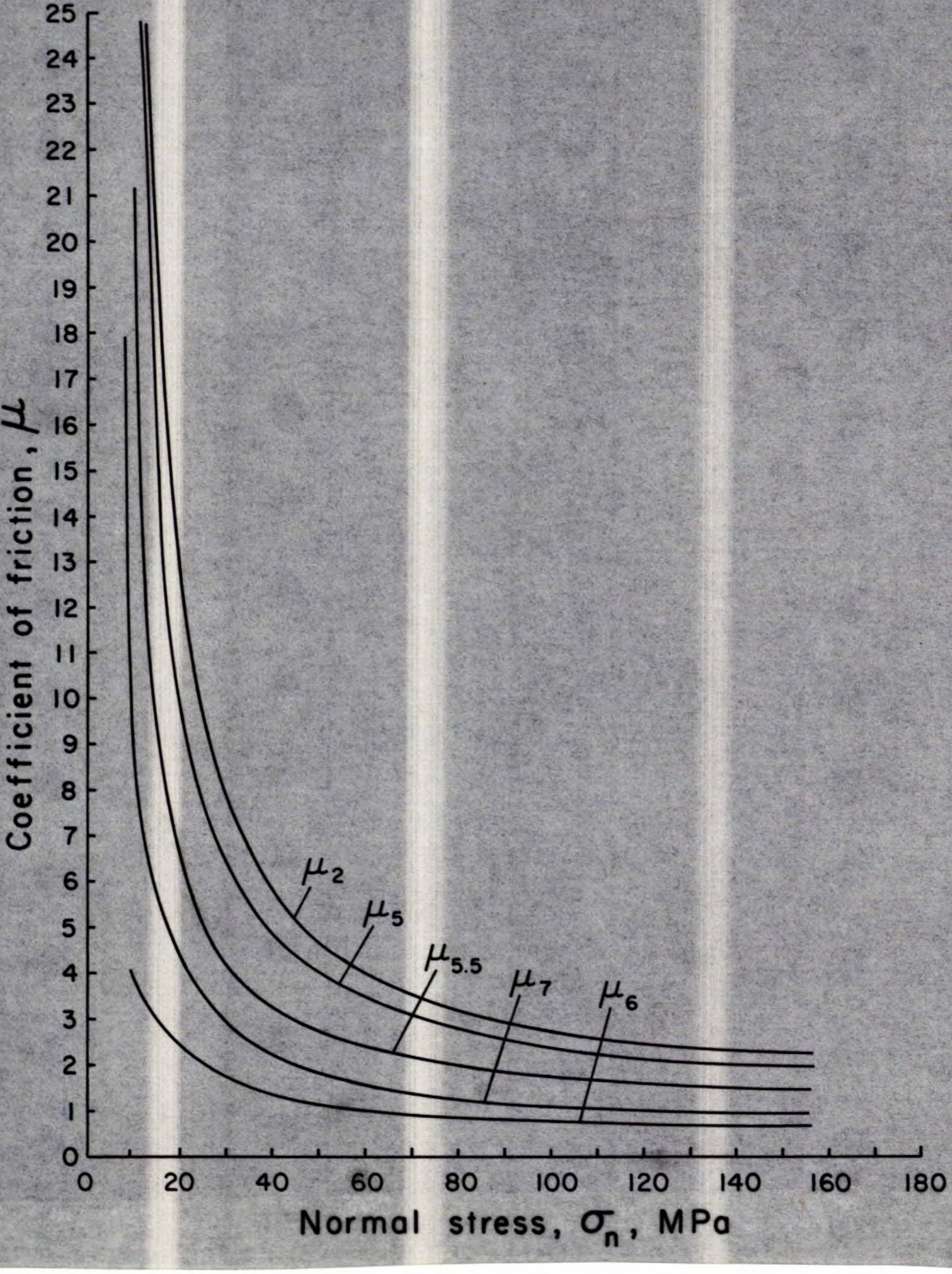

Fig. 48 - Coefficient of friction versus normal stress for granite specimens with single large asperity.

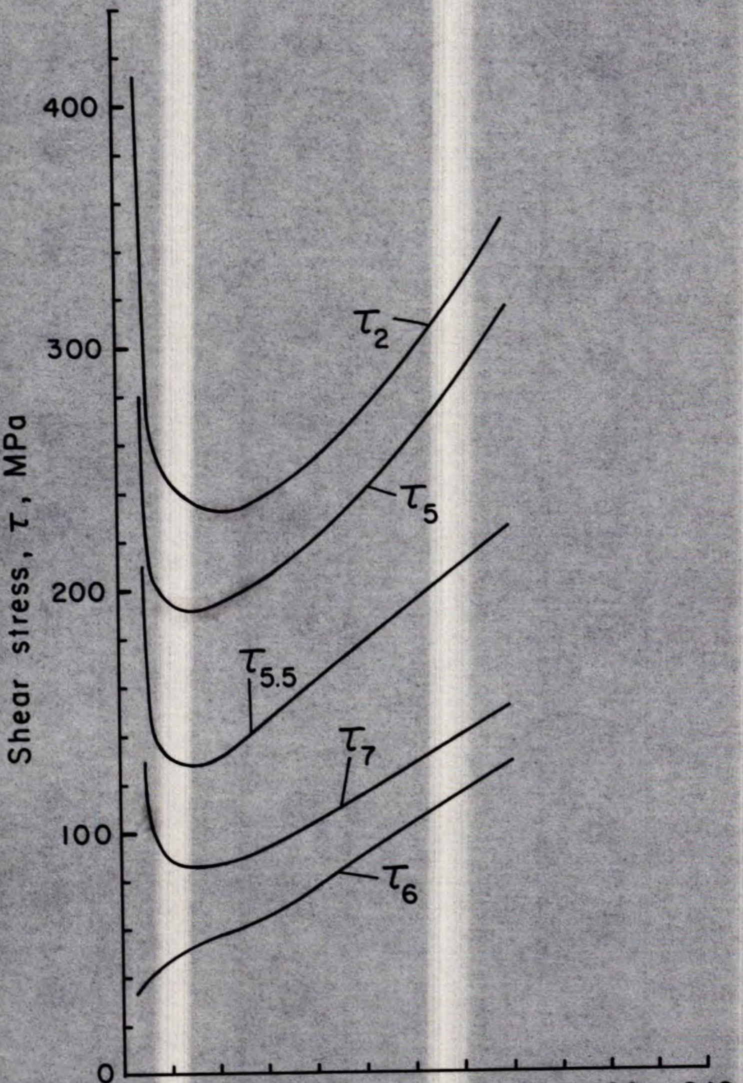

Fig. 49 - Shear stress versus normal stress for granite specimens with single large asperity.

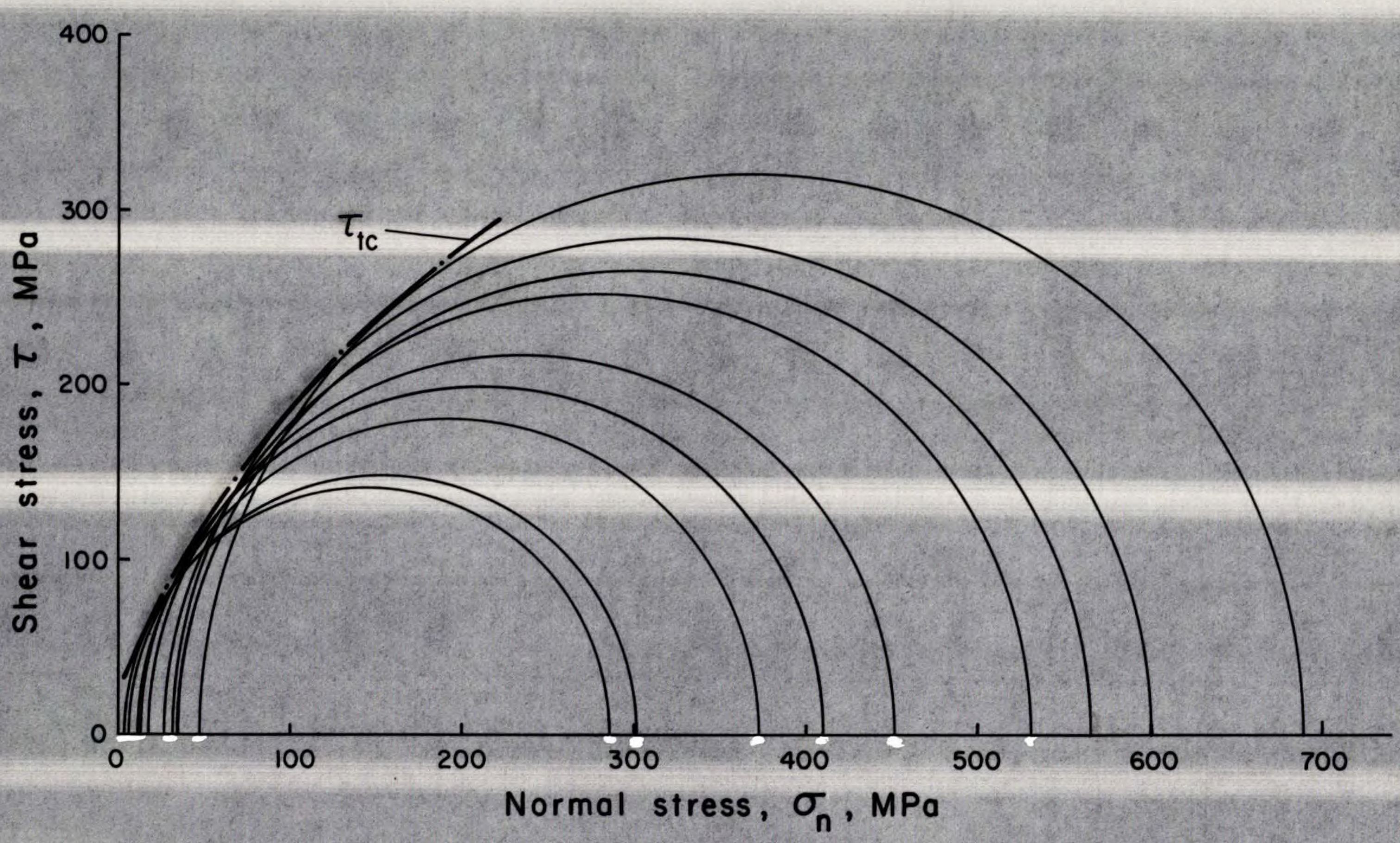

Fig. 50 - Peak strength envelope established by conventional triaxial test method.

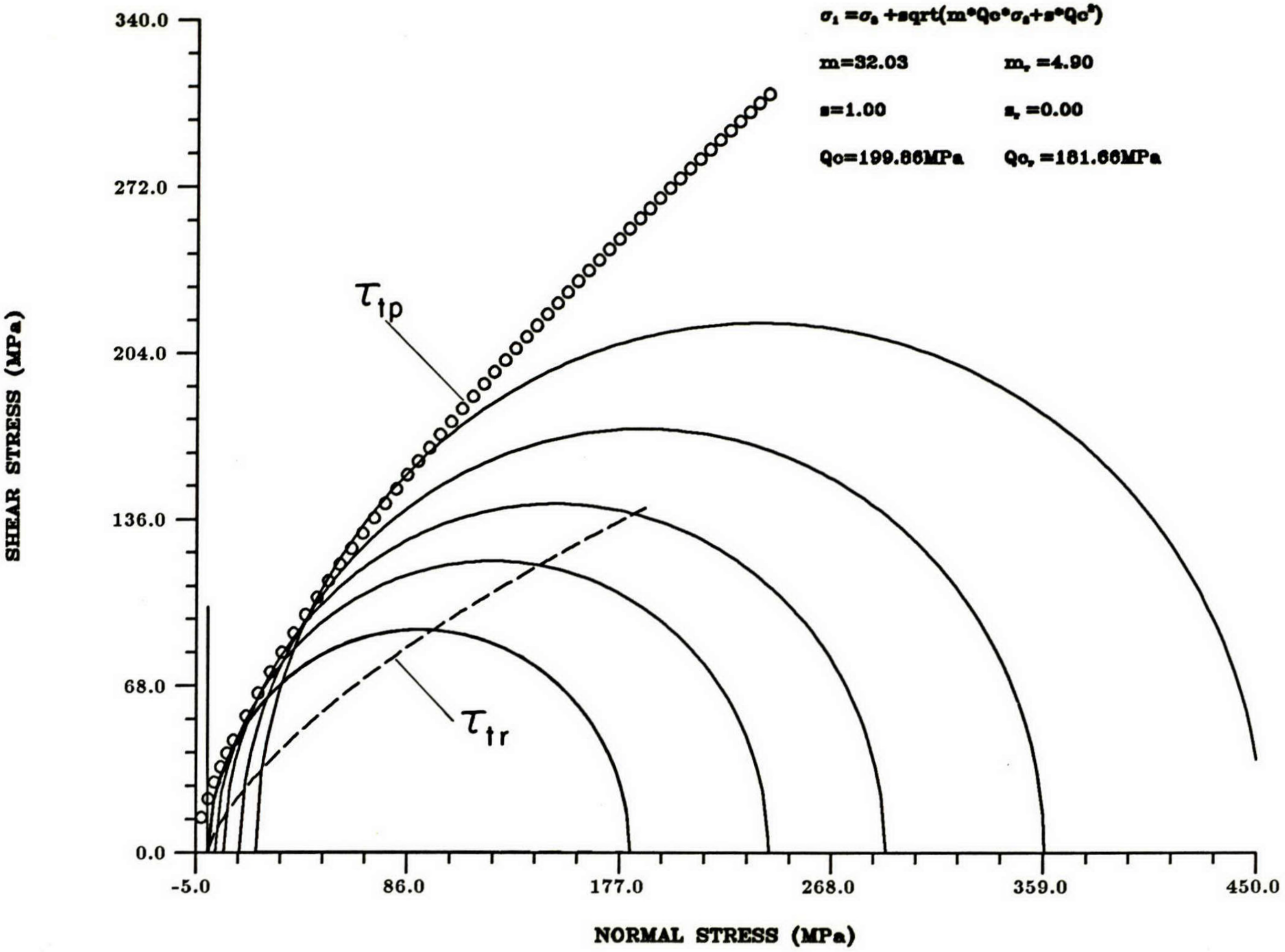

Fig. 51 - Peak and residual strength envelopes established by multi-stage triaxial test method.

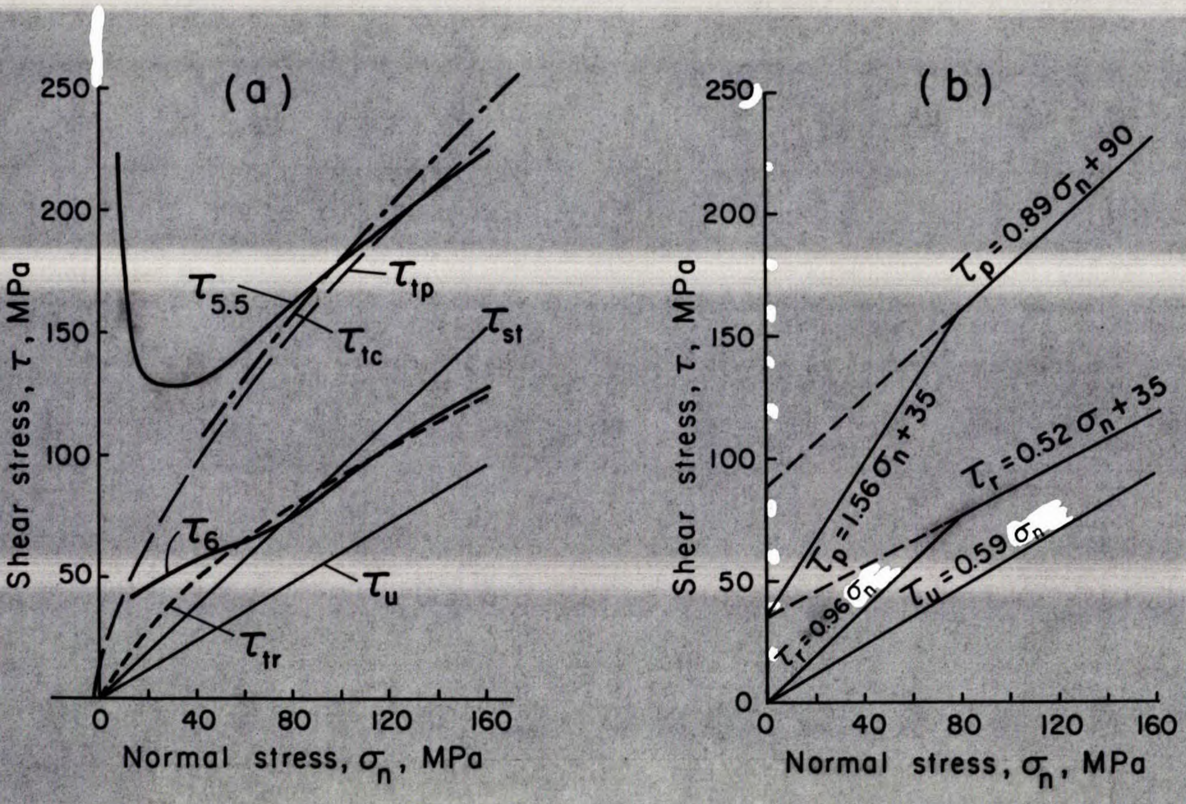

Fig. 52 - Summary of test results for granite; (a) strength envelopes obtained by various tests, (b) peak and residual strength envelopes.

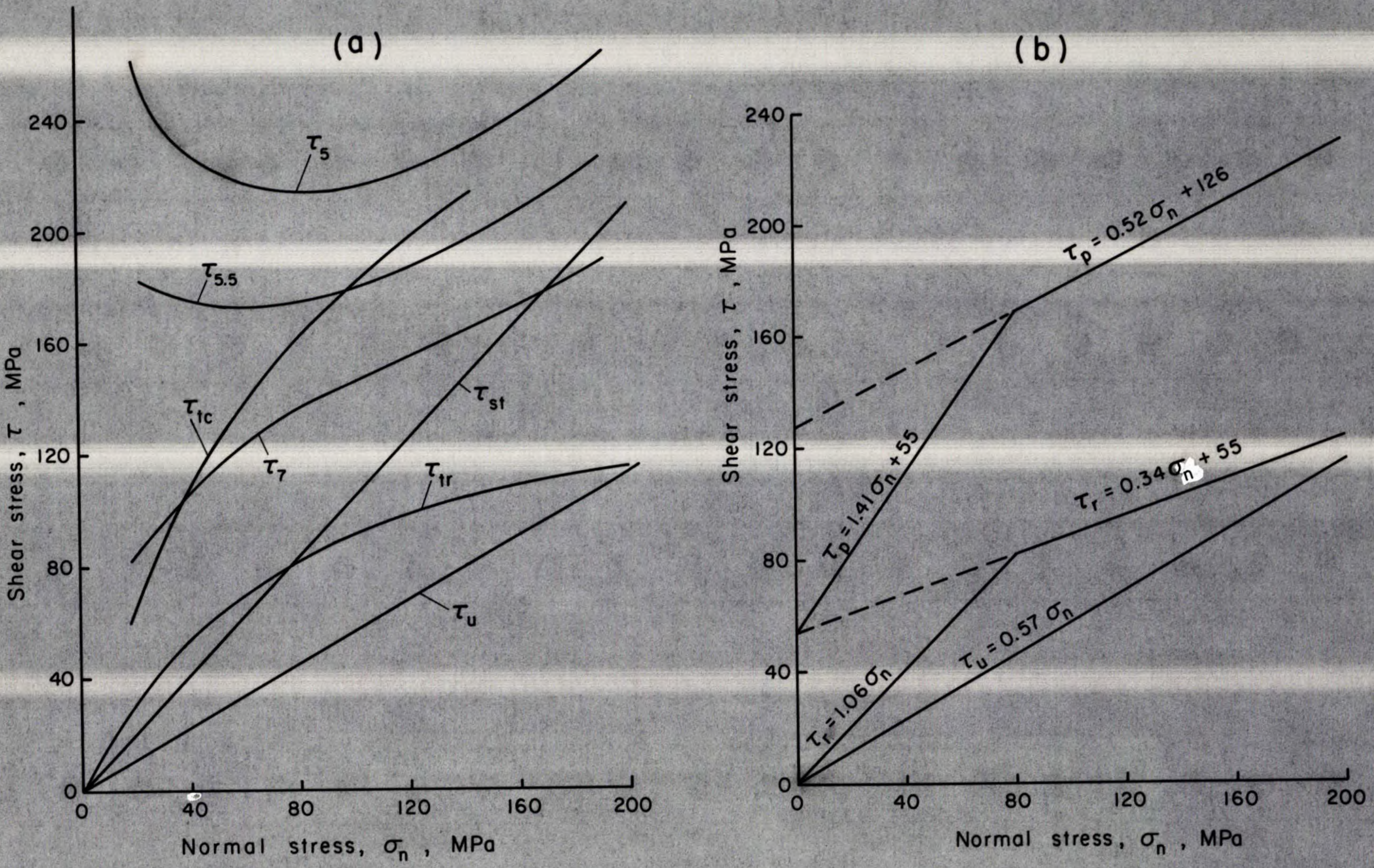

Fig. 53 - Summary of test results for diabase; (a) strength envelopes obtained by various tests, (b) peak and residual strength envelopes.

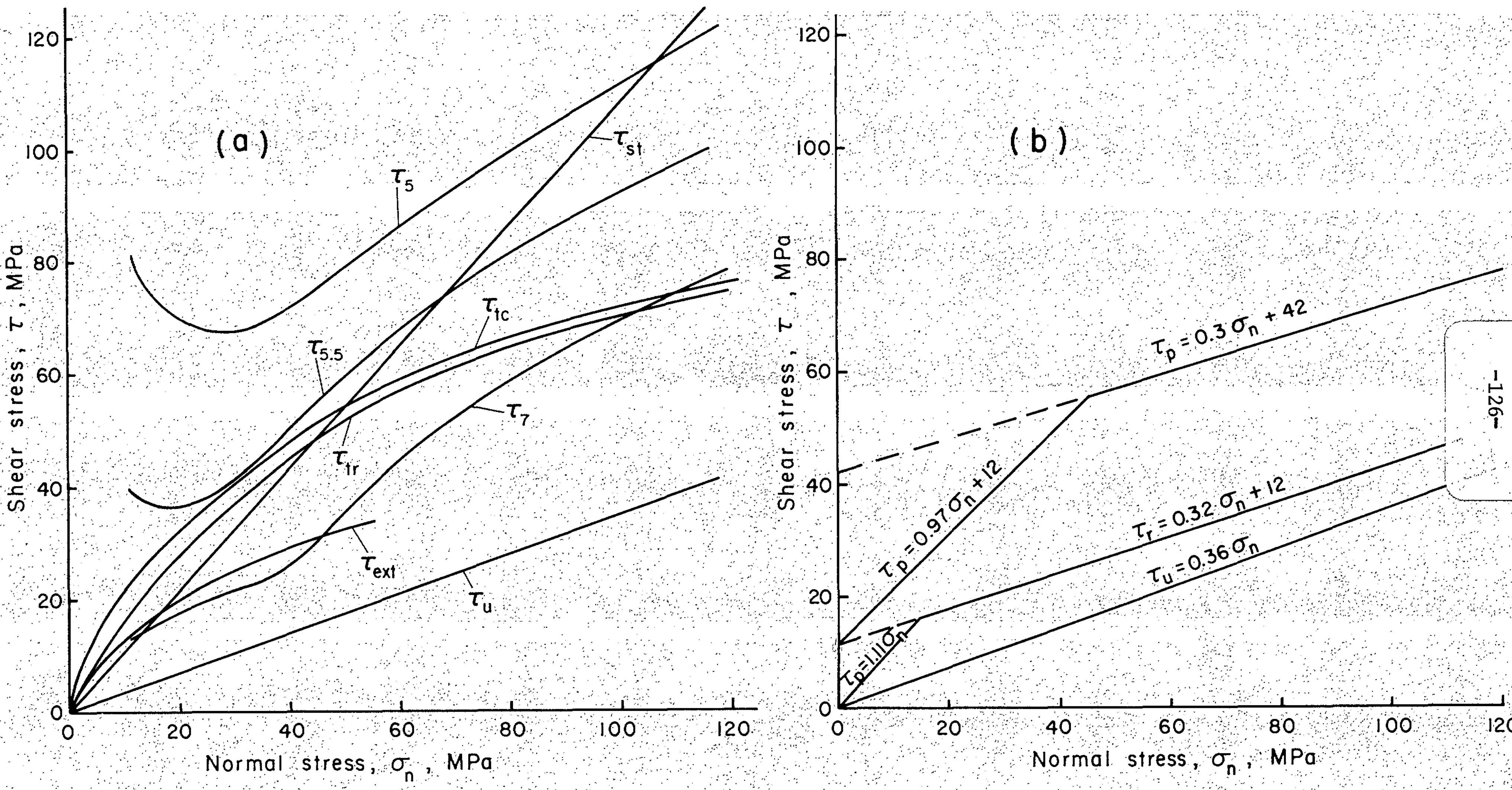

Fig. 54 - Summary of test results for Indiana limestone; (a) strength envelopes obtained by various tests, (b) peak and residual strength envelopes.